Review Article

Nano Research
2024, 17(11): 10134–10161

ISSN 1998-0124 CN 11-5974/O4
https://doi.org/10.1007/s12274-024-6936-3

Progress and prospects of Moiré superlattices in twisted TMD heterostructures

Syed Jamal Shah[1,2], Junying Chen[1,2], Xing Xie[1,2], Xinyu Oyang[2], Fangping Ouyang[1,3], Zongwen Liu[4,5], Jian-Tao Wang[6,7,8], Jun He[1], and Yanping Liu[1,2] (✉)

[1] *Institute of Quantum Physics, School of Physics, Central South University, Changsha 410083, China*
[2] *State Key Laboratory of Precision Manufacturing for Extreme Service Performance, Central South University, Changsha 410083, China*
[3] *School of Physics and Technology, State Key Laboratory of Chemistry and Utilization of Carbon Based Energy Resources, Xinjiang University, Urumqi 830046, China*
[4] *School of Chemical and Biomolecular Engineering, The University of Sydney, NSW 2006, Australia*
[5] *The University of Sydney Nano Institute, The University of Sydney, NSW 2006 Australia*
[6] *Beijing National Laboratory for Condensed Matter Physics, Institute of Physics, Chinese Academy of Sciences, Beijing 100190, China*
[7] *School of Physical Sciences, University of Chinese Academy of Sciences, Beijing 100049, China*
[8] *Songshan Lake Materials Laboratory, Dongguan 523808, China*

© Tsinghua University Press 2024

Received: 19 June 2024 / **Revised:** 31 July 2024 / **Accepted:** 2 August 2024

ABSTRACT

Moiré superlattices based on twisted transition metal dichalcogenide (TMD) heterostructures have recently emerged as a promising platform for probing novel and distinctive electronic phenomena in two-dimensional (2D) materials. By stacking TMD monolayers with a small twist angle, these superlattices create a periodic modulation of the electronic density of states, leading to the formation of mini bands. These mini bands can exhibit intriguing properties such as flat bands, correlated electron behavior, and unconventional superconductivity. This review provides a comprehensive overview of recent progress in Moiré superlattices formed from twisted TMD heterostructures. It covers the theoretical principles and experimental techniques for creating and studying these superlattices, and explores their potential applications in optoelectronics, quantum computing, and energy harvesting. The review also addresses key challenges, such as improving the scalability and reproducibility of the fabrication process, emphasizing the exciting opportunities and ongoing hurdles in this rapidly evolving field.

KEYWORDS

Moiré superlattices, twisted transition metal dichalcogenides, heterostructures, electronic properties, optical properties, transport properties, valleytronics, optoelectronics, quantum information processing

1 Introduction

In the field of condensed matter physics, the concept of Moiré superlattices has emerged as a valuable platform avenue for investigating novel electronic properties in low-dimensional materials [1–4]. These superlattices are formed by stacking two-dimensional (2D) materials with a slightly mismatched lattice structure with either twist angle or lattice mismatch, resulting in a periodic Moiré pattern with a longer wavelength than either individual lattice [5–8]. Recent advancements in the synthesis of twisted transition metal dichalcogenide (TMD) heterostructures have opened up exciting possibilities for studying Moiré superlattices across a range of new materials systems [9–11]. There has been significant interest in various two-dimensional materials, including graphene, hexagonal boron nitride (h-BN), and various TMDs. The main focus of this paper is on TMD materials. TMDs have been selected as the primary research object for several compelling reasons. Firstly, TMDs exhibit a range of electronic, optical, and mechanical properties that can be finely tuned by varying the composition and structure of the material. This tunability makes them highly versatile for various applications in electronics, photonics, and catalysis [12, 13]. Secondly, unlike graphene, TMDs possess a natural bandgap, which is essential for the development of semiconductor devices. Additionally, the strong spin-orbit coupling in TMDs opens up opportunities for spintronic applications. The ease of creating heterostructures with other 2D materials further enhances their utility in research and development of novel devices. Given these advantages, TMDs are particularly well-suited for exploring new physical phenomena and advancing technology in various fields.

This review paper aims to provide an overview of the latest progress in this field, focusing on the experimental and theoretical studies of TMD Moiré superlattices. We highlight key results in areas such as electronic transport, optical properties, and magnetism, and discuss the potential for future applications in areas such as quantum computing and optoelectronics. Overall, this review aims to provide a comprehensive overview of the state-of-the-art research in the field of Moiré superlattices based on TMD heterostructures. The paper begins with an introduction to the basic concepts of Moiré superlattices, including their formation and the unique properties they exhibit. Subsequently,

Address correspondence to liuyanping@csu.edu.cn

we discuss the specific properties of TMD materials, such as their strong electron–electron interactions and their strong optical response. Following this, we focus on recent progress in the field, covering topics like the observation of superconductivity in TMD Moiré superlattices, the emergence of new electronic phases, and the development of new techniques for probing these systems. We also address the challenges that remain in the field, such as the need to control and manipulate the Moiré patterns in a precise and reliable way. Finally, we discuss the potential future applications of TMD Moiré superlattices in areas such as quantum computing, optoelectronics, and energy harvesting. Overall, this review aims to serve as a valuable resource for researchers interested in the latest developments in this exciting and rapidly evolving field.

In this review paper, we provide a detailed analysis of recent progress in Moiré superlattices based on twisted TMD heterostructures. We begin by discussing the basics of Moiré superlattices and their electronic properties, followed by a thorough analysis of twisted TMD heterostructures, including the synthesis methods and their structural and electronic properties. Figure 1 provides a visual representation of this review paper. We also discuss the recent experimental and theoretical studies on the electronic and optical properties of Moiré superlattices based on twisted TMD heterostructures, which have demonstrated a wide range of phenomena, including the emergence of new electronic bands, novel transport properties, and unusual optical properties. Furthermore, these studies have also identified a number of challenges that need to be addressed to fully realize the potential of Moiré superlattices based on twisted TMD heterostructures. Finally, we offer a perspective on the future research directions and potential applications of Moiré superlattices based on twisted TMD heterostructures. We highlight the potential for developing novel electronic and optical devices, such as ultrafast transistors, valleytronics, and quantum emitters, and identify the need for further studies to understand the underlying physics and to address the challenges associated with the fabrication and characterization of these structures. Overall, this review highlights the recent progress in Moiré superlattices based on twisted TMD heterostructures and provides a roadmap for future research in this exciting field. We believe that these Moiré superlattices have the potential to revolutionize electronic and optical devices, and we anticipate many exciting discoveries in the future. Figure 1 summarizes the topics covered in this review.

1.1 Overview of Moiré superlattices and their applications

The word "Moiré" derives from the French term for a certain type of watered textile pattern, often seen in silk and taffeta fabrics. This pattern is characterized by its wavy, rippled appearance,

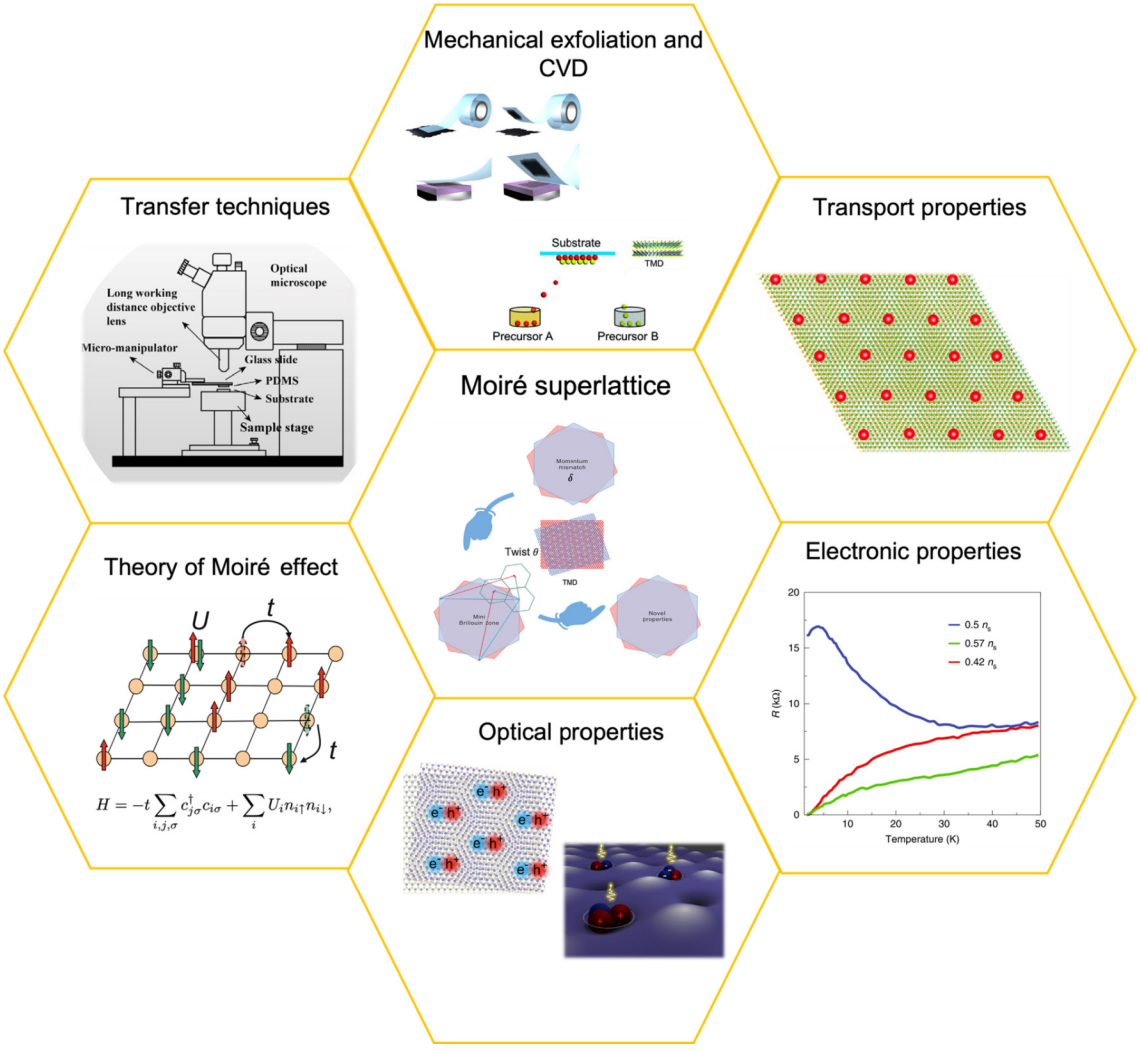


Figure 1 Schematic overview of the review topics, highlighting fabrication methods such as mechanical exfoliation, CVD, transfer techniques, and the unique characteristics of TMDs Moiré superlattices. Reproduced with permission from Refs. [6, 14–21], © Elsevier Inc. 2020, © Wiley-VCH GmbH 2023, © American Chemical Society 2023, © Tsinghua University Press and Springer-Verlag GmbH Germany, part of Springer Nature 2021, © Wang, L. et al. under exclusive licence to Springer Nature Limited 2020, © Springer Nature Limited 2021, © Wang, X. et al. under exclusive licence to Springer Nature Limited 2021, © Regan, E. C. et al. under exclusive licence to Springer Nature Limited 2020, and © Yamada, S. et al. 2018, respectively.

reminiscent of the way light dances on the surface of water. The term has been adopted in various fields to describe similar patterns or phenomena. In condensed matter physics, the concept of a Moiré pattern or Moiré superlattice has taken on a particular significance. Moiré superlattices are artificial structures, artificially crafted by stacking two layers of 2D materials with a slight twist angle (θ) relative to each other in both homostructures and heterostructures, or with a lattice mismatch (θ) for heterostructures [22] as shown in Figs. 2(a) and 2(b) [23] respectively.

This manipulation creates a periodic modulation in the electronic and optical properties of the combined material, giving rise to new phenomena and potential applications. When studying layered materials, the Moiré lattice constant, denoted by λ_m, plays a key role. It is influenced by two main factors: θ, which measures how the layers are rotated, especially compared to common positions like 0° or 60° in hexagonal patterns, and δ, which captures the differences in their lattice structures [24, 25]. These two factors (θ and δ) come together in the following Eq. (1)

$$\lambda_m = \frac{(1+\Delta)\,a}{\sqrt{2\,(1+\Delta)\,[1-\cos(\theta)]+\Delta^2}} \quad (1)$$

where λ_m is the Moiré lattice constant, δ is the lattice mismatch, θ is the twist angle, and a signifies the lattice constant for one of the combined layers. Moiré superlattices typically range from tens to hundreds of nanometers in dimension. Such variations often correlate with slight alterations in twist angle or minimal inconsistencies in lattice arrangements. The size of the Moiré pattern is inversely dependent on the twist angle between the two layers. When the twist angle is large (like 15°), the mismatch between the lattices is also large, resulting in a smaller Moiré pattern. Conversely, when the twist angle is smaller (like 5°), the lattices are more closely aligned, creating a larger Moiré pattern [26].

The superlattice can have properties that are distinct from those of the individual layers. Initially, twisted layers were investigated mostly through theoretical calculations, with experimental progress being limited due to poorly controlled samples [27–29]. In 2018, Cao et al. demonstrated the concept of graphene superlattices, famously recognized as the magic-angle phenomenon ($\theta \approx 1°$), through their experimentation with twisted bilayer graphene (TBG). This breakthrough not only showcased the existence of correlated insulators [30] and unconventional superconductivity [31] (see Fig. 2(h)) but also set the stage for future developments in other twisted 2D systems [32–41]. Notably, their work has paved the way for the exploration of TMD based twisted heterostructures as potential candidates for similar studies [17, 20, 42–45]. It is believed that flat bands can be observed in both graphene and TMDs, indicating a promising area for future research. Noval characteristics are enabled by flat bands in both magic-angle TBG (MATBG) and twisted TMD heterostructures. Graphene and TMD heterostructures are both quintessential examples of 2D materials that exhibit fascinating electronic properties due to their reduced dimensionality and unique band structures. One of the notable phenomena observed in these materials is the formation of flat bands, which can lead to a variety of interesting physical effects, including correlated electron behavior and potential superconductivity. In twisted bilayer graphene, when two graphene layers are stacked with a slight rotational misalignment, the resulting Moiré pattern creates a periodic potential that can significantly alter the electronic band structure. At certain "magic angles", this periodic potential flattens the electronic bands near the Fermi level, resulting in high density of states and strong electron correlations. This has been experimentally observed and theoretically predicted, leading to discoveries such as superconductivity and correlated insulating states in TBG [27, 30–32]. Similarly, in twisted TMDs, the stacking of two TMD layers with a twist angle can also create Moiré superlattices. These superlattices induce periodic potentials that modify the electronic band structure, potentially leading to

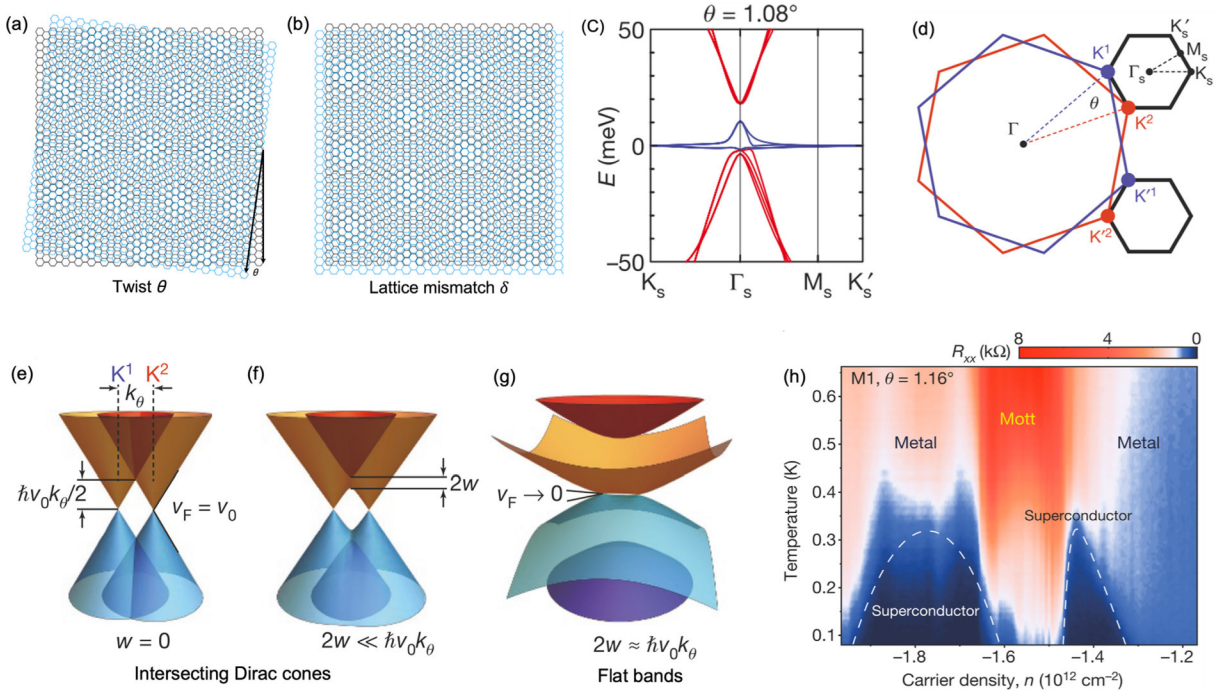


Figure 2 (a) Schematic illustration depicting Moiré patterns emerging from a distinct twist angle. (b) Schematic illustration showing Moiré patterns resulting from disparate lattice misalignments. Reproduced with permission from Ref. [23], © Elsevier Ltd. 2023. (c) Band energy diagram (E) highlighting flat bands (in blue) in TBG at the magic angle (θ = 1.08°). (d) Illustration showing the difference between the two K (or K') wavevectors, forming the mini-Brillouin zone in TBG. (e)–(g) Visualization of intersecting Dirac cones and flat bands in TBG due to the influence of interlayer hybridization. Reproduced with permission from Ref. [30], © Macmillan Publishers Limited, part of Springer Nature 2018. (h) Temperature-dependent four-probe resistances R_{xx} of TBG Moiré superlattice at magic-angle revealing two superconducting domes. Reproduced with permission from Ref. [31], © Macmillan Publishers Limited, part of Springer Nature 2018.

the formation of flat bands [42, 43, 46, 47]. Recent studies have shown that flat bands can emerge in twisted TMDs, analogous to the behavior observed in twisted bilayer graphene. For example, twisted homobilayer WSe_2 have been found to exhibit flat band physics, leading to enhanced electron–electron interactions and novel correlated states [17]. The observation of flat bands in both graphene and TMDs underscores the similarities in their electronic structures despite differences in their material composition. The ability to tune the electronic properties through twisting and stacking opens up new avenues for exploring strongly correlated phenomena and potential applications in electronic and optoelectronic devices.

Correlated electronic phases have been intriguingly observed in TBG, even though monolayer graphene, by itself, does not exhibit any such correlated phenomena. A compelling explanation for this behavior is provided by the Bistritzer-MacDonald model [27]. According to their model, the fermi velocity of the electronic states vanishes at a particular "magic angle" denoted by θ. To understand the emergence of these correlated phases in TBG, it is paramount to focus on its low-energy electronic structure. As depicted in Fig. 2(d), the two Dirac cones correspond to each of the graphene layers, layer 1 and layer 2. This scenario is further visualized in Fig. 2(e), where the Dirac cones are separated by a momentum, the magnitude of which is determined by the twist angle θ. Notably, the cones intersect at certain points. The introduction of interlayer hybridization can transform these intersections into potential energy gaps, as highlighted in Fig. 2(f). At a critically tuned angle, the strength of the interlayer tunneling precisely matches the separation between the Dirac cones, leading to the formation of exceptionally flat electronic bands as shown in Fig. 2(g). It is this flattening of the bands that paves the way for the manifestation of the correlated physics observed in both TBG and Twisted TMDs.

The potential of TMDs for exhibiting correlated properties akin to TBG has been under theoretical scrutiny [42, 43, 46–48]. Wang et al. presented observable, tunable correlated phases in twisted bilayer WSe_2. Specifically, correlated insulator and potential superconductivity phases were noted at twist angles (θ) of 4°–5.1° and temperatures under 3 K [17]. These findings elevate twisted bilayer TMDs as a crucial platform for delving into 2D correlated physics within a triangular lattice, underscoring the versatility of TMDs in exploring new quantum states. The tunability of correlated phases in twisted bilayer WSe_2 suggests that precise control over twist angles and temperature conditions can be pivotal for realizing desired electronic states. Future research should also explore the integration of TMDs with other 2D materials to discover novel properties and functionalities. Such advancements could pave the way for significant breakthroughs in quantum computing and advanced electronic applications. Additionally, understanding the interplay between different degrees of freedom, such as spin, valley, and layer pseudospins, is crucial for harnessing the full potential of these materials.

Moiré superlattices possess distinctive properties that find applications across various fields. They provide a dynamic platform for quantum simulations, enabling researchers to explore complex quantum phenomena [18, 49–51]. The altered band structures of Moiré superlattices hold promise for photonics and optoelectronics, contributing to the development of advanced LEDs, lasers, and photodetectors [25, 52–55]. A notable application is the modulation of band structures in 2D layered materials, introducing a myriad of novel properties and applications. This modulation creates strong coupling in Moiré superlattices, forming flat minibands that enhance electronic interactions and generate strongly correlated states [56]. Such advancements have catalyzed developments like quantum emission arrays, low-energy flat bands, and Mott insulators, garnering interest in optoelectronics, materials science, and energy research [25]. Moreover, the global structural periodicity and symmetry inherent in Moiré superlattices have practical implications for engineering 2D materials [7]. Building on these advancements, the dynamic tunability of Moiré superlattices makes them particularly well-suited for valleytronics and quantum information processing. Future research should focus on refining these parameters and exploring other TMD combinations to expand the range of observable phenomena. Integrating these materials with other 2D systems could lead to the discovery of novel functionalities and enhance device performance. Exploring new combinations of TMDs with 2D magnetic materials, for instance, could yield interesting results in terms of magnetic properties and spintronics applications. Advancements in understanding and manipulating these correlated phases could lead to significant breakthroughs in quantum computing and advanced electronic applications.

The discovery of superconductivity in certain Moiré systems hints at innovative superconducting materials [17, 31, 57–60]. This discovery not only opens up possibilities for developing new superconductors but also demonstrates the ability of Moiré superlattices to manipulate electronic properties at a fundamental level. Beyond superconductivity, Moiré superlattices have emerged as a promising platform for quantum emission applications, providing a controlled environment for the generation and manipulation of quantum light sources. Furthermore, the controlled twisting of van der Waals homostructures at specific angles, combined with strain manipulation, facilitates the fine adjustment of electronic properties. This capability lays a robust foundation for two-dimensional electronic and optoelectronic applications [61]. For instance, the precise tuning of the band structure in these systems enables the design of novel electronic devices with tailored functionalities. Moiré superlattices also play a crucial role in modulating the band structure of 2D layered materials, offering a new realm of properties and applications [6]. This modulation can lead to the emergence of new quantum phases and enhance the performance of devices in fields such as photodetectors, transistors, and sensors. Beyond practical applications, these superlattices are reshaping fundamental physics by aiding in the understanding of correlated electron systems and topological phases. The study of these phenomena not only advances theoretical physics but also informs the development of new materials and technologies. Moreover, the interdisciplinary nature of Moiré superlattice research brings together concepts from quantum mechanics, materials science, and electrical engineering. This convergence fosters innovation, as insights from one field can drive advancements in another. For example, understanding the quantum mechanical behavior of electrons in Moiré patterns can lead to the development of highly sensitive sensors and advanced communication technologies. The ability to design materials with specific electronic properties also has implications for energy storage and conversion, highlighting the broad impact of Moiré superlattice research on future technological developments.

In essence, Moiré superlattices bridge advanced research with technological advancements in condensed matter physics. Their ability to influence electronic properties, enable new quantum phenomena, and support diverse applications illustrates the interconnected nature of their impact on both fundamental science and practical technology.

1.2 Twisted transition metal dichalcogenide heterostructures

The inception of "twistronics" has profoundly impacted 2D

materials science, emphasizing lattice orientation's pivotal role in modulating electronic and optical properties [62–64]. Pioneering insights from studies on TBG [30, 31] have catalyzed a wave of investigations into twisted TMDs. Recognized for their broad spectrum of electronic and optical characteristics, TMDs have long been integral to the progress of 2D materials research. TMDs are a family of semiconducting materials composed of layers of transition metal atoms (such as molybdenum or tungsten) sandwiched between layers of chalcogen atoms (such as sulfur or selenium). By stacking two TMD layers with a twist angle, a Moiré pattern is formed that can dramatically alter the electronic band characteristics and optical behaviors of the material. When a layer of homobilayer TMDs (MX_2-MX_2, with M representing Mo or W and X being S, Se, or Te) or heterobilayer TMDs (MX_2-MY_2, where M stands for Mo or W, and X/Y signifies S, Se, or Te, ensuring X is not equal to Y) undergoes a twist or lattice mismatch, it gives rise to pronounced periodic structures resembling Moiré superlattices [65]. Such configurations are often referred to as twisted Moiré TMDs.

Although research into TMD Moiré systems began more recently than research into TBG, TMD Moiré systems have quickly attracted significant interest in both experimental and theoretical studies due to their various advantages over TBG. Unlike TBG, twisted TMDs do not exhibit a singular magic angle. Instead, they feature a "magic continuum", a range of angles that foster correlated electronic behaviors. This continuum of angles represents a broader regime in which correlated physics can be observed [17], marking a significant departure from the discrete magic angle characteristic of TBG. Furthermore, the practicality of applying a tight-binding model to semiconducting TMD Moiré systems is well-established, making these structures particularly apt for studies in the realm of Hubbard model physics[42, 44].

Additionally, many TMD materials possess the property of being direct-bandgap semiconductors, known for their strong light-matter interaction [66]. Owing to this trait, a variety of well-known optical techniques, including photoluminescence, reflectance spectroscopy, and ultrafast spectroscopy, can be effectively utilized to probe electronic correlations and analyze many-body effects in Moiré superlattices made from TMDs. Moreover, TMD monolayers are distinguished by their significant spin-orbit interactions and the availability of a wide range of materials [65]. This combination enables enhanced control over various properties, such as the degree of electron degeneracy, the symmetry of the crystal lattice, and the characteristics of the Moiré potentials [67]. Such control facilitates a dynamic interplay among multiple variables, potentially leading to a richer spectrum of interaction phenomena and unveiling new and fascinating aspects of physics. This makes TMD monolayers a versatile and valuable area of study in material science and condensed matter physics.

One of the most remarkable features of twisted TMD heterostructures is the emergence of new electronic states near the Fermi level that arise due to the coupling between the Moiré pattern and the underlying electronic structure of the TMD layers. These states are often described as "flat bands" [42, 43, 46, 68–70] because they are extremely narrow and have a nearly constant energy over a large range of momenta. Flat bands are of great interest because they can exhibit strong electronic correlations and can potentially lead to unconventional superconductivity [17, 71] or other exotic phases of matter such as generalized Wigner crystals [20, 44], Mott insulating state [20], stripe phases [72].

In addition to their fundamental physics, twisted TMD heterostructures also have potential applications in a variety of electronic and optoelectronic devices. For instance, the narrow bandwidth of the flat bands can enhance the performance of transistors and other electronic devices by reducing scattering and improving carrier mobility. The strong coupling between the Moiré pattern and light can also lead to novel optical phenomena, such as strong photoluminescence and valley-selective optical transitions. Overall, twisted TMD heterostructures represent a fascinating and rapidly developing field of research with a wide range of potential applications in electronics, optoelectronics, and quantum technologies.

2 Fabrication of twisted TMD heterostructures

The breakthrough in fabricating twisted TMD heterostructures represents a significant milestone, seamlessly integrating with the crafting of Moiré superlattices. Together these advancements offer a transformative approach to manipulating electronic and optical phenomena at the nanoscale.

2.1 Mechanical exfoliation and transfer techniques

Mechanical exfoliation, often referred to as the "Scotch tape method", epitomizes the "top–down" approach in 2D materials science due to its straightforward yet effective strategy in peeling off layers from bulk materials. This technique has been pivotal in the preparation of 2D crystals, especially following the groundbreaking isolation of graphene, which marked a significant advancement in the study of 2D materials [73].

The efficacy of this method in isolating graphene has subsequently led to its widespread application across a variety of other 2D materials, including TMDs, h-BN, and more. Figure 3(a) demonstrates the typical steps involved in the mechanical exfoliation method: first, a piece of Scotch tape is applied to the surface of a bulk 2D material, and then used to peel off thin layers from it. This process is repeated multiple times, gradually obtaining thinner layers until atomically thin, often single-layer sheets of the material are isolated.

The pristine nature of the materials obtained via mechanical exfoliation has been instrumental in advancing our understanding of their fundamental properties and behaviors. Recognized for its simplicity and cost-effectiveness, the mechanical exfoliation method offers significant accessibility for research applications, particularly for procuring high-quality, defect-free materials.

Despite these benefits, the method has notable limitations concerning scalability, and the control over the thickness and size of the resultant flakes. Recent developments have addressed these limitations enhancing yield, flake size, and consistency. Methods such as gold (Au)-assisted [74–79] (see Fig. 3(b)) and silver (Ag)-assisted exfoliation (see Fig. 3(c)) [80–82] have efficiently separated 2D layers, overcoming traditional method shortcomings.

In the realm of TMDs, the exfoliation of monolayers represents a crucial step in the fabrication of complex twisted heterostructures. Exfoliation of these materials can be performed using different mechanical methods or by employing chemical vapor deposition (CVD). Once obtained, these monolayers can be used to fabricate Moiré superlattices using common techniques reported in literature such as wet and dry transfer. Sections 2.1.1 and 2.1.2 will provide an overview of these transfer techniques, focusing on wet and dry transfer methods, respectively.

While these methods differ, they typically rely on similar dedicated experimental setup involving an optical inspection system with a long working distance, coupled with precision micro positioning systems, often including three-axis micro positioners and rotational stages [84] (see Fig. 4(a)). These tools are critical for achieving sub-micrometer precision in lateral positioning and rotational accuracy to less than 1°. Such precision

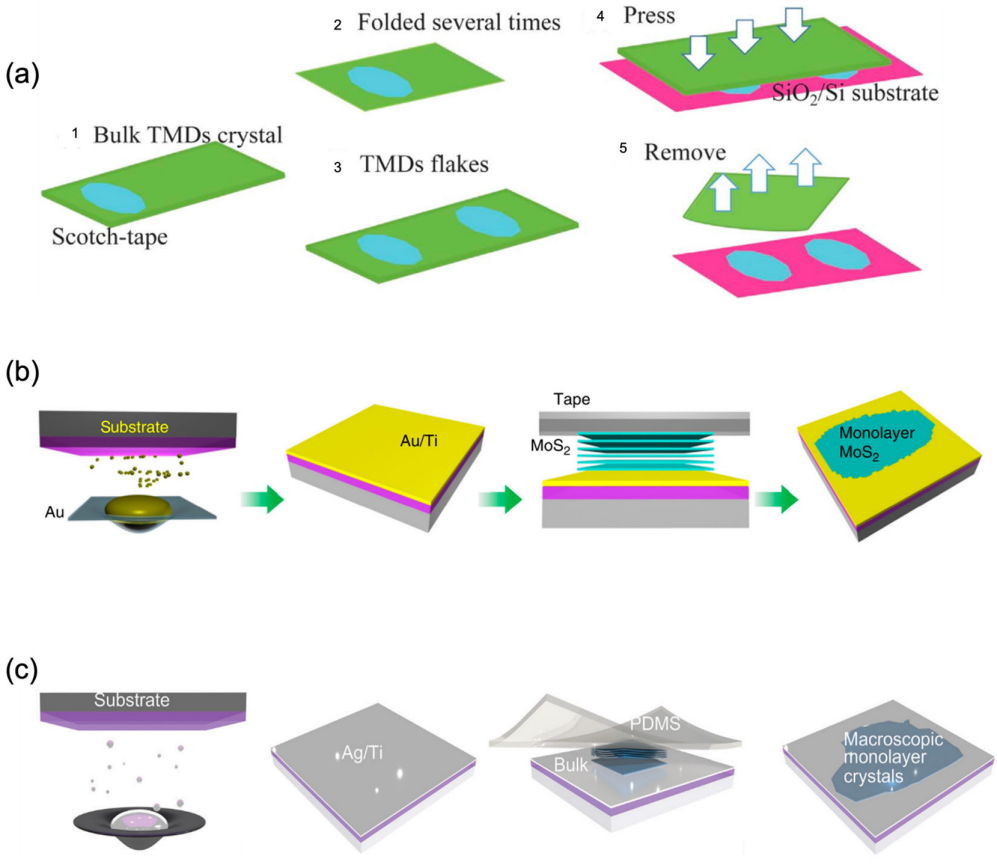


Figure 3 Schematic depiction of different methods for exfoliating TMD monolayers: (a) Mechanical exfoliation using scotch-tape. Reproduced with permission from Ref. [83], © Li, Y. G. et al. 2022. (b) Au-assited exfolaition. Reproduced with permission from Ref. [77], © Huang, Y. et al. 2020. (c) Ag-assisted exfoliation. Reproduced with permission from Ref. [81], © Fu, Q. et al. 2022.

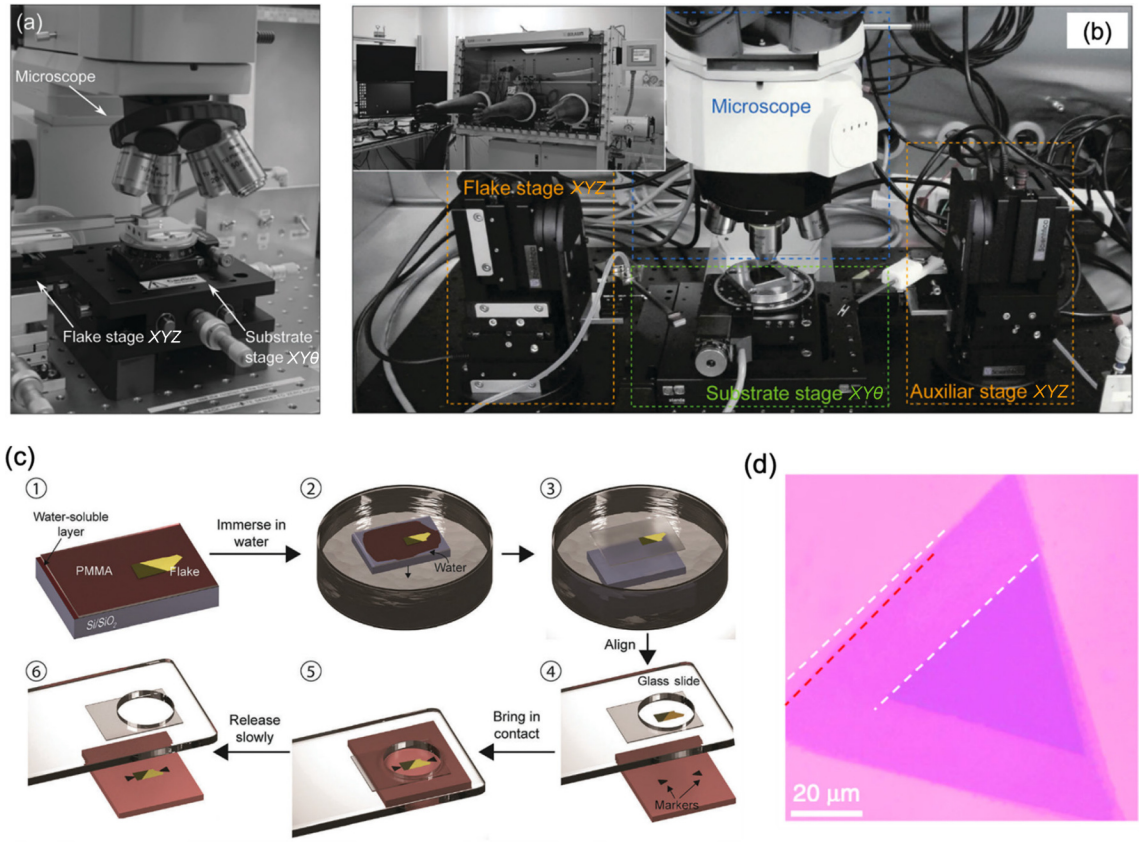


Figure 4 Wet transfer technique. (a) Experimental arrangement depicting a precise transfer mechanism, utilizing an optical microscope equipped with objectives optimized for extended working distances. (b) Experimental setup enclosed within a glove box to ensure consistent environmental conditions during the entire transfer operation. (c) Schematic illustration detailing the step-by-step procedure for a wet transfer technique. Reproduced with permission from Ref. [84], © Royal Society of Chemistry 2018. (d) Optical image showcasing a twisted heterostructure fabricated using the wet-transfer technique. Reproduced with permission from Ref. [56], © Zheng, H. H. et al. 2023.

is essential for manipulating the delicate TMD flakes, ensuring their accurate placement and orientation, especially when constructing layers with a user-defined twist angle [85–87].

Furthermore, installing this setup in controlled environments such as gloveboxes can help reduce contamination and enhance the uniformity of transfer processes (see Fig. 4(b)). This standardized experimental framework underscores the converging practices in the assembly of TMD heterostructures, emphasizing the shared focus on precision and control across different fabrication techniques in this advanced field of materials science.

2.1.1 *Wet transfer technique:*

The pioneering wet transfer technique, also known as the poly methyl methacrylate (PMMA) transfer method, was developed by Dean et al. in 2010. This method begins with the systematic preparation of a Si/SiO_2 substrate. Initially, the substrate is coated with a water-soluble polymer and then overlaid with PMMA. Subsequently, a target flake, characterized by its atomic thinness, is delicately exfoliated onto this dual-layer substrate.

The key step in this method involves immersing the substrate in water, which dissolves the underlying water-soluble polymer while leaving the PMMA layer, now carrying the ultra-thin flake, floating on the water surface. The next critical procedure is the careful retrieval of this PMMA layer, with the attached flake, using a glass slide equipped with a three-axis micromanipulator. This allows for precise alignment with the intended target substrate.

The final phase of the method entails placing the PMMA, with the flake facing downwards, onto the designated substrate. The PMMA is subsequently removed, typically by immersion in acetone, completing the heterostructure. Figure 4(c) visually represents this step-by-step process. Over time, this method has evolved, with modifications aimed at reducing contamination risks by eliminating the use of water solvents [88–93]. This technique has been effectively applied in the fabrication of TMDC Moiré superlattices. For instance, Zheng et al. successfully fabricated a Moiré heterotrilayer of $WSe_2/WS_2/WSe_2$, using a wet-transfer technique incorporating PMMA [56] (see Fig. 4(d)). This method is widely used due to its effectiveness in creating high-quality heterostructures, despite the challenges associated with potential contamination

2.1.2 *Dry transfer technique*

The wet transfer technique is notably susceptible to contamination due to its reliance on wet chemistry. Addressing this concern, Castellanos-Gomez et al. pioneered an all-dry transfer method [94]. This innovative approach introduces the use of polydimethylsiloxane (PDMS) stamps, a type of viscoelastic material, which significantly reduces contamination risks inherent in traditional wet transfer techniques. Illustrated in Fig. 5(a), this method outlines a sophisticated procedure for precisely placing atomically thin crystals onto a specific substrate. Initially, these crystals are mechanically separated and identified on a silicon dioxide/silicon substrate. A PDMS stamp, known for its ability to conform flexibly and adhere due to its viscoelastic properties, is then carefully positioned over the substrate. This precise alignment is achieved using a lever-arm mechanism, where the stamp, attached to a glass slide, is maneuvered into place over the target area with the aid of an optical microscope for enhanced accuracy. The PDMS stamp's capacity to conform to the substrate and crystals ensures secure capture of the flakes. During the removal process, the stamp is lifted from the original substrate with precision. By gently peeling it away while adjusting the height of the glass slide, the flakes are deposited onto the designated substrate. This technique not only enables precise positioning of the flakes but also leverages PDMS's unique properties to assemble twisted Moiré heterostructures, showcasing a delicate balance between accuracy and meticulous manipulation in crafting layered configurations. Over time, numerous variations of this original method have emerged [91, 95–98]. This technique has been effectively employed in the fabrication of TMDC Moiré superlattices. For example, Dai et al. [99] successfully fabricated a twisted WSe_2 homogeneous structures by using dry transfer method (see Figs. 5(b)–5(d)).

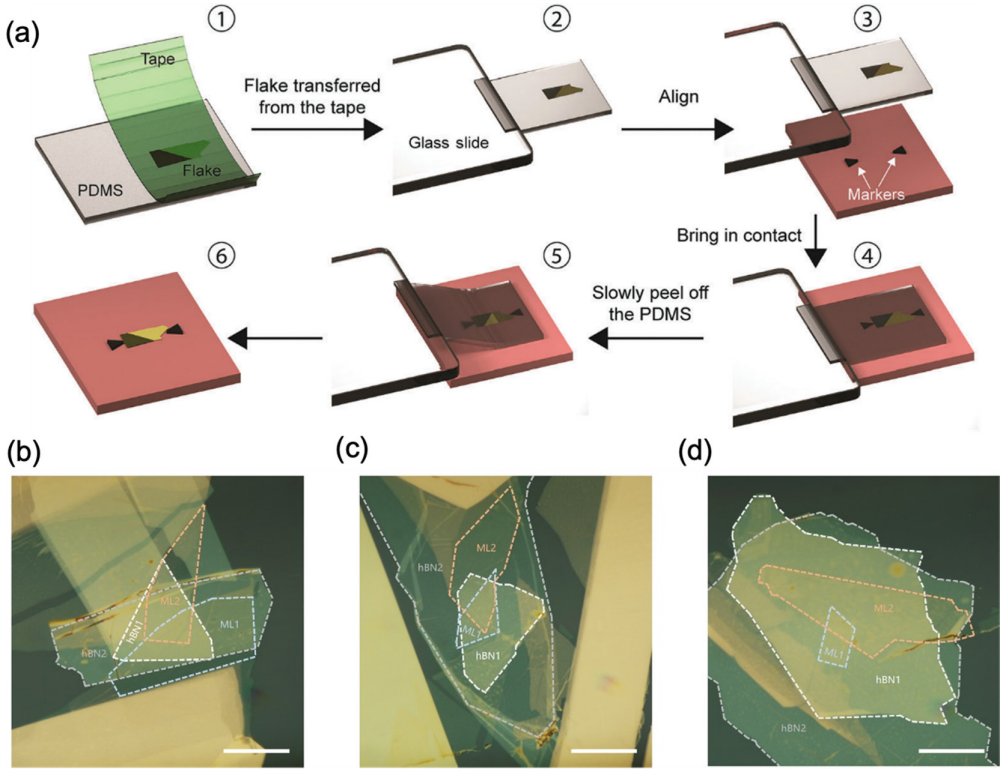


Figure 5 Dry transfer technique. (a) Schematic representation of the dry transfer technique. Reproduced with permission from Ref. [94], © IOP Publishing Ltd. 2014. Optical microscopy images showing twisted bilayer WSe_2 samples rotated at angles of (b) 1.1°, (c) 5.5°, and (d) 13.8°, with a scale bar represents 20 μm. Reproduced with permission from Ref. [99], © Dai, Y. C. et al. 2023.

2.2 Chemical vapor deposition

CVD is a sophisticated bottom-up fabrication method that enables the direct construction of Moiré superlattices without the need for transfer processes, offering a significant advantage over conventional methods [100]. Eliminating transfer processes is pivotal as traditional methods, which rely on mechanical layer transfer, can introduce contaminants such as dust particles and induce strains and defects that compromise superlattice performance. In contrast, CVD facilitates the *in-situ* growth of Moiré superlattices, ensuring pristine integration directly onto the substrate. This approach not only guarantees higher material quality and device reliability but also simplifies the fabrication process, reducing both complexity and cost. By bypassing mechanical transfer, CVD preserves intrinsic material properties like electrical conductivity and mechanical strength, providing a cleaner, more efficient pathway to developing high-performance material systems. This makes CVD an invaluable technique in materials science, driving advances in device engineering and scientific exploration by efficiently and cost-effectively producing pristine Moiré superlattices.

Zhang et al. [101] developed an innovative sequential thermal CVD technique to enable robust epitaxial fabrication of monolayer lateral heterostructures, multi-heterostructures, and superlattices (Figs. 6(a) and 6(b)). Sahoo et al. [102] introduced a one-pot growth or a single-step CVD synthesis approach for the *in-situ* fabrication of TMD lateral superlattices. Besides lateral

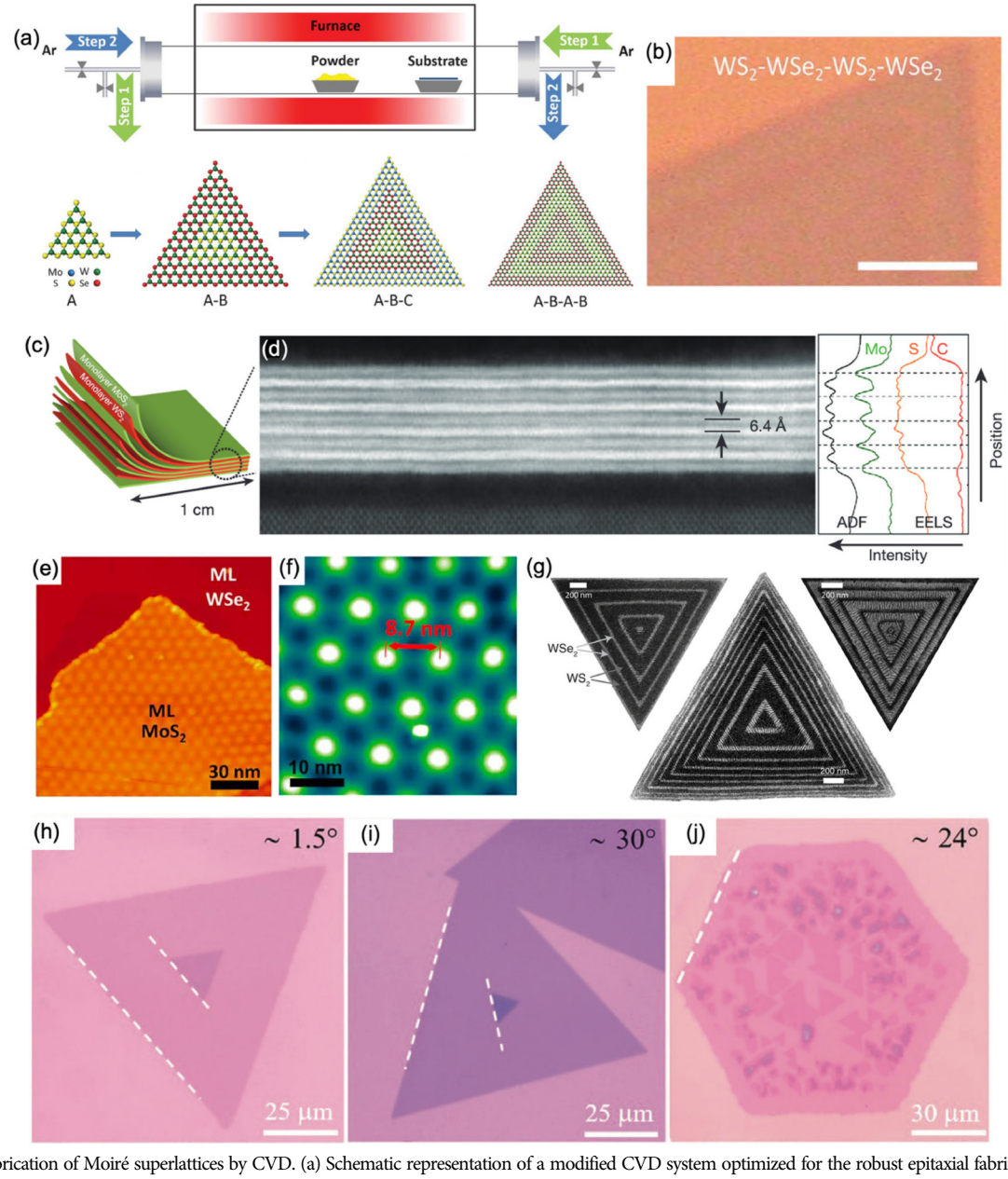


Figure 6 Fabrication of Moiré superlattices by CVD. (a) Schematic representation of a modified CVD system optimized for the robust epitaxial fabrication of lateral heterostructures. (b) Microscopic optical image showing a superlattice of WS_2 and WSe_2 layers on a SiO_2/Si substrate. Reproduced with permission from Ref. [101], © Zhang, Z. W. et al. 2017. (c) Schematic illustration of a superlattice composed of vertically stacked MoS_2/WS_2 layers. (d) ADF STEM image of a superlattice film on a SiO_2/Si substrate (left). The bright and dark regions correspond to WS_2 and MoS_2 layers, respectively, with the Si crystal lattice visible at the bottom. Intensity profiles obtained from the ADF STEM image and EELS mapping in the out-of-plane direction are shown (right): black (ADF STEM), green (EELS for Mo), orange (EELS for S), and red (EELS for C). Reproduced with permission from Ref. [103], © Macmillan Publishers Limited, part of Springer Nature 2017. (e) STM image of a MoS_2/WSe_2 van dar Waals heterostructure on HOPG substrate. (f) Zoomed-in STM image revealing the hexagonal Moiré pattern with a periodicity of 8.7 nm. Reproduced with permission from Ref. [104], © Zhang, C. D. et al. 2017. (g) SEM images showing three monolayer WS_2/WSe_2 superlattices. Scale bars, 200 nm. Reproduced with permission from Ref. [109], © Xie, S. E. et al. 2018. (h)–(j) Optical microscopy images depicting as-grown twisted bilayer homostructures with a twist angle of approximately 1.5°, 30°, and 24°; scale bars: 25 and 30 μm. Reproduced with permission from Ref. [112], © Wiley-VCH GmbH 2023.

superlattices, Kang et al. [103] introduced a modified CVD method, specifically the programmed vacuum stack (PVS) process, to fabricate vertically stacked TMD superlattices (Figs. 6(c) and 6(d)). Zhang et al. [104] fabricated a vertically stacked Moiré superlattice of WSe_2/MoS_2 (Fig. 6(e)), featuring a Moiré pattern with a lattice constant of 8.7 ± 0.2 nm (Fig. 6(f)), using a developed two-step CVD method [105, 106]. Yuan et al. [107] also synthesized vertically stacked WS_2/WSe_2 heterostructures via a modified two-step CVD method. TMD Moiré superlattices can also be synthesized through modulated metal-organic chemical vapor deposition (MOCVD). This variant of the traditional MOCVD technique [108] enables layer-by-layer deposition. Xie et al. [109] synthesized a WS_2/WSe_2 superlattice (Fig. 6(g)) using MOCVD. Jin et al. [110] reported the direct growth of TMD superlattice using MOCVD. In a recent study, Zhou et al. [111] developed an approach to directly synthesize Moiré superlattices by combining CVD with plasma treatment on highly ordered pyrolytic graphite (HOPG) substrates. Additionally, Zheng et al. [112] fabricated WSe_2/WSe_2 Moiré superlattices with different twist angles using CVD, employing a heteroatom-assisted growth technique for synthesis (Figs. 6(h)–6(j)).

2.3 Other methods

In addition to the fabrication techniques discussed earlier in this review, the "tear-and-stack" method represents another pivotal approach for synthesizing Moiré superlattices. This method is characterized by its capability to produce bilayer systems with precisely controlled twist angles, a feature that has enabled meticulous control over the twist angle itself. Since its introduction by Kim et al. [113], the "tear-and-stack" method has gained increasing underscoring its role in exploring new physical phenomena. The ability of the method to create bilayer systems with well-defined twist angles has been effectively leveraged, particularly in the fabrication of TBG [30, 31, 114], highlighting its utility and impact. Subsequently, the technique has been applied to twisted TMDs, showcasing its versatility and broad applicability in the study of two-dimensional materials. For example, Andersen et al. [115] fabricated the twisted WSe_2/WSe_2 homobilayers using tear-and-stack technique, Wu et al. [116] employed the method to fabricate twisted double-bilayer WSe_2 Moiré superlattices. Another cutting-edge method, the van der Waals assembly technique, developed by Wang et al. [117], stands out as a cornerstone in Moiré superlattice fabrication. This approach delicately layers materials with such precision that it unveils entirely new properties, akin to uncovering a hidden layer of reality at the nanoscale. For instance, Xu et al. [118] utilized the method to fabricate a Moiré superlattice composed of WSe_2 and WS_2 layers, with a near-zero twist angle.

To provide a comprehensive overview, the advantages and disadvantages of various methods for fabricating twisted TMD heterostructures have been compared. The overall benefits and limitations of current fabrication techniques for TMD Moiré superlattices are summarized in Table 1.

Following the comparison of various fabrication methods for twisted TMD heterostructures, it is crucial to highlight the ongoing trends and future directions in this field. Advances in nanotechnology and materials science are pushing towards more precise and controllable fabrication techniques. Methods like dry transfer and tear and stack are being refined to allow for even finer control over the alignment and thickness of layers, which is essential for the reproducibility and scalability of high-quality heterostructures. CVD is gaining traction due to its scalability and ability to produce uniform films over large areas. Research is focused on reducing the cost and complexity of CVD setups to make this method more accessible for large-scale production [119–121]. Both wet and dry transfer methods are being improved to minimize contamination and defects during the transfer process. Innovations in cleaner transfer techniques and better handling protocols are critical to achieving high-performance TMD heterostructures. There is a growing trend towards integrating these fabrication methods with other advanced technologies such as atomic layer deposition (ALD) and molecular beam epitaxy (MBE) to create hybrid structures with enhanced properties. For instance, van der Waals epitaxy combining ALD and MBE has shown promising results in synthesizing high-quality 2D materials with controlled properties [122, 123]. Additionally, the automation of fabrication processes and the application of machine learning algorithms for process optimization are emerging trends. These technologies aim to enhance the efficiency and consistency of fabrication methods, thereby accelerating the development of next-generation TMD heterostructures. Recent studies have shown the potential of using machine learning to predict optimal conditions for material growth and to automate the intricate processes involved in fabrication [124–127]. By addressing these trends, we can better understand the future landscape of TMD heterostructure fabrication and guide ongoing research and development efforts towards the most promising directions.

3 Theoretical background of the Moiré effect

The investigation of TMDs Moiré superlattices has emerged as a central focus in condensed matter physics and materials science, driven by their unique electronic, optical, and mechanical properties. The dynamic interplay between the Moiré effect and the intrinsic characteristics of TMDs opens avenues for revolutionary applications in nanoelectronics, optoelectronics, and quantum information technologies. The development of Moiré superlattices is significantly driven by the synergy between theoretical predictions and experimental validations. Both theoretical and experimental research methods are crucial in advancing our understanding of these complex systems, as they mutually inform and guide each other. One prominent example is

Table 1 Comparison of TMDs Moiré superlattices fabrication methods

Method	Advantages	Disadvantages
Wet transfer	High quality of transferred layers; compatible with a wide range of materials	Potential contamination from solvents; difficult to control thickness and alignment
Dry transfer	Cleaner process with less contamination; better control over alignment and thickness	Requires precise handling and equipment; limited to certain material combinations
CVD	Scalable for large area production; produces high-quality, uniform films	High temperatures required; complex and costly setup
Tear and stack	Allows for precise control of angle and stacking order; versatile for various material systems	Time-consuming; requires high precision and can be technically challenging
Van der Waals assembly technique	Enables construction of high-quality heterostructures; flexibility in material choice	Labor-intensive; requires advanced equipment and techniques for precise assembly

the prediction and experimental observation of flat bands in Moiré superlattices. Theoretical studies predicted that TBG at a "magic angle" would result in flat electronic bands, leading to correlated electronic states such as superconductivity and Mott insulating behavior [27]. Experimental studies subsequently confirmed these predictions by fabricating TBG with precise control over the twist angle and measuring the electronic properties that matched the theoretical predictions [30, 31]. Similar to TBG, theoretical studies on TMD homo- and heterostructures predicted the presence of flat bands [42, 43, 46, 47] capable of supporting emergent electronic phases. Based on these theoretical predictions, experimental observations have demonstrated a correlated insulating state and the potential for a transition to a superconducting state in twisted bilayer WSe_2 [17]. Another example is that, unlike graphene, TMDs exhibit reduced degeneracy due to coupled spin and valley degrees of freedom, along with unique material properties such as strong spin-orbit coupling. These characteristics indicate that twisted bilayer TMDs could exemplify a solid-state single-band Hubbard model on a triangular lattice, where various correlated states may emerge [42]. Based on these theoretical predictions, Tang et al. [44] experimentally simulated Hubbard model physics in TMDs [42] for WSe_2/WS_2 Moiré superlattices [44].

Another significant area of study is Moiré excitons in TMD heterostructures. Recent theoretical predictions have indicated that Moiré superlattices could exhibit Moiré excitons, which are excitonic states modulated by the periodic potential of the Moiré pattern [128–130]. Experimental research has validated these predictions, demonstrating Moiré excitons in WSe_2/WS_2 heterostructures [131]. These experiments revealed that Moiré excitons have lifetimes significantly longer than those observed in traditional monolayer or bilayer TMDs without Moiré patterns, highlighting their potential for various optoelectronic and quantum information applications. These examples illustrate how theoretical predictions guide experimental efforts, and experimental findings, in turn, refine and validate theoretical models. This iterative process accelerates the development of Moiré superlattices and opens new avenues for research and technological applications. This section further delves into the theoretical underpinnings of the Moiré effect as applied to TMDs Moiré superlattices.

3.1 Basic principles of the Moiré effect

The Moiré effect occurs when two periodic structures are overlaid with a slight misalignment or twist. In TMDs Moiré superlattices, this effect arises when layers of TMDs are stacked with rotational misalignment or different lattice constants [49, 118]. This misalignment creates a larger periodic pattern known as the Moiré pattern, profoundly influencing the electronic band structure and localized states within the material. The unique properties of these Moiré superlattices are influenced by several factors, including the twist angle between layers, which determines the periodicity and scale of the Moiré pattern. Smaller twist angles result in larger superlattices that can more effectively localize electrons and enhance interaction effects. Additionally, the stacking configuration, whether AA stacking with direct atom alignment or AB stacking where atoms of one layer sit atop the hollow spaces of the other, plays a crucial role in defining the electronic properties of the superlattice. Moreover, the combination of TMD materials (e.g., MoS_2/WS_2 or $MoSe_2/WSe_2$) leads to diverse electronic and optical properties due to differences in band alignment and interlayer coupling strength, highlighting the complex nature of Moiré superlattices.

Theoretical findings by Wu et al. [42] demonstrate that achieving flat electronic bands in TMDs Moiré superlattices does not necessarily require a specific "magic angle". Through their theoretical investigation, they show that twisted heterobilayers of TMDs exhibit distinct flat Moiré bands described by generalized triangular lattice Hubbard models. They illustrate how parameters such as hopping and interaction strengths within the Hubbard model can be finely tuned by adjusting structural factors like the twist angle and environmental conditions like the dielectric environment. Their study focuses on Moiré band Hamiltonians for holes in twisted heterobilayers, specifically $WSe_2/MoSe_2$ combinations (Fig. 7(b)), which display a pair of low-energy valence bands aligned with the chemical potential (Fig. 7(a)). They emphasize that if the twist angle remains below 3.5°, a Moiré pattern forms with a lattice constant of approximately 6 nm, the initial Moiré sub-bands exhibit flat characteristics (Fig. 7(c)). Furthermore, the periodic potential, bandwidth, and interaction energies within these Moiré superlattices are highly adaptable, theoretically positioning them as effective quantum simulators for various complex models, including the Hubbard models [42, 46, 132, 133], Kane-Mele models [46, 134, 135], and Kondo lattice models [136], among others.

3.2 Mathematical modeling of Moiré superlattices

Moiré patterns emerge from the overlay of two distinct periodic structures. In quantum mechanics and condensed matter physics, the Hamiltonian describes the total energy of a system. Constructing a Hamiltonian that incorporates the periodic potential of each layer, along with their relative displacement and twist angle, is a foundational approach for understanding the energy dynamics of electrons of electrons in Moiré superlattices. Wu et al. [42] present numerical calculations of $\Delta(d)$ for the AA-aligned $WSe_2/MoSe_2$ bilayer as depicted in Fig. 7(b). When the bilayer is twisted ($\theta \neq 0$), resulting in a Moiré pattern, the local parameter d undergoes gradual changes across the Moiré period (a_M). Simultaneously, the maximum of the valence band, acting as a spin-neutral external potential, mirrors the spatial fluctuations of d, showing periodic variations. The Moiré band Hamiltonian obtained is

$$\mathcal{H} = -\frac{\hbar Q^2}{2m^*} + \Delta(r) \tag{2}$$

$$\Delta(r) = \sum_b V(b) \exp[ib \cdot r] \tag{3}$$

The terms $-\hbar Q^2/(2m^*)$ and $\Delta(r)$ represents the kinetic and potential energy components within the Moiré band. The potential $\Delta(r)$, depicted in Fig. 7(d), can be effectively approximated using a Fourier series expansion [36]. Furthermore, Angeli et al. [137] have developed a continuum model Hamiltonian to characterize the miniband structures emerging within the valence bands of Γ-valley bilayers due to slight rotational misalignment between the layers. Through advanced ab initio calculations, they have formulated a model that accurately describes the band structure of these bilayer systems. The simplified single-band $k{\cdot}p$ Hamiltonian is as follows

$$\mathcal{H} = -\frac{\hbar^2 k^2}{2m^*} + \Delta(d) \tag{4}$$

Here, m^* represents the effective mass of the particle, and $\Delta(d)$ is the potential that holes experience at the valence band. This potential shift depending on the in-plane displacement d between the two layers. A small twist angle θ leads to an interlayer displacement d that varies gradually with the spatial position r, given by $\mathrm{d}(r) = \theta\hat{z} \times r$. Substituting d with r in Eq. (3) preserves the

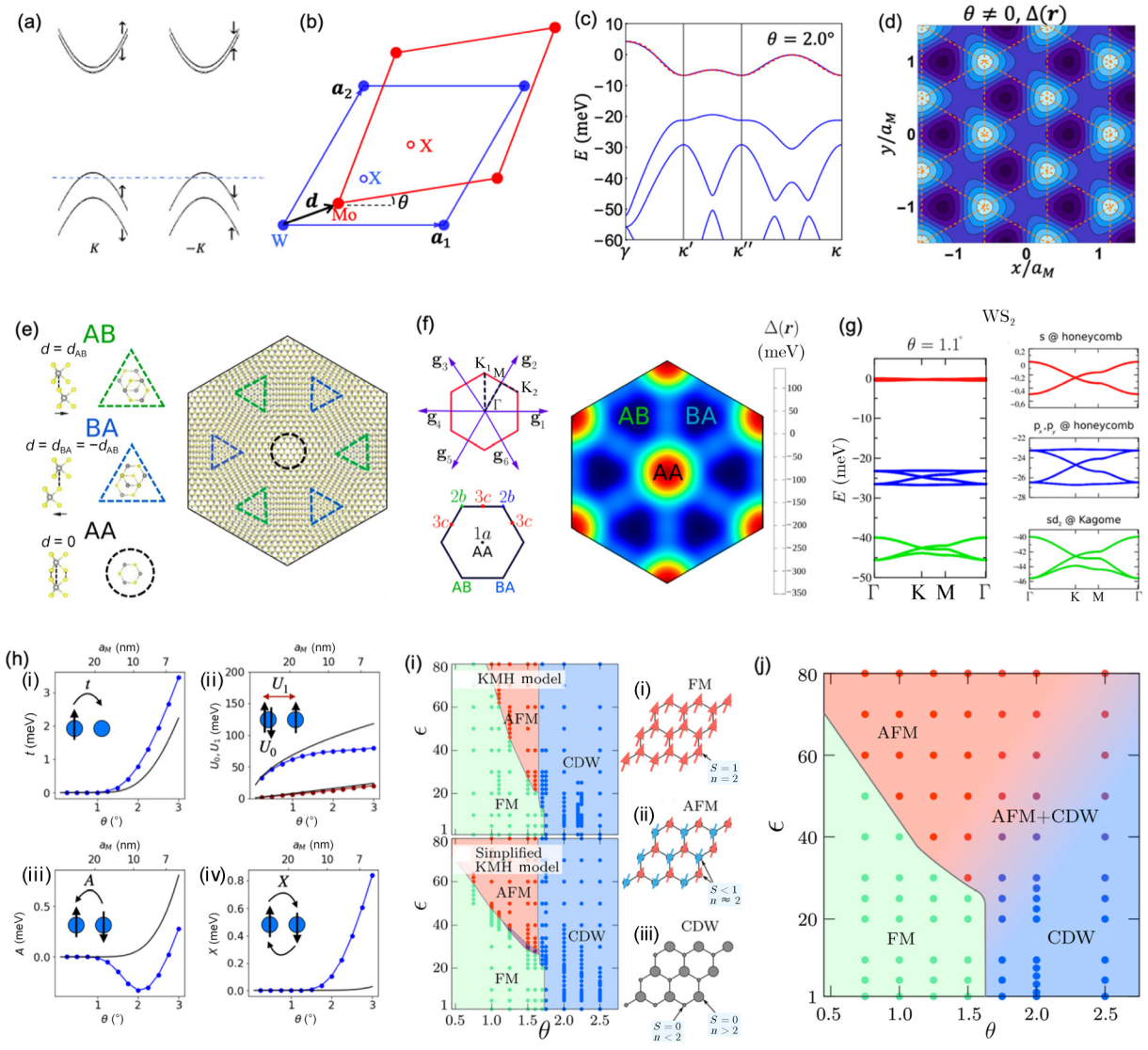


Figure 7 Mathematical modeling of Moiré superlattices. (a) Schematic band structure of monolayer WSe_2 with pronounced spin-splitting at valence band extrema (large) and conduction band extrema (small) situated at the $\pm K$ valleys. (b) schematic depiction of AA stacked WX_2/MoX_2 bilayers with an additional in-plane displacement d and a twist angle θ. a_1 and a_2 represents primitive translation vectors of WX_2. (c) Moiré bands at twist angle $\theta = 2.0°$. The red dashed line denotes a tight-binding-model fit to the highest valence band, incorporating hopping up to the third nearest neighbor. (d) Amplification of band maximum variation from atomic to Moiré pattern scale upon Moiré pattern formation. The orange dashed lines indicate near-neighbor links connecting $\Delta(r)$ maxima. Reproduced with permission from Ref. [42], © American Physical Society 2018. (e) Three high-symmetry configurations in β homobilayers: AB, BA, and AA. The right panel illustrates the Moiré pattern formed in a $\theta = 3.15°$ β homobilayer. Bernal stacked regions, forming a honeycomb lattice, are denoted by green and blue triangles, and the AA region is indicated by a black circle. (f) Schematic illustration of the first shell ($S = 1$) of Moiré reciprocal lattice vectors used for expanding the Moiré potential and the maximal Wyckoff positions. The right panel displays the Moiré potential $\Delta(r)$ for MoS_2, effective for holes on the hexagonal network formed by the AB/BA regions. (g) Band structure of WS_2 with a twist angle of 1.1°. (Top right) The first band set with a bandwidth of approximately 0.5 meV, is formed by s orbitals on a honeycomb lattice. (Middle right) The second band set, with a bandwidth of ≈ 3.2 meV, formed by $p_x \pm ip_y$ orbitals on the honeycomb. (Bottom right) The third set of bands, with a bandwidth a bandwidth of ≈ 5.75 meV, is formed by hybridized sd^2 orbitals on a kagome lattice, has. Reproduced with permission from Ref. [137], © National Academy of Sciences 2021. (h) Comparison between harmonic approximation (solid black lines) and exact continuum model results (lines with dots) for (i) hopping, (ii) on-site (blue) and first-neighbor (dark red) interactions, (iii) assisted hopping, and (iv) intersite exchange interactions. Interaction parameters are plotted against twist angle (bottom axes) and Moiré length (top axes). Insets provide schematic illustrations of each process. Reproduced with permission from Ref. [133], © American Physical Society 2022. (i) phase diagrams of effective dielectric constant ε vs. twist angle θ for the full Kanamori-Moiré Hubbard (KMH) model and the simplified KMH model, both constructed via unrestricted Hartree-Fock. Panels (i), (ii), and (iii) depict ferromagnetic (FM), antiferromagnetic (AFM), and charge density wave (CDW) states, respectively. The small violet regions in the simplified KMH model correspond to non-collinear and non-coplanar phases. (j) Phase diagram of the effective dielectric constant ε versus twist angle θ for the simplified KMH model, obtained using the Lanczos technique. Reproduced with permission from Ref. [141], © American Physical Society 2023.

symmetry of the potential and amplifies the positional values, resulting in a Moiré potential characterized by the subsequent Fourier series expansion

$$\Delta(r) = \sum_{S}\sum_{j=1}^{6} V_S \exp(i g_j^S \cdot r + \phi_S) \quad (5)$$

Here, $g_{j+1}^S = C_{6\mathbb{Z}} g_j^S$ represents $\mathbb{Z}$ the s-th shell of six Moiré wave vectors organized by their ascending magnitudes $|g|$ (Fig 7(f)). The phase factor ϕ_S are constrained by the hexagonal $C_{6\mathbb{Z}}$ symmetry, allowing them to assume values of either zero or π [137].

Their findings indicate that the moiré pattern serves as a long-wavelength modulation potential, which introduces a sixfold rotational symmetry absent in the original lattice structure. This modulating potential serves to narrow the bandwidth of hole bands, effectively localizing electrons or holes at sites corresponding to honeycomb or kagome lattices (Fig. 7(g)). Unlike graphene, twisted TMDs can adopt two specific

configurations, α and β, distinguished by 180° rotation of the top layer along the metal axis. Figure 7(e) illustrates a β twisted bilayer configuration where AA-stacked regions from a triangular lattice, surrounded by six Bernal-stacked regions, creating a comprehensive honeycomb pattern. The efficacy of their continuum model is demonstrated by its ability to predict the band structure of twisted TMDs, particularly at twist angles where a complete microscopic analysis is impractical (Fig. 7(g)).

Moreover, employing a projection technique [138–140], Durán et al. [133] obtained Wannier functions for holes localized at sites within TMDs Moiré superlattice. These functions served as the basis for calculating parameters in a generalized Hubbard model. The derived parameters supported the establishment of a low-energy spin model that accounts for strong interaction strengths at filling factor $\nu = 1$. The study also notes that at smaller twist angles or larger Moiré lattice constants, Wannier orbitals can be well approximated by eigenstates of harmonic potentials, justifying an on-site Hubbard model representation. Additionally, significant non-local interactions in TMDs Moiré materials influence electronic properties, potentially leading to Moiré Mott-Hubbard ferromagnets. These interactions become more pronounced with larger twist angles and weaker Moiré modulation, validating the approach used. (see Fig. 7(h)).

The continuum model proposed by Wu et al. [46] represents a sophisticated framework for describing the electronic properties of twisted bilayer systems. This model, based on an effective mass approximation, accurately simulates the formation of Moiré bands arising from periodic variations in the potential caused by the Moiré pattern. Furthermore, their continuum model provides insights into the Kane-Mele model for TMDs. Key aspects of the Hamiltonian in this model, particularly for the ±K valley bands, include the spatial modulation of interlayer tunneling, $\Delta_T(r)$, and layer-dependent potentials, $\Delta_{1,2}(r)$.

$$\mathcal{H}_{\downarrow} = \begin{pmatrix} -\frac{\hbar^2(k-\kappa_+)^2}{2m^*} + \Delta_1(r) & \Delta_T(r) \\ \Delta_T^{\dagger}(r) & -\frac{\hbar^2(k-\kappa_-)^2}{2m^*} + \Delta_2(r) \end{pmatrix} \quad (6)$$

The continuum model approach is particularly suited for scenarios involving slight rotational discrepancies between layers, resulting in Moiré patterns with sufficiently large wavelengths.

In a recent study, Kaushal et al. [141], uncovered that twisted TMD homobilayers can exhibit behaviors predicted by the multi-orbital Hubbard model within a Moiré honeycomb lattice, through a combination of *ab-initio* calculations and continuum modeling. This investigation has led to the development of the Kanamori-Moiré-Hubbard model, an advanced framework that incorporates complex electron interactions. By employing Wannierization for detailed electronic structure analysis, along with unrestricted Hartree-Fock and Lanczos methods to explore half-filled Moiré bands, the study unveils a diverse range of quantum states, including antiferromagnetic, spin-1 ferromagnetic insulator, and charge density wave states (see Figs. 7(i) and 7(j)). This research not only advances the understanding of many-body physics in twisted TMD homobilayers but also establishes a groundwork for future experimental investigations, representing a significant leap forward in the mathematical modeling of Moiré superlattices and the study of condensed matter physics.

3.3 Density functional theory (DFT) calculations

DFT calculations have emerged as a crucial tool for unraveling the intricate electronic behaviors of twisted TMDs Moiré superlattices. Given the complex interplay of atomic arrangements and electronic interactions in these materials, DFT provides a comprehensive framework for predicting and analyzing their electronic structures and related properties. This section explores the foundational principles of DFT calculations applied to TMDs Moiré superlattices, highlighting key discoveries and insights that have significantly advanced our understanding in this field.

In the exploration of electronic properties and structural transformations in Moiré superlattices based on twisted TMD heterostructures, DFT calculations play a pivotal role. A seminal work by Naik et al. [43] explores the complexities of twisted bilayer MoS_2, (Figs. 8(a) and 8(b)), reveling the formation of ultraflat bands, depicted in Fig. 8(c), and shear solitons, shown in Fig. 8(d), at the valence band edge.

These phenomena are fundamental to understanding electronic interactions in these heterostructures. Shear solitons, localized distortions within the crystal lattice that move without altering their shape, significantly influence the structural dynamics of these systems. Through extensive DFT analyses, the study not only underscores the profound impact of structural transformations on electronic structure but also extends these implications to other TMDs, such as WS_2, $MoSe_2$, and WSe_2. This broad applicability underscores the generality of Moiré-induced phenomena across different TMD materials, offering valuable insights on the uniformity and variability of electronic properties within these complex systems. Detailed investigations into atomic relaxations and their effects on the localization of flat bands provide essential foundations for understanding the exotic electronic phases that Moiré superlattices may exhibit. Consequently, insights garnered from their work are instrumental in advancing our comprehension of how DFT calculations elucidate the novel physical properties of twisted TMD heterostructures, marking a significant contribution to the field.

While DFT is adept at establishing the ground-state electronic structure of twisted TMD heterostructures, the exploration of optical phenomena in these materials, particularly the relationship between twist angle and excitonic properties, requires a more detailed approach. Integrating DFT with advanced computational techniques such as many-body perturbation theory (MBPT) bridges this gap. Specifically, methods like the GW approximation and the Bethe-Salpeter equation (GW-BSE) enable the exploration of excitonic states from the Moiré Brillouin zone (MBZ) to the unit-cell Brillouin Zone (UBZ), offering comprehensive insights into excitonic landscapes in Moiré superlattices. This combined approach not only deepens our understanding of ground-state properties illuminated by DFT but also provides insightful forays into excited-state dynamics critical for accurately characterizing optical responses. In the work by Kundu et al. [11], this methodology is applied to twisted $MoS_2/MoSe_2$ heterostructures, revealing how twist angle modulates excitonic properties and highlighting the potential of these heterostructures in optoelectronic applications. The study's findings (Figs. 8(e)–8(g)), underscore the pivotal role of both DFT and MBPT in elucidating the nuanced excitonic behaviors induced by Moiré patterns, representing a significant advancement in our understanding of TMD heterostructures.

However, exploring Moiré excitons in twisted heterostructures, quasi-particles indicative of bound states of electrons and holes influenced by their micro-environment, demands a more nuanced computational strategy beyond conventional DFT. Guo et al. [142] expend DFT's capabilities by incorporating time-dependent DFT (TDDFT) [143, 144] with optimally tuned range-separated hybrid functionals [145–148]. This methodological innovation allows for the direct study of Moiré excitons in twisted MoS_2/WS_2 heterostructures (see Fig. 8(h)), revealing their localized nature and how their properties are significantly influenced by twist angles and external electric fields. Through the advanced integration of DFT and TDDFT, this study not only deepens the

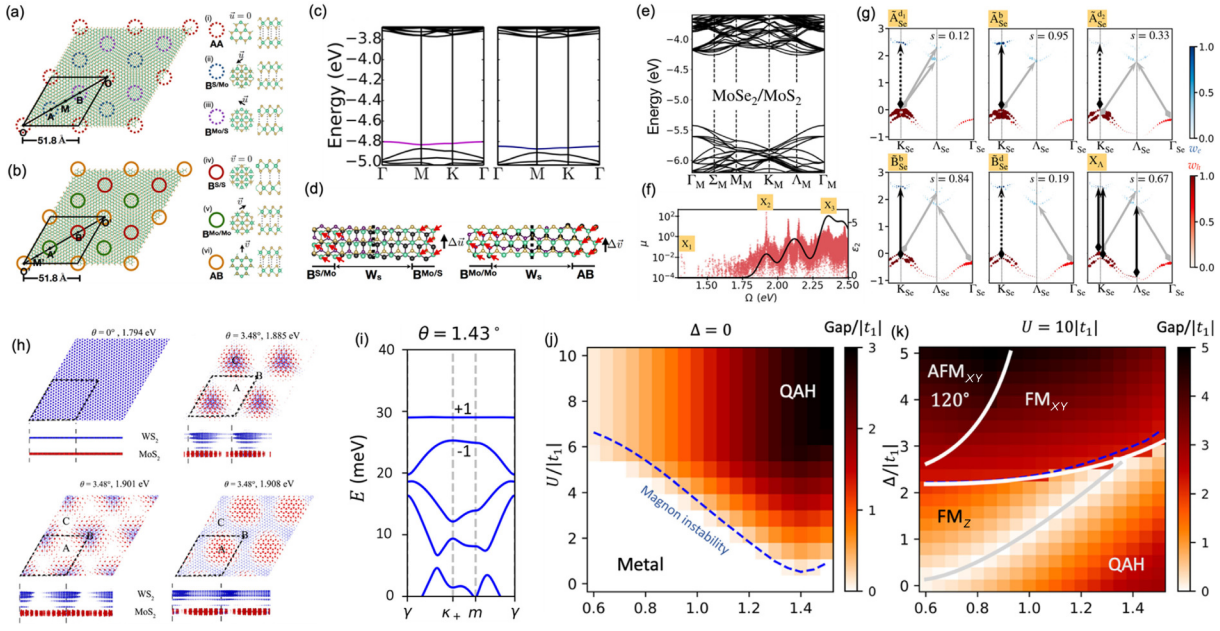


Figure 8 DFT calculations. (a) and (b) Moiré superlattice formed by twisting bilayer MoS_2 by 3.5° and 56.5°, respectively. High symmetry stackings are highlighted within circles. Stacking configurations within the circle is shown in (i)–(vi). The vectors $\vec{u}$ or $\vec{v}$denote the direction of the order parameter. (c) Illustration of flat bands near the valence band edge, depicted in magenta and blue colors, respectively. (d) Representation of shear-strain soliton between $B^{S/Mo}$ and $B^{Mo/S}$ stackings, and between AB and $B^{Mo/Mo}$, respectively. The width of the soliton is approximately 1.5 nm, denoted as Ws, while the red arrows represent the order parameter. Reproduced with permission from Ref. [43], © American Physical Society 2018. (e) DFT band structure of the 16° twisted $MoSe_2/MoS_2$ heterostructure in the MBZ. (f) Dipole matrix elements (μ) and the absorption spectrum ($\varepsilon 2$) of the heterostructure, shown as pink dots and a black line, respectively. Interlayer and intralayer exciton regions are marked. (g) GW band-resolved unfolded exciton contribution within the UBZ of $MoSe_2$. Red and blue colors denote hole and electron state contributions, respectively. Black arrows represent direct and optically bright (solid lines) or dark (dashed lines) transitions in the UBZ, while gray arrows indicate the additional momentum indirect contributions in the UBZ. "s" is the spin-allowed probability for direct transitions in the UBZ, averaged over all excitons within 10 meV around each marked state. Reproduced with permission from Ref. [11], © Kundu, S. et al. 2023. (h) Localized Moiré excitons in the twisted MoS_2/WS_2 heterostructure (θ = 3.48°). Charge density and energy for the lowest energy exciton in the MoS_2/WS_2 heterostructure with θ = 0° (upper panel, top view; bottom panel, side view). Charge density and for the three lowest-energy excitons with MoS_2/WS_2 heterostructure with θ = 3.48° (upper panel, top view; bottom panel, side view). The dashed box indicates the unit cell of the Moiré superlattice. Red and blue colors represent electron and hole charge densities, respectively. Reproduced with permission from Ref. [142], © American Chemical Society 2023. (i) Band dispersion in the continuum model, flattest at approximately 1.43°. (j) Phase diagram based on the twist angle and interaction strength U,with fixed displacement field (Δ = 0), or specified $U = 10|t_1|$. Insulating phases labeled QAH, FM_z, 120° AFM_{xy}, and FM_{xy}, are depicted. A blue dashed line marks the FM_z phase boundary, identified by the initial magnon instability. Colors indicate the charge gap. Reproduced with permission from Ref. [135], © Devakul, T. et al. 2021.

understanding of Moiré excitons but also demonstrates the evolving landscape of computational techniques designed to tackle the challenges presented by novel quantum materials.

The concept of the "magic angle", originally identified in TBG, extends intriguingly to twisted TMDs. In these materials, a specific small twist angle introduces flat bands, creating a fertile ground for electron localization and phenomena enhanced by interactions. Devakul et al. [135] leverage a combination of DFT calculations, continuum modeling, and the Hartree-Fock method to construct a solid theoretical framework for delving into the properties of twisted TMD homobilayers, particularly WSe_2, at twist angles less than 4°. Notably, at a specific angle of θ = 1.43° (see Fig. 8(i)), the top valence Moiré band becomes nearly flat. Near this angle, the study anticipate the emergence of a generalized Kane-Mele model characterized by a topological flat band alongside novel electronic states such as the Haldane insulator and Mott insulators (Figs. 8(j) and 8(k)).

The field of "twistronics" highlights how the relative rotation, or "twist", between two layers of TMDs can profoundly influence their electronic and optical properties by generating Moiré patterns. These patterns can significantly modify the material's band structure, leading to emergent properties such as unconventional superconductivity and topological conducting channels. Adjusting the twist angle allows precise control over band gaps, enabling phase transitions from direct to indirect bandgap semiconductors. This capability enhances the material's optical absorption in the visible spectrum, particularly advantageous for photovoltaic applications.

A recent study by Gupta et al. [149] investigates the intriguing domain of twisted TMD bilayers, including combinations of $MoSe_2/WSe_2$, MoS_2/WSe_2, WS_2/WSe_2, and $MoSe_2/WS_2$, employing DFT based first-principles calculations. Their investigation explores how twisting introduces a new array of electronic and optical properties that can be leveraged for various technological applications, such as solar cells and light-emitting diodes. These materials exhibit direct bandgap semiconductor characteristics coupled with high absorption coefficients, making them promising candidates for next-generation optoelectronic devices.

4 Electronic properties of Moiré superlattices

Investigating Moiré superlattices in twisted TMD heterostructures has uncovered new opportunities for modifying electronic features essential for the development of advanced electronic, optoelectronic, and quantum devices. This section highlights the significant advancements in understanding and tailoring the electronic properties of these complex structures. Through meticulous research and experimentation, scientists have identified the unique interactions within these superlattices that lead to groundbreaking electronic behaviors, opening the door to innovative applications and technologies. This enhanced understanding of the electronic dynamics within twisted TMD heterostructures represents a significant leap forward in the realms of materials science and nanotechnology.

4.1 Band structure engineering

The deliberate manipulation of a material's electronic band structure, which governs the range of energy levels available for electrons, represents a powerful tool for influencing its electronic, optical, and magnetic properties. This capability opens up new avenues for innovations in electronics, optoelectronics, and quantum computing devices. By precisely tailoring these energy levels, such as adjusting the bandgap, the energy difference between the valence band (where electrons are bound) and the conduction band (where electrons are free to move), materials can be transformed from insulators to metals or into semiconductors with specific conductivity characteristics.For instance, Wang et al. [17] have elucidated layered electronic phenomena of TMDs, focusing particularly on twisted bilayer WSe_2. Their research reveals the appearance of low-energy flat bands (see Fig. 9(a)), underscoring the pivotal role of Moiré superlattices in finely tuning electronic band structures. They also uncover a correlated insulator phase that can be precisely manipulated at half-band filling (see Fig. 9(b)). achieved through careful adjustments of the twist angle and application of a displacement field. This highlights the intricate balance between the material's structural configuration and its electronic properties.

Twisting a crystal structure fundamentally alters the atomic arrangement, influencing orbital hybridization. Such changes in orbital hybridization are crucial as they lead to shifts in the positions of the conduction band minimum (CBM) and valence band maximum (VBM) [62]. Gupta et al. [149], utilizing first-principles DFT calculations, demonstrate that by varying the twist angle between TMD layers, one can modulate the bandgaps, thereby facilitating transitions between direct and indirect bandgap semiconductors (see Fig. 9(c)).

Interlayer interactions also significantly impact the modification of electronic band structures. A study by Liu et al. highlights that the indirect bandgap in MoS_2 bilayers is notably influenced by the twist angle between layers, exhibiting significant variations across different stacking configurations [150]. For AA and AB-stacked bilayers, a pronounced redshift in the bandgap size is observed, contrasting with a smaller, more consistent redshift for bilayers with other twist angles (see Figs. 9(d) and 9(e)). This phenomenon is attributed to repulsive steric effects that alter interlayer separations depending on the stacking configuration, emphasizing the intricate relationship between structural arrangements and electronic properties in TMD heterostructures.

In the quest for advanced materials with customizable electronic properties, band gap engineering stands out as a crucial technique, especially for enhancing the optoelectronic capabilities of 2D materials. An influential exploration in this domain is carried out by Zhao et al. [151], explored the manipulation of band structures in TMDs superlattices. Their systematic computational study shows that by varying the composition and stacking order of TMDC superlattices, significant modifications in band behavior, such as indirect-to-direct band gap transitions and semiconductor-to-metal transitions, can be achieved (see Fig. 9(f)). This is particularly evidenced in their demonstration of how band offsets and in-plane strain from lattice mismatches contribute to these transitions, providing a comprehensive understanding of the underlying mechanisms at play.

4.2 Tuning of electronic properties via electric and magnetic fields

Beyond mechanical manipulation, external electric and magnetic fields offer additional means to tune the electronic properties of TMD-based Moiré superlattices. Applying an electric field

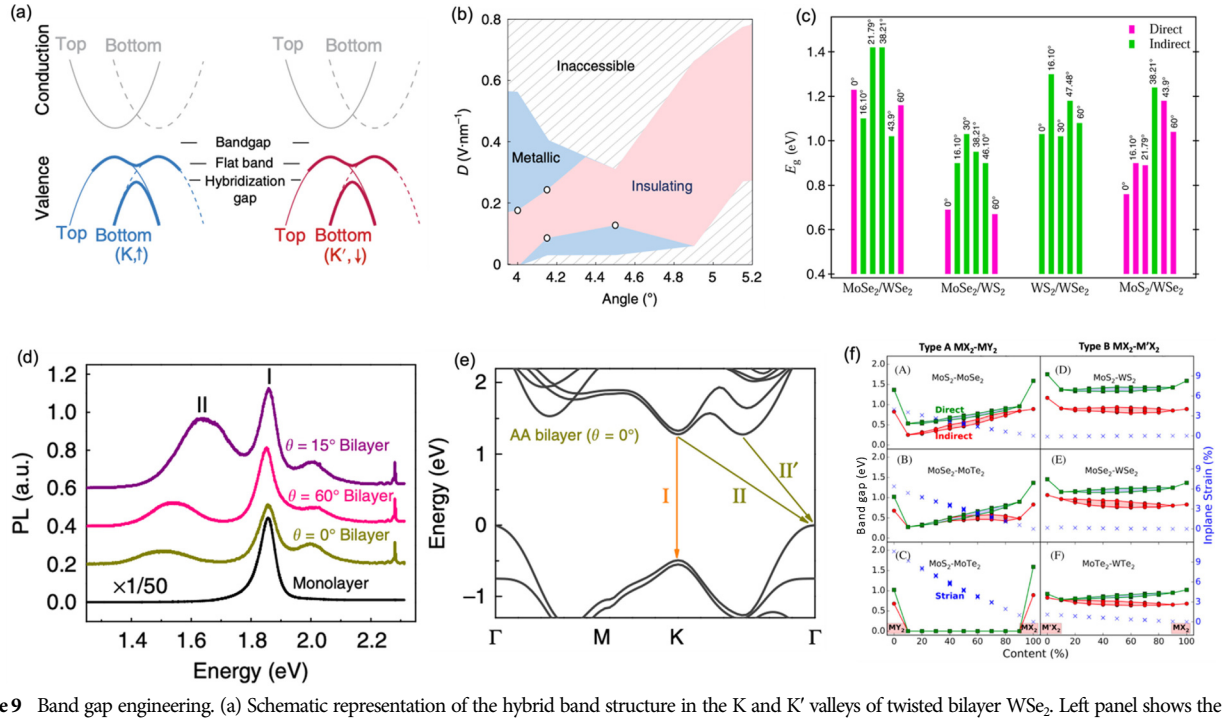


Figure 9 Band gap engineering. (a) Schematic representation of the hybrid band structure in the K and K′ valleys of twisted bilayer WSe_2. Left panel shows the spin-up configuration in the K valley, while the right panel shows the spin-down configuration in the K′ valley. (b) Phase diagram illustrating the influence of displacement field and twist angle on twisted bilayer WSe_2, delineating metallic and insulating states at half filling. Transition points from metal to insulator are marked by white circles. Reproduced with permission from Ref. [17], © Wang, L. et al. under exclusive licence to Springer Nature Limited 2020. (c) Modulation of bandgaps in $MoSe_2/WSe_2$, $MoSe_2/WS_2$, WS_2/WSe_2, and MoS_2/WSe_2 heterostructures at various twist angles. Reproduced with permission from Ref. [149], © Gupta, N. et al. 2024. (d) Photoluminescence (PL) emission spectra for monolayer and bilayer MoS_2 at twist angles of 0°, 15°, and 60°. (e) Correlation of PL emission peaks with direct bandgap transitions in MoS_2, with transitions labeled I and II'. Peaks I and II correspond to distinct energy levels observed in the PL spectra. Reproduced with permission from Ref. [150], © Liu, K. H. et al. 2014. (f) Band gap variations for type A and type B superlattices as a function of composition n, with indirect band gaps indicated by red circles and direct band gaps by green squares. In-plane strain relative to bulk MX_2 is depicted with blue crosses. Shaded regions represent band gap variability due to different stacking sequences. Reproduced with permission from Ref. [151], © Zhao, X. G. et al. 2020.

perpendicular to the layers can further modulate the band structure, enabling control over the charge carrier density and type (electrons or holes). This electric field effect facilitates the fine-tuning of the material's conductivity, work function, and can even induce superconductivity in some cases.

In the study by Wang et al. [17], the emergence of superconductivity within twisted bilayer WSe_2 was closely examined. Remarkably, upon fine-tuning the carrier concentration away from half-filling through the application of a displacement field, regions exhibiting zero resistance were detected at temperatures below 3 K, specifically at a twist angle of 5.1° (see Figs. 10(a) and 10(b)). This observation strongly suggests a transition to a superconducting state, highlighting the critical role of electric field-induced tuning in realizing superconductivity within engineered materials. The displacement field not only alters the band structure but also stabilizes correlated electronic states, creating conditions conducive for the emergence of the superconducting phase upon deviating from the half-filled insulating state. Li et al. [152] investigate the metal-insulator transition (MIT) in $MoTe_2/WSe_2$ semiconductor Moiré superlattices through the application of an out-of-plane electric field. Their findings reveal a continuous MIT at a critical juncture marked by one electron per unit cell, highlighting the ability to finely tune electronic interactions and achieve quantum criticality (see Fig. 10(c)). This transition is characterized by a diminishing charge gap, an increase in quasiparticle effective mass, and a gradual change in magnetic susceptibility, culminating in a magnetic-field-induced MIT showcased in Fig. 10(d). The findings demonstrate the significant role of electric fields in modulating electronic properties, providing insights into the manipulation of quantum states in two-dimensional materials. In the pioneering work by Xu et al. [118] unveiled a series of nearly two dozen correlated insulating states within WSe_2/WS_2 Moiré superlattices, observable at fractional electron or hole fillings (see Figs. 10(e) and 10(f)). A key breakthrough in this research is the development of a novel optical sensing technique that uses exciton excited states in monolayer WSe_2 as a sensitive probe to detect changes in the dielectric environment induced by these insulating states. This method allows for an unprecedented view into the Moiré superlattice's electronic properties without necessitating direct electrical contact, a significant advancement in the study of 2D materials.

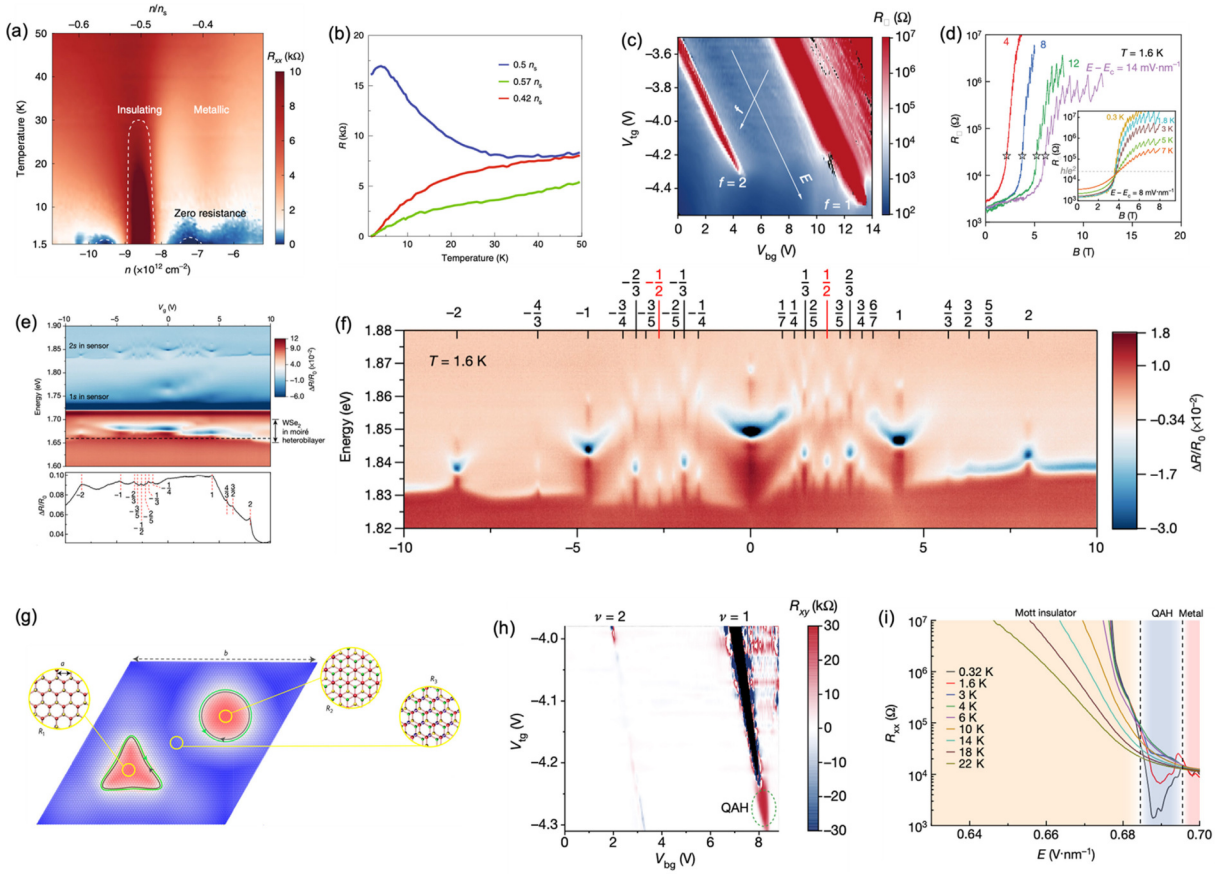


Figure 10 Electronic and topological properties. (a) Resistance as a function of temperature and density at a 5.1° twist angle and D = 0.45 V nm^{-1}, showing two instances of zero resistance indicative of superconductivity away from the insulating phase. (b) Resistance near half-filling densities illustrates insulating behavior starting at 35 K (blue) and transitioning to superconductivity (red and green) below 3 K. Reproduced with permission from Ref. [17], © Wang, L. et al. under exclusive licence to Springer Nature Limited 2020. (c) an electric-field induced MIT is detected at f = 1 and f = 2. (d) Magnetoresistance at various electric fields surpassing the critical electric field at 1.6 K. Inset shows magnetoresistance at different temperatures for one electric field, indicating a magnetic-field-induced MIT. Reproduced with permission from Ref. [152], © Li, T. X. et al. under exclusive licence to Springer Nature Limited 2021. (e) Gate-dependent reflection contrast spectrum of a WSe_2/WS_2 Moiré structure at 1.6 K (top) with a line-cut at 1.66 eV (black dashed line in bottom panel). The red dashed lines indicate the correlated insulating states shown in (f). (f) Blueshifts in the 2s exciton resonance, highlighted by the sensor in (e), reveal multiple insulating states and enhanced spectral intensity, with the top axis showing the corresponding filling factor. Reproduced with permission from Ref. [118], © Xu, Y. et al. under exclusive licence to Springer Nature Limited 2020. (g) Three locations (highlighted in yellow circles) within a Moiré supercell, where the length scale is significantly larger than the lattice constant a yet considerably smaller than the Moiré period b. Local atomic registries exhibit minimal deviation from commensurate TMD bilayers, with regions in the topological insulating phase (red) or normal insulating phase (blue). Grey and green colors represent expected spin up and spin down helical modes at the boundaries between the topological insulator (TI) and normal insulator (NI) phases. Reproduced with permission from Ref. [153], © Springer Nature Limited 2016. (h) Dashed lines encircle areas of a quantum anomalous Hall (QAH) insulator. Dark areas represent zones that are highly insulating and cannot be probed experimentally. (i) Three distinct regions identified as Mott insulator, QAH insulator, and metallic state, respectively. Reproduced with permission from Ref. [154], © Li, T. X. et al. under exclusive licence to Springer Nature Limited 2021.

4.3 Topological properties

The investigation into topological properties within TMDC Moiré superlattices represents a rapidly evolving field, where theoretical predictions and experimental discoveries continuously expand our knowledge of these intricate systems. The interplay of topology, electron correlations, and quantum geometry in these materials holds significant promise for uncovering novel physical phenomena and advancing next-generation electronic, photonic, and quantum technologies. A study by Tong et al. [153], Moiré superlattices formed from van der Waals heterobilayers of TMDs were found to host topological mosaics, characterized by a periodic modulation between topological insulator (TI) and normal insulator (NI) regions (see Fig. 10(g)). This phenomenon arises due to incommensurate stacking and/or lattice mismatch of two-dimensional atomic crystals, which can be dynamically tuned via interlayer bias, thereby enabling electrically switchable topological superstructures. Leveraging symmetry-based k·p and tight-binding models, the study predicts the emergence of topologically protected helical modes at the boundaries between TI and NI phases, opening new avenues for applications in quantum electronics and spintronics. A significant contribution by Li et al. [154] reveals the observation of the Quantum anomalous Hall (QAH) effect in AB-stacked $MoTe_2/WSe_2$ Moiré heterobilayers, demonstrating the profound interplay between electron correlation and band topology. The study identifies a quantized Hall resistance and vanishing longitudinal resistance at half-band filling ($\nu = 1$) under zero magnetic field, indicative of the QAH effect (see Fig. 10(h)). Moreover, it explores an electric-field-induced topological phase transition from a Mott insulator to a QAH insulator at $\nu = 1$, a phenomenon not accompanied by the closure of a bulk charge gap (see Fig. 10(i)). The subtle topological properties of TMDs Moiré superlattices not only deepen our understanding of quantum materials but also pave the way for groundbreaking applications in electronics, spintronics, and quantum computing, marking a transformative era in materials science.

5 Optical properties of Moiré superlattices

Moiré superlattices based on TMDs display distinctive optical phenomena arising from their periodic potential landscapes and the strong interactions between electronic and photonic states. This section delves into pivotal aspects such as excitonic effects and the amplification of light-matter interactions.

5.1 Excitonic effects

In recent years, significant experimental and theoretical advancements have enhanced our understanding of optically excited Moiré excitons in Moiré systems based on TMDs. In isolated TMD monolayers, optical spectra are primarily influenced by excitons, pairs of electrons and holes held together by Coulomb interactions. However, when two TMD monolayers are overlaid with a small angle or lattice mismatch, the periodic Moiré potential introduces new optical resonances beyond fundamental excitons, known as Moiré excitons (Fig. 11(a)). In conventional 2D semiconductors, excitons are mobile across the two-dimensional surface. In Moiré lattices, however, these excitons become confined, emitting light at energy minima within the potential landscape.

Experimental evidence of Moiré excitons has been reported in various TMD Moiré bilayers, such as WSe_2/WS_2 [131], $MoSe_2/WSe_2$ [155], and $WS_2/MoSe_2$ [156] as well as in trilayer configurations [56, 157, 158]. Moiré excitons encompass several

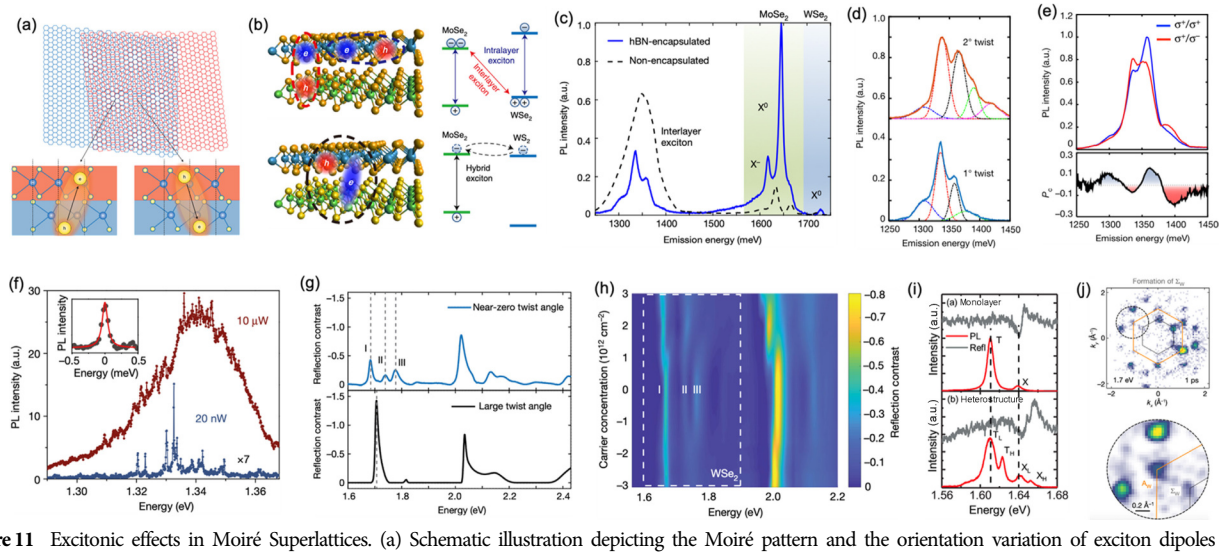


Figure 11 Excitonic effects in Moiré Superlattices. (a) Schematic illustration depicting the Moiré pattern and the orientation variation of exciton dipoles across different regions of a Moiré superlattice. Reproduced with permission from Ref. [179], © Springer Nature Limited 2020. (b) Spatial and energy diagrams for intralayer, interlayer, and hybrid excitons. Reproduced with permission from Ref. [180], © Springer Nature Limited 2022. (c) PL spectra illustrating differences between an uncapped heterostructure (dashed black curve) and an hBN-encapsulated heterostructure (solid blue curve). Emissions of neutral (X^0) and charged (X^-) excitons are observed in $MoSe_2$ and WSe_2 layers, respectively. Interlayer exciton emission appears approximately 300 meV below the intralayer exciton peaks. (d) PL spectra displayed for heterobilayers with twist angles of 1° (bottom) and 2° (top). Each spectrum is fitted with four (1°) or five (2°) Gaussian functions (dot-dashed lines). (e) Top panel: Circularly polarized PL spectrum under σ+ excitation of 1° sample in (d). Bottom panel: Degree of circular polarization as a function of emission wavelength, obtained from the spectra in the top panel. Reproduced with permission from Ref. [159], © Tran, K. et al. under exclusive licence to Springer Nature Limited 2019. (f) Interlayer exciton PL in a 2° twisted heterobilayer under 10 μW (dark red) and 20 nW (blue, amplified 7×) excitation. Inset: Lorentzian fit of PL peak shows ~ 100 μeV linewidth at 20 nW. Reproduced with permission from Ref. [160], © Seyler, K. L. et al. under exclusive licence to Springer Nature Limited 2019. (g) Reflection contrast spectrum of device D1 (light blue) compared to a WSe_2/WS_2 heterostructure with a large twist angle (black). The large twist shows a single WSe_2 A exciton peak (1.6–1.8 eV), while Moiré superlattice in device D1 exhibits three distinct Moiré exciton peaks (I to III). (h) Gate-tuned reflection contrast spectrum of device D1, illustrating electron and hole doping. The dashed box indicates the WSe_2 A exciton energy range, revealing three Moiré exciton states (I, II, III). Reproduced with permission from Ref. [131], © Jin, C. H. et al. under exclusive licence to Springer Nature Limited 2019. (i) PL and reflectivity spectra of $MoSe_2$ in monolayer (top) versus heterostructure (bottom). Reproduced with permission from Ref. [161], © American Chemical Society 2018. (j) Momentum fingerprint of the dark Σ_W exciton. Reproduced with permission from Ref. [171], © Schmitt, D. et al. under exclusive licence to Springer Nature Limited 2022.

types, including interlayer [131, 159, 160], intralayer [10, 161–163], and layer-hybridized excitons [164, 165], each distinguished by its unique interaction within the Moiré lattice (see Fig. 11(b)). For instance, Tran et al. [159] present compelling evidence of multiple interlayer exciton resonances with circularly polarized emission in hexagonal boron nitride (hBN) encapsulated $MoSe_2/WSe_2$ heterobilayers (Figs. 11(c)–11(e)). These resonances exhibit a systematic dependence on the twist angles and temperature, underscoring the complex relationship between structural configurations and optical properties in van der Waals heterostructures.

In Moiré lattices, excitons manifest as distinct peaks in photoluminescence and reflection spectra, indicating their confinement either at specific positions within the Moiré supercell or by spatial variations of the Moiré potential. Seyler et al. [160] demonstrate, for instance, that in twisted $MoSe_2/WSe_2$ heterobilayers, interlayer valley excitons are confined by a Moiré potential, evidenced by narrowed photoluminescence linewidths around 100 μeV at low temperatures (Fig. 11(f)), showcasing potential applications in excitonic devices [166–170]. Moreover, Jin et al. [131], observed Moiré exciton states within WSe_2/WS_2 heterostructure Moiré superlattices, where the A exciton resonance in WSe_2 splits into several peaks (Fig. 11(g)). revealing unique doping dependencies distinct from both WSe_2 monolayer A excitons and WSe_2/WS_2 heterostructures with large twist angles (Fig. 11(h)). Zhang et al. [161] reported the formation of intralayer excitons in a $MoSe_2/MoS_2$ heterostructure encapsulated in hBN, where the Moiré pattern splits the $MoSe_2$ exciton and trion in both emission and absorption spectra (Fig. 11(i)). These observations align with theoretical models, illustrating the profound influence of Moiré patterns on TMD heterostructure optical and electronic features [104, 128–130]. Furthermore, Alexeev et al. [164] observe hybrid Moiré excitons in $MoSe_2/WS_2$ heterostructures, demonstrating an interplay between inter- and intralayer Moiré excitons that induces significant energy level shifts, particularly in nearly aligned structures. Schmitt et al. [171] pioneer the observation of "dark" Moiré interlayer excitons (Σ_W) at the Σ valleys of the hexagonal Brillouin zones (Fig. 11(j)), employing femtosecond photoemission momentum microscopy with time-resolved Angle-resolved photo emission spectroscopy (ARPES). providing unprecedented insights into exciton dynamics and properties.

Moreover, experiments have also identified Moiré trions, bound states of Moiré excitons with additional charges, providing further insights into excitonic and electronic interactions within Moiré systems. These Moiré trions are influenced by the spatially varying electronic environments created by Moiré patterns, significantly impacting their binding energies, mobility, and responses to external fields. Liu et al. [172] investigate the quantum interactions within $WSe_2/MoSe_2$ heterobilayers unveiling sharp emission lines' complex dependence on charge density, contrasting with conventional trion behaviors. Kim et al. [173] provide insights into the temperature-dependent behavior of Moiré trions and their valley dynamics within $WSe_2/MoSe_2$ heterobilayers. The researchers introduce a novel microfabrication technique using focused Ga^+ ion beams, enabling precise control over the number of peaks arising from Moiré potentials. The valley dynamics of Moiré trions are governed by a lengthy valley relaxation process lasting about 700 ns, significantly longer than that of typical exciton or trion states.

Additionally, Moiré excitons have been observed in homostructures, where stacked layers of the same material exhibit similar phenomena [158, 163, 174–178]. Techniques such as ARPES, scanning transmission electron microscopy, and femtosecond photoemission momentum microscopy have been instrumental in studying Moiré excitons, providing insights into their spatial and momentum-space characteristics.

Theoretical calculations have significantly advanced our understanding of Moiré excitons [142, 181, 182], proposing novel configurations such as intralayer charge-transfer excitons that help elucidate the observed optical properties of Moiré superlattices [183]. The study of optically excited Moiré excitons in TMD Moiré systems has provided profound insights into their distinctive electronic and optical characteristics. These experimental findings, coupled with theoretical insights, collectively enhance our understanding of Moiré exciton phenomena and lay the groundwork for potential applications in optoelectronic devices and quantum technologies.

Moiré excitons have garnered significant interest due to their unique properties and potential for realizing Bose-Einstein condensation (BEC). Recent studies have shown that the periodic potential of Moiré patterns can trap excitons, leading to the formation of localized states and enabling the study of strongly correlated excitonic systems [131, 159]. Researchers have demonstrated that these excitons can exhibit long-range coherence and interaction effects, which are crucial for BEC [184, 185]. For instance, experiments conducted on $MoSe_2/WSe_2$ heterobilayers have revealed the presence of Moiré excitons with lifetimes significantly longer than those in conventional TMDs, suggesting enhanced stability and interaction capabilities [186–189]. Furthermore, theoretical models predict that under appropriate conditions, such as low temperatures and high exciton densities, Moiré excitons could condense into a coherent quantum state, exhibiting properties akin to a Bose-Einstein condensate [190–192]. These models are supported by experimental evidence showing exciton localization and the formation of quantum-dot-like potentials in Moiré superlattices. Research is also focused on manipulating the Moiré pattern by twisting the layers at specific angles, which can tune the excitonic properties and interactions. This tunability is essential for exploring various quantum phases and achieving the conditions necessary for BEC. The realization of BEC in Moiré excitons represents a groundbreaking leap in the field of quantum materials, promising to unlock new realms of quantum coherence and interaction. This phenomenon, where particles condense into a single quantum state, could pave the way for unprecedented advancements in optoelectronic devices and quantum computing.

5.2 Enhancement of light-matter interactions

Moiré superlattices in TMDs utilize Moiré potentials to study light-matter interactions, leading to strongly correlated quantum phenomena influenced by interlayer coupling. Zheng et al. present compelling insights into how intentional variations in twist angles between layers of WSe_2 profoundly affect Moiré potentials and excitonic behaviors within these structures [112]. Their study measures Moiré potential depths of 115 and 180 meV for twist angles of 1.5° and 2.5°, respectively, highlighting the fine-tunability of these potentials through structural adjustments. This strong interlayer coupling enables the capture of Moiré excitons (see Fig. 12(a)), directly influencing the splitting of exciton peaks in photoluminescence spectra, as shown in Figs. 12(b) and 12(c). This precise control over exciton energy marks a significant advancement, promising applications in efficient solar cells, sensors, and innovative photonic devices.

Excitons confined within Moiré potentials exhibit valley-dependent characteristics and significant circular polarization, as detailed in Fig. 12(d). This polarization underscores Moiré superlattices' potential to influence excitonic behavior, enhancing interactions between light and matter. Additionally, Baek et al. demonstrate that Moiré-trapped excitons within $MoSe_2/WSe_2$

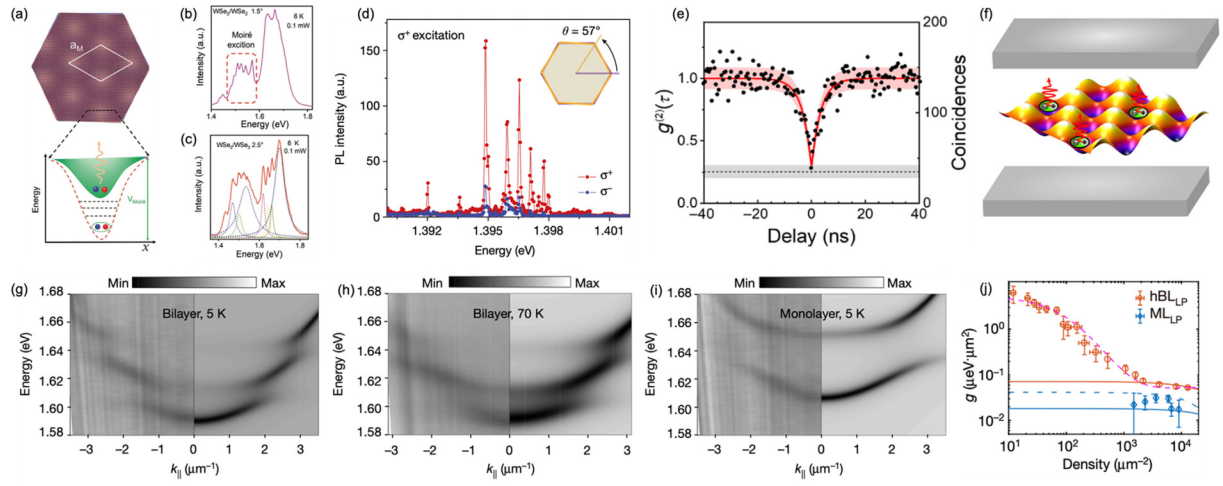


Figure 12 Enhancement of light-matter interactions. (a) Top: Schematic depiction of Moiré superlattice in real space. Bottom: Schematic depiction of exciton entrapment within Moiré potential wells. (b) and (c) Representative PL spectra of WSe_2/WSe_2 homostructures featuring twist angles of 1.5° and 2.5°, with each peak split modeled using Gaussian functions. Reproduced with permission from Ref. [112], © Wiley-VCH GmbH 2023. (d) Circularly polarized PL spectra depicting Moiré confined interlayer excitons in $MoSe_2/WSe_2$ heterobilayers with a twist angle of 57°. Reproduced with permission from Ref. [160], © Seyler, K. L. et al. under exclusive licence to Springer Nature Limited 2019. (e) Second-order photon correlation statistics of Moiré-trapped interlayer excitons (black dots) clearly show antibunching, confirming single-photon behavior. Reproduced with permission from Ref. [193], © American Chemical Society 2023. (f) schematic depiction of the Moiré polariton system, where excitons are trapped within a Moiré lattice and interact with a flat cavity. (g)–(i) Angle-dependent white-light reflectance spectra showing the robust interaction between Moiré excitons and cavity photons at temperatures of (g) 5 and (h) 70 K, (i) compared with the interaction between monolayer (ML) excitons and cavity photons at 5 K. (j) Experimental (symbols) and modeled (lines) non-linear coefficient, g, as a function of carrier density for Moiré hBL LPs (red) and ML LPs (blue). Reproduced with permission from Ref. [194], © Zhang, L. et al. under exclusive licence to Springer Nature Limited 2021.

Moiré heterobilayers serve as foundational single-photon emitters [193]. Their study confirms photon antibunching (see Fig. 12(e)), indicating that photons are emitted individually, validating the quantum nature of emitted light. Moreover, they show the ability to tune emission properties of these excitons up to 40 meV using an electric field (DC Stark effect), showcasing advanced methods to enhance quantum-level light-matter interactions.

Furthermore, the periodic modulation of the electronic landscape in Moiré superlattices enhances light-matter interactions, giving rise to exciton-polaritons. These hybrid light-matter quasiparticles emerge from the strong coupling regime and exhibit properties that can be dynamically controlled by adjusting the twist angle. Zhang et al. [194] explores van der Waals heterostructure polaritons with Moiré-induced nonlinearity within $WS_2/MoSe_2$ heterobilayers integrated into a microcavity, as depicted in Fig. 12(f). Their research demonstrates the formation of Moiré polaritons through strong coupling between cavity photons and excitons trapped within Moiré potentials, detailed in Figs. 12(g)–12(i). The study highlights the unique density-dependent behavior of these Moiré polaritons compared to monolayer exciton polaritons, indicating a potential for substantially increased polariton nonlinearity, even at elevated temperatures. Figure 12(j) illustrates the measured nonlinear coefficients g for both Moiré heterobilayer (hBL) and monolayer (ML) lower polaritons (LP), underscoring the introduction of substantial nonlinearities into the system [165, 195]. This interaction not only highlights the ability to manipulate exciton properties through microcavity adjustments but also enables effective control of light at the nanoscale. Complementing experimental insights, Fitzgerald et al. [196] provided a theoretical exploration into the impact of varying twist angles between layers in $WS_2/MoSe_2$ heterostructures on exciton-light coupling and polariton energy dynamics. The minimal gap between Moiré excitons and their strong interaction with light in TMDs result in unique polariton branches, potentially involving multiple excitons due to photon-induced hybridization. The pronounced dependence on twist angle and cavity configuration elucidates their dual light-matter nature. This control over exciton quantum states facilitates groundbreaking advancements in quantum and optoelectronic technologies, offering precise manipulation of light-matter interactions at the quantum level.

6 Transport properties of Moiré superlattices

The study of transport properties in TMD Moiré superlattices represents a compelling frontier in condensed matter physics. These properties are essential not only for unraveling the intricate electronic interactions within these complex systems but also for advancing future technologies. The distinct periodic potential created by Moiré patterns profoundly alters the electronic landscape, influencing how charge carriers react to external stimuli. This section delves into key aspects of transport phenomena in Moiré superlattices, emphasizing electrical conductivity and magnetotransport properties.

6.1 Electrical conductivity

Electrical conductivity in Moiré superlattices of TMDs unveils a spectrum of intricate physical phenomena shaped by lattice geometry, electronic interactions, and external influences. These two-dimensional materials exhibit diverse electronic behaviors spanning insulating, semiconducting, metallic, and even superconducting states [17], underscoring the need to explore conductivity within these systems. Central to this exploration is the profound influence of Moiré patterns, arising from the relative twisting or alignment of TMD layers, which significantly alter the electronic band structure and local properties. These changes are pivotal for leveraging the unique quantum and electronic characteristics of TMD Moiré superlattices in advanced technological applications, making the study of their conductivity a focal point in contemporary condensed matter physics. A study by Tang et al. [44] on WSe_2/WS_2 Moiré superlattices illustrates substantial impact of hole interactions on electrical conductivity by revealing the formation of a Mott insulating state at half-filling of the first hole Moiré superlattice band. Figure 13(a) depicts the relationship between gate voltage, hole density, and Moiré band filling factors, clearly indicating the emergence of the Mott insulating state at half-filling through detailed measurements of reflectance peak amplitude and two-terminal resistance. This

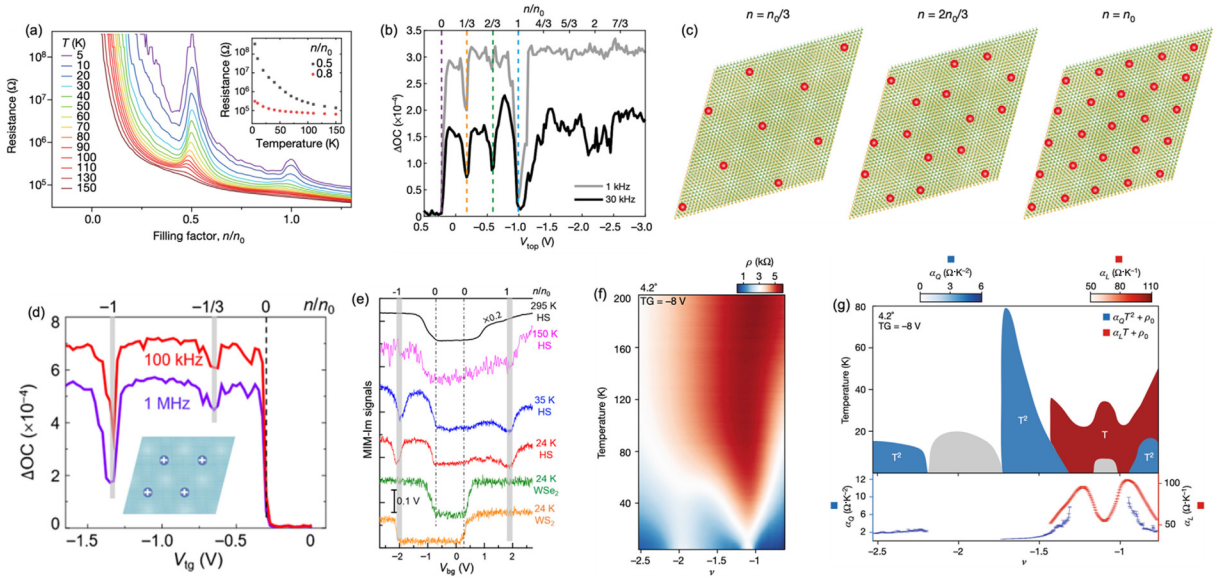


Figure 13 Electrical conductivity in TMDs Moiré superlattices. (a) Temperature-dependent two-terminal resistance in WSe_2/WS_2 Moiré superlattices relative to Moiré filling factors. Inset: Resistance variations at temperatures corresponding to $n/n_0 = 0.5$ (black) and 0.8 (red). Reproduced with permission from Ref. [44], © Tang, Y. H. et al. under exclusive licence to Springer Nature Limited 2020. (b) ODRC signals at 1 kHz (grey) and 30 kHz (black) from charge neutrality to moderate hole doping. Gap-like features appear at $n = n_0/3$ (orange), $n = 2n_0/3$ (green), and $n = n_0$ (blue) with $n = 0$ marked by purple line. (c) Schematic shows Wigner crystal states ($n = n_0/3$, $n = 2n_0/3$) and Mott insulator states ($n = n_0$) in a WSe_2/WS_2 Moiré superlattice. Reproduced with permission from Ref. [20], © Regan, E. C. et al. under exclusive licence to Springer Nature Limited 2020. (d) ODRC signals at two AC frequencies plotted against top-gate voltage and filling factors. A dashed line marks the charge-neutral point. Shaded areas highlight the Mott insulator state at $n/n_0 = (-1)$ and correlated insulating state at −1/3. Inset: Mott insulator with one hole per Moiré unit cell. (e) MIM-Im (imaginary) signals across different locations and temperatures. Shaded regions indicate the Mott insulating states at $n/n_0 = \pm 1$. The data recorded at 295K HS is scaled by 0.2 for clearer visualization. Reproduced with permission from Ref. [197], © American Physical Society 2020. (f) Color plot showing resistivity as a function of temperature and doping for a 4.2° device with a constant top gate voltage of −8 V. (g) The upper panel shows varying temperature behaviors: T^2 behavior in blue, T-linear in red, and insulating in grey. Two quantum critical fans are observed near half-filling, absent near the full filling trivial insulator. The bottom panel illustrates the evolution of fit parameters with doping: the T^2 coefficient α_Q, in blue, significantly increases as the quantum critical point is approached from the metallic phase. The T-linear coefficient α_L, in red, peaks at the quantum critical points where T-linear resistivity persists to the lowest temperatures. Reproduced with permission from Ref. [45], © Ghiotto, A. et al. under exclusive licence to Springer Nature Limited 2021.

study provides compelling evidence that hole mobility is blocked under such conditions, rendering the material insulating and underscores the ability to manipulate electrical conductivity in these materials by altering hole density. This highlights a fundamental mechanism for controlling charge flow in next-generation electronic devices. Expanding on electronic phenomena within Moiré superlattices, Regan et al. [20] reported a Mott insulator state in which each superlattice site hosts a single hole, with the state being stable up to 45 K, using the innovative optically detected resistance and capacitance (ODRC) technique. The study also revealed unexpected insulating phases at 1/3 and 2/3 fillings, attributed to generalized Wigner crystals, as illustrated in Figs. 13(b) and 13(c). Additionally, twisted homobilayer WSe_2 exhibits characteristics of a correlated insulator, modifiable through variations in twist angle and displacement field [17]. Notably, at a twist angle of 5.1°, regions of zero resistance were observed upon deviation from half-filling at temperatures below 3 K, suggesting a potential transition to a superconducting state.

However, previous studies predominantly focus on hole-doped correlated insulators, leaving electron-doped aspects less explored. Addressing this gap, Chu et al. [197] introduced a novel noncontact technique that integrates ODRC with Microwave Impedance Microscopy (MIM). Applied to angle-aligned WSe_2/WS_2 Moiré heterobilayers, their method measured electrical conductivity on both electron and hole-doped sides, revealing nanoscale conductivity features within correlated electronic states. They identified a Mott insulating state at one electron per Moiré unit cell, a novel finding not previously reported. The robustness of these electronic phases is confirmed across temperatures up to 150 K (see Fig. 13(e)), indicating their stability under varying thermal conditions. Furthermore, the observation of a resistivity peak at one hole per lattice site (Fig. 13(d)) aligns with characteristics typical of a Mott insulator, as reported in earlier studies [20, 44]. Microwave imaging further highlighted spatial inhomogeneities in the correlated states, likely stemming from localized irregularities in the Moiré potential or variations in electrostatic doping.

In their study, Xu et al. [118] developed an optical sensing technique for 'exciton detection,' uncovering a series of generalized Wigner crystal states at various filling factors ν = 1/2, 2/5, 3/5, 1/4, 3/4, 1/7, 6/7 within the WSe_2/WS_2 Moiré superlattice system. These findings underscore the significant role of long-range electron-electron interactions, which spanning one to several lattice constants. Concurrently, Jin et al. [72] confirmed through optical anisotropy measurements that states at ν = 1/2, 2/5, and 3/5 in the WSe_2/WS_2 Moiré superlattices arise from spontaneous rotational symmetry breaking driven by these interactions, forming electronic stripe states. Li et al. [198] employed a graphene layer for charge detection, using scanning tunneling microscopy to map the lattice structure of generalized Wigner crystal states within WSe_2/WS_2 Moiré superlattice. Various experimental techniques have contributed significantly to the study of electron correlation effects in these systems, including microwave impedance [197, 199], quantum capacitance [200], reflection fluorescence spectroscopy [165, 201–204], scanning tunneling spectroscopy [69, 205–207], and angle-resolved photoemission spectroscopy [1]. These studies highlight the profound electron correlation effects in TMDC Moiré superlattices, particularly when the Coulomb interaction strength U significantly exceeds the electron hopping term t. Another fascinating aspect of these investigations is the exploration of reducing the U/t ratio to induce a transition from a Mott insulator to a metallic state, known as a Mott transition. In many materials, this transition involves magnetic and structural transformations

and is typically a first-order process [208]. However, continuous Mott transitions, occurring without symmetry breaking, have drawn considerable interest in condensed matter physics [209–212]. Theoretical predictions suggest that on a triangular lattice, frustration may allow for such a continuous Mott transition, potentially leading to a quantum spin liquid state near the critical point [209, 210].

TMDC Moiré superlattices constitute a strongly correlated system on a triangular lattice. A key question involves the feasibility of continuously and *in situ* adjusting the *U*/*t* ratio. Recent experimental work by Ghiotto et al. [45] and Li et al. [152] has shown that in optimal TMDC Moiré superlattice systems, the *U*/*t* ratio can be effectively modulated by applying an electric field through a gate. This modulation facilitates a bandwidth-controlled transition from a Mott insulator to a metallic state. Specifically, Ghiotto et al. [45] investigated the transport properties near the Mott insulator-to-metal transition, observing a metallic state in the critical region that deviates from Fermi liquid behavior (Figs. 13(f) and 13(g)). Wang et al. [17] reported on insulating states and preliminary signs of superconductivity in twisted WSe_2, where theoretical calculations suggested tuning the *U*/*t* ratio by adjusting the relative band positions of two WSe_2 layers using an external electric field. Furthermore, Li et al. [152] studied the transport and spectroscopic properties of the Moiré sub-bands in the valence band of the $MoTe_2/WSe_2$ Moiré heterostructure stacked in an AA configuration. At zero electric field, the energy difference between the valence bands of $MoTe_2$ and WSe_2 was approximately 200 meV [213]. Applying an external electric field brought their band edges closer together, significantly altering the interlayer coupling strength and thus affecting the system's *U*/*t* ratio. They observed a continuous Mott transition controlled by an external electric field, with resistance measurements near the transition exhibiting scaling behavior typical of quantum critical regions. Furthermore, near half-filling of Moiré sub-bands (ν = 1), a notable Pomeranchuk effect was observed, where increasing temperature stabilized the insulating state. Magneto-optical measurements revealed frustration effects in the system at ν = 1, where no long-range ordered states appeared at temperatures around 5% of the Curie-Weiss temperature. These experimental observations confirm the presence of frustration effects in the system at ν = 1. These findings provide foundational insights into Mott transitions in twisted WSe_2 and $MoTe_2/WSe_2$ Moiré superlattices, paving the way for future explorations of potential quantum spin liquid states in two-dimensional semiconductor Moiré superlattice systems

6.2 Magnetotransport properties

Magnetotransport properties elucidate how a magnetic field influences the transport behavior of charge carriers in a material. In TMDs, strong spin-orbit coupling and valley degrees of freedom give rise to unique electronic behaviors. In TMD Moiré superlattices, the interaction between magnetic fields and the periodic potential landscapes formed by Moiré patterns results in distinctive magnetotransport phenomena crucial for advancing electronic and optoelectronic devices.

Seyler et al. [160] conducted a thorough investigation into magneto-photoluminescence properties of $MoSe_2/WSe_2$ Moiré heterobilayers to explore the influence of Moiré potentials on valley excitons. They observed significant Zeeman splitting in the photoluminescence spectra of interlayer excitons under an applied magnetic field. This splitting allowed them to determine the effective g-factors of the excitons, which varied with the twist angle of the heterobilayers. For instance, the g-factor was approximately 6.7 for a 2° twist angle and around −15.9 for a 57° twist angle (see Fig. 14(a)). These variations highlight the strong dependence of magnetic properties on the Moiré potential and the local atomic registry within the heterobilayers.

Meanwhile, Tang et al. [44] investigated the effects of an out-of-plane magnetic field on the electronic and magnetic properties of WSe_2/WS_2 Moiré superlattices. The study also observed significant Zeeman splitting in the photoluminescence spectra of interlayer excitons, revealing twist-angle-dependent effective g-factors. At half-filling, the study identified a Mott insulating state displaying antiferromagnetic Curie-Weiss behavior (see Fig. 14(b)), evidenced by a negative Weiss constant, indicating antiferromagnetic interactions between localized moments. The Zeeman splitting exhibited linear behavior at low magnetic fields and saturation at higher fields, revealing a significant exciton valley g-factor around 270 (see Fig. 14(c)). The study also suggested a potential quantum phase transition from an antiferromagnetic state to a weak ferromagnetic state at certain filling factors, characterized by a divergence in magnetic susceptibility. These findings highlight the significant impact of magnetic fields on the electronic and magnetic behavior of TMD Moiré superlattices, offering valuable insights into their magnetotransport properties.

Further exploring the influence of magnetic fields, Ghiotto et al. [45] demonstrated anomalous magnetotransport behavior in twisted WSe_2, revealing that the longitudinal magnetoresistance (ρ_{xx}) transitions from a quadratic (B^2) to a linear (B) dependence near the MIT, indicative of quantum criticality. As depicted in the left panel of Fig. 14(d), at low magnetic fields (0–1 T), resistivity evolves with doping, displaying *B*-linear behavior near the quantum critical point. Significant changes in Hall resistivity ρ_{xy}) near this point, shown in the middle panel of Fig. 14(d), reflect the collapse of the Fermi surface, emphasizing the impact of magnetic fields on the electronic structure. The right panel of Fig. 14(d) highlights the critical enhancement in longitudinal resistivity as it transitions from B^2 to *B*-linear behavior, underscoring the role of magnetic fields in driving and revealing quantum critical phenomena. These findings underscore the interplay between magnetic fields and electronic properties in TMD Moiré superlattices, emphasizing *B*-linear magnetoresistance and variations in Hall resistivity as key to understanding magnetic field effects on quantum phase transitions. This research positions twisted WSe_2 as a valuable platform for exploring the effects of magnetic fields on quantum phase transitions and magnetotransport properties in TMD Moiré superlattices. Addressing the role of magnetic fields in TMD Moiré superlattices, Li et al. [152] investigated the effects on $MoTe_2/WSe_2$ Moiré superlattice, using Magnetic Circular Dichroism (MCD) to measure magnetization. They observed linear increases in magnetization at low fields, saturating at higher fields, with distinctions between metallic and insulating states. Magnetic susceptibility remained significant at low temperatures without long-range order, indicating low- energy spin excitations. Magnetoresistance measurements revealed magnetic field-induced metal-insulator transitions and Shubnikov-de Haas oscillations, indicative of Landau level formation. The study also observed the Pomeranchuk effect, linking increased spin entropy to charge localization, highlighting the profound influence of magnetic fields on electronic behavior in these superlattices. Expanding on the understanding of TMD Moiré superlattices, Zhang et al. [214] examined the specific effects of magnetic fields on 3L-$MoTe_2/WSe_2$ Moiré superlattice, through transport measurements, magnetoresistance, and Shubnikov-de Haas oscillations analysis. They identified a magnetic-field-induced MIT at a critical magnetic field (Bc ≈ 6 T), where increasing field strength led to a progressive closure of the charge gap and divergence of the effective quasiparticle mass, indicating quantum critical behavior (see Fig. 14(e)). The study also noted the Pomeranchuk effect, where elevated temperatures enhanced

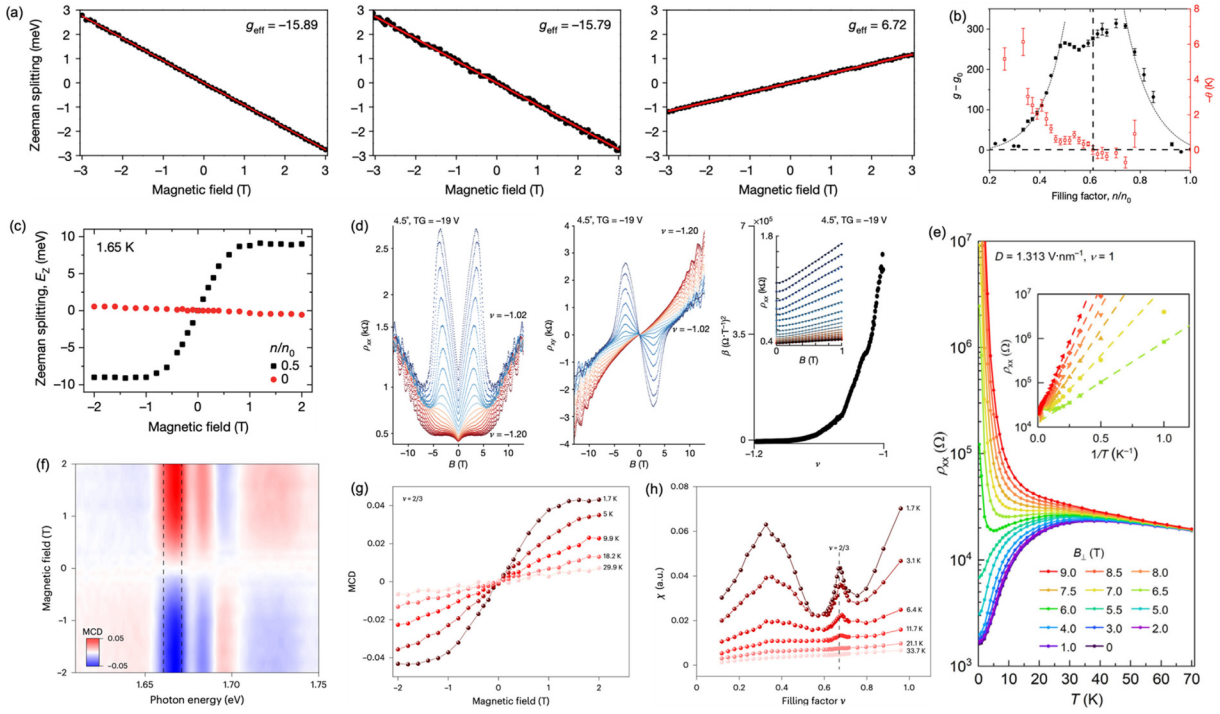


Figure 14 Magnetotransport properties in TMDs Moiré superlattices. (a) Zeeman splitting observed in polarization-resolved photoluminescence across varying magnetic field strength. The effective g-factors determined for three distinct samples are: −15.89 ± 0.02, −15.79 ± 0.05, and 6.72 ± 0.02, respectively. Reproduced with permission from Ref. [160], © Seyler, K. L. et al. under exclusive licence to Springer Nature Limited 2019. (b) Variation of the magnetic susceptibility ($g - g_0 \propto \chi$at 1.65 K, plotted against the filling factor. The corresponding Weiss constant θ is shown on the right axis with red empty symbols. (c) Exciton Zeeman splitting (E_Z) as a function of the magnetic field strength, shown for two distinct filling conditions: half-filling (black squares) and zero filling (red circles). Reproduced with permission from Ref. [44], © Tang, Y. H. et al. under exclusive licence to Springer Nature Limited 2020. (d) Left panel: Longitudinal magnetoresistance plotted against doping near the quantum critical point for a sample with a 4.5° twist angle. In low magnetic fields (0–1 T), resistivity transitions from B^2 behavior (bottom curve) to B-linear behavior near the quantum critical point (top curves). Middle panel: Doping dependence of the Hall resistance, showing significant shifts indicating Fermi surface collapse near the quantum critical point. Right panel: Parameter β versus doping as the system approaches half filling, highlighting the shift B^2 to B-linear behavior. Inset shows corresponding sample fits. Reproduced with permission from Ref. [45], © Ghiotto, A. et al. under exclusive licence to Springer Nature Limited 2021. (e) Temperature dependence of ρ_{xx} at various $B_\perp$, illustrating the magnetic-field-induced MIT. Inset: Arrhenius fits (dashed lines) used for determining activation gap magnitudes for $B_\perp > 6$ T. Reproduced with permission from Ref. [214], © Zhang, M. J. et al. Published by the American Physical Society under the terms of the Creative Commons Attribution 4.0 International license 2022. (f) MCD spectrum versus magnetic field strength at $\nu = 2/3$ and $T = 1.7$ K. The spectrum, integrated around the Moiré exciton resonance (between the vertical lines), reflects the sample's magnetization. (g) Integrated MCD versus magnetic field strength at selected temperatures. At 1.7 K, MCD saturates above ~1 T. The zero-field slope is used to determine χ. (h) Magnetic susceptibility (χ) plotted against filling factor across different temperatures, highlighting a distinct peak at 2/3 filling with decreasing temperature. Reproduced with permission from Ref. [215], © Tang, Y. H. et al. under exclusive licence to Springer Nature Limited 2023.

charge localization due to increased spin entropy, emphasizing the system's proximity to the metal-insulator transition point in the triangular lattice Hubbard model. These findings underscore the significant influence of magnetic fields on the transport properties and phase transitions in 3L-$MoTe_2$/WSe_2 Moiré superlattices. Furthermore, Tang et al. [215] utilized MCD to study the magneto-optical properties of WSe_2/WS_2 Moiré superlattices. They investigated two device types: one with negligible screening and another with strong Coulomb screening. Their results indicated antiferromagnetic net exchange interactions for filling factors below one, with pronounced suppression at 2/3 filling, indicative of frustrated magnetic interactions in the Wigner-Mott insulator state. This suppression was mitigated by screening long-range Coulomb interactions. The temperature dependence of magnetic susceptibility X) followed the Curie–Weiss law, with a negative Curie–Weiss temperature, highlighting antiferromagnetic interactions. MCD measurements revealed enhanced signals near the Moiré exciton resonance, saturating at around 1 T at low temperatures (Fig. 14(f)), with decreasing saturation at higher temperatures (Fig. 14(g)). The study also demonstrated a strong dependence of magnetic properties on filling, particularly the suppression of antiferromagnetic exchange at 2/3 filling (Fig. 14(h)), supporting the role of Coulomb screening. To explain these findings, the study proposed a spin model with antiferromagnetic nearest-neighbour coupling and ferromagnetic second-neighbour coupling, providing insights into the competition between magnetic interactions in the Moiré superlattice. These magneto-optical properties, significantly influenced by frustrated magnetic interactions, are crucial for understanding the magnetotransport properties of WSe_2/WS_2 Moiré superlattices and similar two-dimensional materials.

7 Conclusion and outlook

Recent advancements in Moiré superlattices formed from TMD heterostructures have significantly enhanced electronic and optoelectronic devices. By stacking 2D TMD materials with a slight twist or lattice mismatch, unique Moiré patterns emerge, leading to novel electronic states and properties. These patterns exhibit intriguing phenomena such as correlated electron behavior, flat bands, superconductivity, and topological phases. TMD materials in Moiré superlattices are particularly suited for optoelectronics due to their natural bandgap and strong light-matter interactions. Moreover, their properties can be dynamically tuned with external stimuli, making them ideal for valleytronics, where manipulation of the valley degree of freedom enhances information storage and processing capabilities. Additionally, these superlattices hold great promise for quantum information processing by enabling precise control over quantum states, facilitating advancements in qubits and other quantum devices.

However, challenges persist, including precise control over the twist angle and interlayer coupling. Reliable fabrication and characterization techniques are essential to fully harness their potential. Nonetheless, rapid progress suggests that these obstacles will be overcome in the near future.

The field of Moiré superlattices in twisted TMD heterostructures is still in its early stages, but the potential for groundbreaking discoveries is immense. By addressing current challenges and exploring new research directions, we can unlock the full potential of these materials.

7.1 Advancements in fabrication techniques

One of the primary challenges is the development of scalable and reproducible fabrication methods for high-quality Moiré superlattices. Future research should focus on refining these techniques. Innovations in fabrication methods will likely enable the production of uniform and large-area Moiré superlattices, which are essential for practical applications.

7.2 Integration with other 2D materials

Exploring new combinations of TMDs with other 2D materials, especially 2D magnetic materials, could lead to the discovery of novel emergent phenomena and enhanced functionalities. This interdisciplinary approach is crucial for the development of advanced heterostructures with tailored electronic and optical properties.

7.3 Application in quantum technologies

The unique electronic properties of Moiré superlattices, such as tunable band structures and strong electron correlations, make them promising candidates for quantum computing, sensing, and communication technologies. Future research should aim to leverage these properties to develop practical quantum devices, including stable qubits and new types of quantum sensors.

7.4 Theoretical and experimental collaboration

Continued collaboration between theoretical and experimental researchers is essential for a deeper understanding of the fundamental interactions within Moiré superlattices. This synergy will drive innovation and lead to the discovery of new quantum states and phases. Translating theoretical models into practical applications is particularly important.

7.5 Emergence of new quantum phases

As the field progresses, we anticipate the discovery of new quantum phases in Moiré superlattices. These phases could reveal unprecedented physical properties and open new avenues for research in condensed matter physics. Understanding these phases will not only advance theoretical physics but also inform the development of new materials and technologies.

7.6 Broader impact on technology and industry

The ability to engineer materials with specific electronic properties will have far-reaching implications for various technological applications, including electronics, optoelectronics, and energy conversion. The advancements in Moiré superlattice research are expected to contribute significantly to the development of next-generation devices and systems, impacting both academic research and industrial applications.

7.7 Machine learning and AI

As the world embraces machine learning (ML) and artificial intelligence (AI), incorporating these technologies into the study of Moiré superlattices offers promising new avenues for discovery and optimization. ML algorithms can predict and optimize the fabrication of Moiré patterns with desirable properties by analyzing large datasets of existing structures and behaviors, significantly accelerating the discovery of novel materials with tailored electronic, optical, and magnetic properties. AI can also optimize fabrication processes for high-quality superlattices, enhancing precision, scalability, and reproducibility for practical applications.

7.8 Interdisciplinary collaboration

The interdisciplinary nature of Moiré superlattice research, involving materials science, physics, and engineering, is essential for overcoming current challenges and driving innovation. Collaboration across these disciplines will foster new insights and accelerate the development of practical applications.

7.9 Policy and funding support

Governmental and institutional support in the form of policy and funding will play a critical role in advancing research in Moiré superlattices. Increased investment in this area will facilitate the development of new technologies and accelerate the transition from fundamental research to industrial applications.

In conclusion, the field of Moiré superlattices in twisted TMD heterostructures is poised for exciting developments. By addressing current challenges and exploring new directions, researchers can unlock the full potential of these materials, bridging the gap between fundamental research and practical applications. The future of Moiré superlattice research promises to be both innovative and transformative, with significant implications for science and technology. The study of these superlattices promises transformative impacts across fundamental physics, optoelectronics, valleytronics, and quantum information processing, thereby paving the way for future scientific and technological breakthroughs.

Acknowledgements

The authors gratefully acknowledge the financial support received from various entities, including the National Natural Science Foundation of China (No. 52373311), and the Key Project of the Natural Science Program of Xinjiang Uygur Autonomous Region (No. 2023D01D03). They also appreciate the support from the High-Performance Complex Manufacturing Key State Lab Project at Central South University (No. ZZYJKT2020-12). ZWL extends thanks to the Australian Research Council (ARC Discovery Project, DP180102976) for their support. J.-T. W. acknowledges funding from the National Natural Science Foundation of China (Nos. 92263202 and 12374020), the Strategic Priority Research Program of the Chinese Academy of Sciences (No. XDB33000000), and the National Key Research and Development Program of China (No. 2020YFA0711502). The authors express gratitude for the resources provided by the High-Performance Computing Center of Central South University and extend their appreciation to the Beijing Super Cloud Computing Center (BSCC, www.blsc.cn) for providing HPC resources that significantly contributed to the research results reported in this paper.

Declaration of competing interest

The authors declare that they have no competing interests.

References

[1] Stansbury, C. H.; Utama, M. I. B.; Fatuzzo, C. G.; Regan, E. C.; Wang, D. Q.; Xiang, Z. Y.; Ding, M. C.; Watanabe, K.; Taniguchi,

T.; Blei, M. et al. Visualizing electron localization of WS_2/WSe_2 moiré superlattices in momentum space. *Sci. Adv.* **2021**, *7*, eabf4387.

[2] Wang, T. G.; Yuan, N. F. Q.; Fu, L. Moiré surface states and enhanced superconductivity in topological insulators. *Phys. Rev. X* **2021**, *11*, 021024.

[3] Ye, Y. S.; Qian, J. M.; Zhang, X. W.; Wang, C.; Xiao, D.; Cao, T. Kekulé moiré superlattices. *Nano Lett.* **2023**, *23*, 6536–6543.

[4] Yang, H.; Liu, L. W.; Yang, H. X.; Zhang, Y.; Wu, X.; Huang, Y.; Gao, H. J.; Wang, Y. L. Advance in two-dimensional twisted moiré materials: Fabrication, properties, and applications. *Nano Res.* **2023**, *16*, 2579–2596.

[5] Shi, B. B.; Qi, P. F.; Jiang, M. L.; Dai, Y. C.; Lin, F.; Zhang, H.; Fang, Z. Y. Exotic physical properties of 2D materials modulated by moiré superlattices. *Mater. Adv.* **2021**, *2*, 5542–5559.

[6] Xiao, Y.; Liu, J. L.; Fu, L. Moiré is more: Access to new properties of two-dimensional layered materials. *Matter* **2020**, *3*, 1142–1161.

[7] Li, Y.; Hua, Y. Q.; Sun, N.; Liu, S. J.; Li, H. X.; Wang, C.; Yang, X. Y.; Zhuang, Z. C.; Wang, L. L. Moiré superlattice engineering of two-dimensional materials for electrocatalytic hydrogen evolution reaction. *Nano Res.* **2023**, *16*, 8712–8728.

[8] Behura, S. K.; Miranda, A.; Nayak, S.; Johnson, K.; Das, P.; Pradhan, N. R. Moiré physics in twisted van der Waals heterostructures of 2D materials. *Emergent Mater.* **2021**, *4*, 813–826.

[9] Götting, N.; Lohof, F.; Gies, C. Moiré-Bose-Hubbard model for interlayer excitons in twisted transition metal dichalcogenide heterostructures. *Phys. Rev. B* **2022**, *105*, 165419.

[10] Brem, S.; Linderälv, C.; Erhart, P.; Malic, E. Tunable phases of moiré excitons in van der Waals heterostructures. *Nano Lett.* **2020**, *20*, 8534–8540.

[11] Kundu, S.; Amit, T.; Krishnamurthy, H. R.; Jain, M.; Refaely-Abramson, S. Exciton fine structure in twisted transition metal dichalcogenide heterostructures. *npj Comput. Mater.* **2023**, *9*, 186.

[12] Han, S. A.; Bhatia, R.; Kim, S. W. Synthesis, properties and potential applications of two-dimensional transition metal dichalcogenides. *Nano Converg.* **2015**, *2*, 17.

[13] Upadhyay, S. N.; Satrughna, J. A. K.; Pakhira, S. Recent advancements of two-dimensional transition metal dichalcogenides and their applications in electrocatalysis and energy storage. *Emergent Mater.* **2021**, *4*, 951–970.

[14] Wang, L.; Yin, S. S.; Yang, J. P.; Dou, S. X. Moiré superlattice structure in two‐dimensional catalysts: Synthesis, property and activity. *Small* **2023**, *19*, 2300165.

[15] Novoselov, K. S.; Castro Neto, A. H. Two-dimensional crystals-based heterostructures: Materials with tailored properties. *Phys. Scr.* **2012**, *2012*, 014006.

[16] Wu, L. S.; Cong, C. X.; Shang, J. Z.; Yang, W. H.; Chen, Y.; Zhou, J. D.; Ai, W.; Wang, Y. L.; Feng, S.; Zhang, H. B. et al. Raman scattering investigation of twisted WS_2/MoS_2 heterostructures: Interlayer mechanical coupling versus charge transfer. *Nano Res.* **2021**, *14*, 2215–2223.

[17] Wang, L.; Shih, E. M.; Ghiotto, A.; Xian, L. D.; Rhodes, D. A.; Tan, C.; Claassen, M.; Kennes, D. M.; Bai, Y. S.; Kim, B. et al. Correlated electronic phases in twisted bilayer transition metal dichalcogenides. *Nat. Mater.* **2020**, *19*, 861–866.

[18] Kennes, D. M.; Claassen, M.; Xian, L. D.; Georges, A.; Millis, A. J.; Hone, J.; Dean, C. R.; Basov, D. N.; Pasupathy, A. N.; Rubio, A. Moiré heterostructures as a condensed-matter quantum simulator. *Nat. Phys.* **2021**, *17*, 155–163.

[19] Wang, X.; Zhu, J. Y.; Seyler, K. L.; Rivera, P.; Zheng, H. Y.; Wang, Y. Q.; He, M. H.; Taniguchi, T.; Watanabe, K.; Yan, J. Q. et al. Moiré trions in $MoSe_2/WSe_2$ heterobilayers. *Nat. Nanotechnol.* **2021**, *16*, 1208–1213.

[20] Regan, E. C.; Wang, D. Q.; Jin, C. H.; Utama, M. I. B.; Gao, B. N.; Wei, X.; Zhao, S. H.; Zhao, W. Y.; Zhang, Z. C.; Yumigeta, K. et al. Mott and generalized Wigner crystal states in WSe_2/WS_2 moiré superlattices. *Nature* **2020**, *579*, 359–363.

[21] Yamada, S.; Imamura, T.; Machida, M. High performance LOBPCG method for solving multiple eigenvalues of Hubbard model: Efficiency of communication avoiding Neumann expansion preconditioner. In *Proceedings of the 4th Asian Conference on Supercomputing Frontiers*, Singapore, 2018, pp 243–256.

[22] Cai, X. B.; Gao, W. B. Moiré synergy: An emerging playground by coupled moirés. *ACS Nano* **2023**, *17*, 9673–9680.

[23] Liu, S.; Yu, G. Fabrication, energy band engineering, and strong correlations of two-dimensional van der Waals moiré superlattices. *Nano Today* **2023**, *50*, 101829.

[24] Zhang, L. F.; Ni, R. H.; Zhou, Y. Controlling quantum phases of electrons and excitons in moiré superlattices. *J. Appl. Phys.* **2023**, *133*, 080901.

[25] Liu, Y. P.; Zeng, C.; Yu, J.; Zhong, J. H.; Li, B.; Zhang, Z. W.; Liu, Z. W.; Wang, Z. M.; Pan, A. L.; Duan, X. D. Moiré superlattices and related moiré excitons in twisted van der Waals heterostructures. *Chem. Soc. Rev.* **2021**, *50*, 6401–6422.

[26] Weston, A. Introduction to 2-dimensional materials and moiré superlattices. In *Atomic and Electronic Properties of 2D Moiré Interfaces*. Weston, A., Ed.; Springer: Cham, 2022; pp 5–28.

[27] Bistritzer, R.; MacDonald, A. H. Moiré bands in twisted double-layer graphene. *Proc. Natl. Acad. Sci. USA* **2011**, *108*, 12233–12237.

[28] Suárez Morell, E.; Correa, J. D.; Vargas, P.; Pacheco, M.; Barticevic, Z. Flat bands in slightly twisted bilayer graphene: Tight-binding calculations. *Phys. Rev. B* **2010**, *82*, 121407(R).

[29] Lopes Dos Santos, J. M. B.; Peres, N. M. R.; Castro Neto, A. H. Continuum model of the twisted graphene bilayer. *Phys. Rev. B* **2012**, *86*, 155449.

[30] Cao, Y.; Fatemi, V.; Demir, A.; Fang, S. A.; Tomarken, S. L.; Luo, J. Y.; Sanchez-Yamagishi, J. D.; Watanabe, K.; Taniguchi, T.; Kaxiras, E. et al. Correlated insulator behaviour at half-filling in magic-angle graphene superlattices. *Nature* **2018**, *556*, 80–84.

[31] Cao, Y.; Fatemi, V.; Fang, S. A.; Watanabe, K.; Taniguchi, T.; Kaxiras, E.; Jarillo-Herrero, P. Unconventional superconductivity in magic-angle graphene superlattices. *Nature* **2018**, *556*, 43–50.

[32] Yankowitz, M.; Chen, S. W.; Polshyn, H.; Zhang, Y. X.; Watanabe, K.; Taniguchi, T.; Graf, D.; Young, A. F.; Dean, C. R. Tuning superconductivity in twisted bilayer graphene. *Science* **2019**, *363*, 1059–1064.

[33] Shi, J. T.; Zhu, J. H.; Macdonald, A. H. Moiré commensurability and the quantum anomalous hall effect in twisted bilayer graphene on hexagonal boron nitride. *Phys. Rev. B* **2021**, *103*, 075122.

[34] Liu, J. P.; Dai, X. Theories for the correlated insulating states and quantum anomalous hall effect phenomena in twisted bilayer graphene. *Phys. Rev. B* **2021**, *103*, 035427.

[35] Arora, H. S.; Polski, R.; Zhang, Y. R.; Thomson, A.; Choi, Y.; Kim, H.; Lin, Z.; Wilson, I. Z.; Xu, X. D.; Chu, J. H. et al. Superconductivity in metallic twisted bilayer graphene stabilized by WSe_2. *Nature* **2020**, *583*, 379–384.

[36] Kwan, Y. H.; Hu, Y. C.; Simon, S. H.; Parameswaran, S. A. Exciton band topology in spontaneous quantum anomalous hall insulators: Applications to twisted bilayer graphene. *Phys. Rev. Lett.* **2021**, *126*, 137601.

[37] Wu, F. C.; Das Sarma, S. Collective excitations of quantum anomalous hall ferromagnets in twisted bilayer graphene. *Phys. Rev. Lett.* **2020**, *124*, 046403.

[38] Shavit, G.; Berg, E.; Stern, A.; Oreg, Y. Theory of correlated insulators and superconductivity in twisted bilayer graphene. *Phys. Rev. Lett.* **2021**, *127*, 247703.

[39] Oh, M.; Nuckolls, K. P.; Wong, D.; Lee, R. L.; Liu, X. M.; Watanabe, K.; Taniguchi, T.; Yazdani, A. Evidence for unconventional superconductivity in twisted bilayer graphene. *Nature* **2021**, *600*, 240–245.

[40] Codecido, E.; Wang, Q. Y.; Koester, R.; Che, S.; Tian, H. D.; Lv, R.; Tran, S.; Watanabe, K.; Taniguchi, T.; Zhang, F. et al. Correlated insulating and superconducting states in twisted bilayer graphene below the magic angle. *Sci. Adv.* **2019**, *5*, eaaw9770.

[41] Serlin, M.; Tschirhart, C. L.; Polshyn, H.; Zhang, Y.; Zhu, J.; Watanabe, K.; Taniguchi, T.; Balents, L.; Young, A. F. Intrinsic quantized anomalous hall effect in a moiré heterostructure. *Science* **2020**, *367*, 900–903.

[42] Wu, F. C.; Lovorn, T.; Tutuc, E.; Macdonald, A. H. Hubbard model physics in transition metal dichalcogenide moiré bands. *Phys. Rev. Lett.* **2018**, *121*, 026402.
[43] Naik, M. H.; Jain, M. Ultraflatbands and shear solitons in moiré patterns of twisted bilayer transition metal dichalcogenides. *Phys. Rev. Lett.* **2018**, *121*, 266401.
[44] Tang, Y. H.; Li, L. Z.; Li, T. X.; Xu, Y.; Liu, S.; Barmak, K.; Watanabe, K.; Taniguchi, T.; MacDonald, A. H.; Shan, J. et al. Simulation of Hubbard model physics in WSe_2/WS_2 moiré superlattices. *Nature* **2020**, *579*, 353–358.
[45] Ghiotto, A.; Shih, E. M.; Pereira, G. S. S. G.; Rhodes, D. A.; Kim, B.; Zang, J. W.; Millis, A. J.; Watanabe, K.; Taniguchi, T.; Hone, J. C. et al. Quantum criticality in twisted transition metal dichalcogenides. *Nature* **2021**, *597*, 345–349.
[46] Wu, F. C.; Lovorn, T.; Tutuc, E.; Martin, I.; Macdonald, A. H. Topological insulators in twisted transition metal dichalcogenide homobilayers. *Phys. Rev. Lett.* **2019**, *122*, 086402.
[47] Ruiz-Tijerina, D. A.; Fal'Ko, V. I. Interlayer hybridization and moiré superlattice minibands for electrons and excitons in heterobilayers of transition-metal dichalcogenides. *Phys. Rev. B* **2019**, *99*, 125424.
[48] Schrade, C.; Fu, L. Spin-valley density wave in moiré materials. *Phys. Rev. B* **2019**, *100*, 035413.
[49] Andrei, E. Y.; Efetov, D. K.; Jarillo-Herrero, P.; MacDonald, A. H.; Mak, K. F.; Senthil, T.; Tutuc, E.; Yazdani, A.; Young, A. F. The marvels of moiré materials. *Nat. Rev. Mater.* **2021**, *6*, 201–206.
[50] Jiang, N.; Wang, L. A novel strategy for quantum image steganography based on moiré pattern. *Int. J. Theor. Phys.* **2015**, *54*, 1021–1032.
[51] Chen, M. Y.; Chen, F. Q.; Cheng, B.; Liang, S. J.; Miao, F. Moiré heterostructures: Highly tunable platforms for quantum simulation and future computing. *J. Semicond.* **2023**, *44*, 010301.
[52] Du, L. J.; Molas, M. R.; Huang, Z. H.; Zhang, G. Y.; Wang, F.; Sun, Z. P. Moiré photonics and optoelectronics. *Science* **2023**, *379*, eadg0014.
[53] Hamer, M. J.; Giampietri, A.; Kandyba, V.; Genuzio, F.; Menteş, T. O.; Locatelli, A.; Gorbachev, R. V.; Barinov, A.; Mucha-Kruczyński, M. Moiré superlattice effects and band structure evolution in near-30-degree twisted bilayer graphene. *ACS Nano* **2022**, *16*, 1954–1962.
[54] Yi, C. H.; Park, H. C.; Park, M. J. Strong interlayer coupling and stable topological flat bands in twisted bilayer photonic moiré superlattices. *Light Sci. Appl.* **2022**, *11*, 289.
[55] Lin, Q. L.; Fang, H. L.; Liu, Y. D.; Zhang, Y.; Fischer, M.; Li, J. T.; Hagel, J.; Brem, S.; Malic, E.; Stenger, N. et al. A room-temperature moiré interlayer exciton laser [Online]. https://arxiv.org/abs/2302.01266 (accessed Feb, 2023).
[56] Zheng, H. H.; Wu, B.; Li, S. F.; Ding, J. N.; He, J.; Liu, Z. W.; Wang, C. T.; Wang, J. T.; Pan, A. L.; Liu, Y. P. Localization-enhanced moiré exciton in twisted transition metal dichalcogenide heterotrilayer superlattices. *Light Sci. Appl.* **2023**, *12*, 117.
[57] Balents, L.; Dean, C. R.; Efetov, D. K.; Young, A. F. Superconductivity and strong correlations in moiré flat bands. *Nat. Phys.* **2020**, *16*, 725–733.
[58] Uri, A.; De La Barrera, S. C.; Randeria, M. T.; Rodan-Legrain, D.; Devakul, T.; Crowley, P. J. D.; Paul, N.; Watanabe, K.; Taniguchi, T.; Lifshitz, R. et al. Superconductivity and strong interactions in a tunable moiré quasicrystal. *Nature* **2023**, *620*, 762–767.
[59] Kezilebieke, S.; Vaňo, V.; Huda, M. N.; Aapro, M.; Ganguli, S. C.; Liljeroth, P.; Lado, J. L. Moiré-enabled topological superconductivity. *Nano Lett.* **2022**, *22*, 328–333.
[60] Lau, C. N.; Bockrath, M. W.; Mak, K. F.; Zhang, F. Reproducibility in the fabrication and physics of moiré materials. *Nature* **2022**, *602*, 41–50.
[61] He, H. R.; Zheng, H. H.; Wu, B.; Li, S. F.; Ding, J. N.; Liu, Z. W.; Wang, J. T.; Pan, A. L.; Liu, Y. P. Unveiling strain-enhanced moiré exciton localization in twisted van der Waals homostructures. *Nano Res.* **2024**, *17*, 3245–3252.
[62] Carr, S.; Massatt, D.; Fang, S. A.; Cazeaux, P.; Luskin, M.; Kaxiras, E. Twistronics: Manipulating the electronic properties of two-dimensional layered structures through their twist angle. *Phys. Rev. B* **2017**, *95*, 075420.
[63] Yang, Y. P.; Li, J. D.; Yin, J.; Xu, S. G.; Mullan, C.; Taniguchi, T.; Watanabe, K.; Geim, A. K.; Novoselov, K. S.; Mishchenko, A. *In situ* manipulation of van der Waals heterostructures for twistronics. *Sci. Adv.* **2020**, *6*, eabd3655.
[64] Jorio, A. Twistronics and the small-angle magic. *Nat. Mater.* **2022**, *21*, 844–845.
[65] Jha, G.; Li, W.; Brumme, T.; Heine, T. Spin orbit coupling effects on the excitonic properties of twisted moiré transition metal dichalcogenides. September 8, 2023.
[66] Liu, Y. P.; Gao, Y. J.; Zhang, S. Y.; He, J.; Yu, J.; Liu, Z. W. Valleytronics in transition metal dichalcogenides materials. *Nano Res.* **2019**, *12*, 2695–2711.
[67] Huang, X. Y.; Han, X.; Dai, Y. Y.; Xu, X. L.; Yan, J. H.; Huang, M. T.; Ding, P. F.; Zhang, D. C.; Chen, H.; Laxmi, V. et al. Recent progress on fabrication and flat-band physics in 2D transition metal dichalcogenides moiré superlattices. *J. Semicond.* **2023**, *44*, 011901.
[68] Zhang, Z. M.; Wang, Y. M.; Watanabe, K.; Taniguchi, T.; Ueno, K.; Tutuc, E.; LeRoy, B. J. Flat bands in twisted bilayer transition metal dichalcogenides. *Nat. Phys.* **2020**, *16*, 1093–1096.
[69] Li, E.; Hu, J. X.; Feng, X. M.; Zhou, Z. S.; An, L. H.; Law, K. T.; Wang, N.; Lin, N. Lattice reconstruction induced multiple ultra-flat bands in twisted bilayer WSe_2. *Nat. Commun.* **2021**, *12*, 5601.
[70] Waters, D.; Nie, Y. F.; Lüpke, F.; Pan, Y.; Fölsch, S.; Lin, Y. C.; Jariwala, B.; Zhang, K. H.; Wang, C.; Lv, H. Y. et al. Flat bands and mechanical deformation effects in the moiré superlattice of MoS_2-WSe_2 heterobilayers. *ACS Nano* **2020**, *14*, 7564–7573.
[71] Scherer, M. M.; Kennes, D. M.; Classen, L. Chiral superconductivity with enhanced quantized hall responses in moiré transition metal dichalcogenides. *npj Quantum Mater.* **2022**, *7*, 100.
[72] Jin, C. H.; Tao, Z.; Li, T. X.; Xu, Y.; Tang, Y. H.; Zhu, J. C.; Liu, S.; Watanabe, K.; Taniguchi, T.; Hone, J. C. et al. Stripe phases in WSe_2/WS_2 moiré superlattices. *Nat. Mater.* **2021**, *20*, 940–944.
[73] Novoselov, K. S.; Geim, A. K.; Morozov, S. V.; Jiang, D.; Zhang, Y.; Dubonos, S. V.; Grigorieva, I. V.; Firsov, A. A. Electric field effect in atomically thin carbon films. *Science* **2004**, *306*, 666–669.
[74] Magda, G. Z.; Petõ, J.; Dobrik, G.; Hwang, C.; Biró, L. P.; Tapasztó, L. Exfoliation of large-area transition metal chalcogenide single layers. *Sci. Rep.* **2015**, *5*, 14714.
[75] Desai, S. B.; Madhvapathy, S. R.; Amani, M.; Kiriya, D.; Hettick, M.; Tosun, M.; Zhou, Y. Z.; Dubey, M.; Ager, J. W.; Chrzan, D. et al. Gold-mediated exfoliation of ultralarge optoelectronically-perfect monolayers. *Adv. Mater.* **2016**, *28*, 4053–4058.
[76] Velický, M.; Donnelly, G. E.; Hendren, W. R.; McFarland, S.; Scullion, D.; DeBenedetti, W. J. I.; Correa, G. C.; Han, Y. M.; Wain, A. J.; Hines, M. A. et al. Mechanism of gold-assisted exfoliation of centimeter-sized transition-metal dichalcogenide monolayers. *ACS Nano* **2018**, *12*, 10463–10472.
[77] Huang, Y.; Pan, Y. H.; Yang, R.; Bao, L. H.; Meng, L.; Luo, H. L.; Cai, Y. Q.; Liu, G. D.; Zhao, W. J.; Zhou, Z. et al. Universal mechanical exfoliation of large-area 2D crystals. *Nat. Commun.* **2020**, *11*, 2453.
[78] Heyl, M.; Burmeister, D.; Schultz, T.; Pallasch, S.; Ligorio, G.; Koch, N.; List-Kratochvil, E. J. W. Thermally activated gold‐mediated transition metal dichalcogenide exfoliation and a unique gold-mediated transfer. *Phys. Status Solidi RRL - Rapid Res. Lett.* **2020**, *14*, 2000408.
[79] Heyl, M.; List-Kratochvil, E. J. W. Only gold can pull this off: Mechanical exfoliations of transition metal dichalcogenides beyond scotch tape. *Appl. Phys. A* **2023**, *129*, 16.
[80] Li, Z. W.; Ren, L. W.; Wang, S. Y.; Huang, X. X.; Li, Q. Y.; Lu, Z. Y.; Ding, S. M.; Deng, H. J.; Chen, P. G.; Lin, J. et al. Dry exfoliation of large-area 2D monolayer and heterostructure arrays. *ACS Nano* **2021**, *15*, 13839–13846.
[81] Fu, Q.; Dai, J. Q.; Huang, X. Y.; Dai, Y. Y.; Pan, Y. H.; Yang, L. L.; Sun, Z. Y.; Miao, T. M.; Zhou, M. F.; Zhao, L. et al. One-step exfoliation method for plasmonic activation of large-area 2D crystals. *Adv. Sci.* **2022**, *9*, 2204247.
[82] Ding, S. M.; Liu, C.; Li, Z. W.; Lu, Z. Y.; Tao, Q. Y.; Lu, D. L.;

Chen, Y.; Tong, W.; Liu, L. T.; Li, W. Y. et al. Ag-assisted dry exfoliation of large-scale and continuous 2D monolayers. *ACS Nano* **2024**, *18*, 1195–1203.

[83] Li, Y. G.; Kuang, G. Z.; Jiao, Z. J.; Yao, L.; Duan, R. H. Recent progress on the mechanical exfoliation of 2D transition metal dichalcogenides. *Mater. Res. Express* **2022**, *9*, 122001.

[84] Frisenda, R.; Navarro-Moratalla, E.; Gant, P.; Pérez De Lara, D.; Jarillo-Herrero, P.; Gorbachev, R. V.; Castellanos-Gomez, A. Recent progress in the assembly of nanodevices and van der Waals heterostructures by deterministic placement of 2D materials. *Chem. Soc. Rev.* **2018**, *47*, 53–68.

[85] Zhao, Q. H.; Wang, T.; Ryu, Y. K.; Frisenda, R.; Castellanos-Gomez, A. An inexpensive system for the deterministic transfer of 2D materials. *J. Phys. Mater.* **2020**, *3*, 016001.

[86] Gant, P.; Carrascoso, F.; Zhao, Q. H.; Ryu, Y. K.; Seitz, M.; Prins, F.; Frisenda, R.; Castellanos-Gomez, A. A system for the deterministic transfer of 2D materials under inert environmental conditions. *2D Mater.* **2020**, *7*, 025034.

[87] Castellanos-Gomez, A.; Duan, X. F.; Fei, Z.; Gutierrez, H. R.; Huang, Y.; Huang, X. Y.; Quereda, J.; Qian, Q.; Sutter, E.; Sutter, P. Van der Waals heterostructures. *Nat. Rev. Methods Primers* **2022**, *2*, 58.

[88] Bertolazzi, S.; Brivio, J.; Kis, A. Stretching and breaking of ultrathin MoS_2. *ACS Nano* **2011**, *5*, 9703–9709.

[89] Taychatanapat, T.; Watanabe, K.; Taniguchi, T.; Jarillo-Herrero, P. Quantum hall effect and landau-level crossing of Dirac fermions in trilayer graphene. *Nat. Phys.* **2011**, *7*, 621–625.

[90] Bonaccorso, F.; Lombardo, A.; Hasan, T.; Sun, Z. P.; Colombo, L.; Ferrari, A. C. Production and processing of graphene and 2D crystals. *Mater. Today* **2012**, *15*, 564–589.

[91] Uwanno, T.; Hattori, Y.; Taniguchi, T.; Watanabe, K.; Nagashio, K. Fully dry PMMA transfer of graphene on *h*-BN using a heating/cooling system. *2D Mater.* **2015**, *2*, 041002.

[92] Tien, D. H.; Park, J. Y.; Kim, K. B.; Lee, N.; Seo, Y. Characterization of graphene-based FET fabricated using a shadow mask. *Sci. Rep.* **2016**, *6*, 25050.

[93] Wang, X. T.; Kang, K.; Chen, S. W.; Du, R. Z.; Yang, E. H. Location-specific growth and transfer of arrayed MoS_2 monolayers with controllable size. *2D Mater.* **2017**, *4*, 025093.

[94] Castellanos-Gomez, A.; Buscema, M.; Molenaar, R.; Singh, V.; Janssen, L.; Van Der Zant, H. S. J.; Steele, G. A. Deterministic transfer of two-dimensional materials by all-dry viscoelastic stamping. *2D Mater.* **2014**, *1*, 011002.

[95] Li, H.; Wu, J.; Huang, X.; Yin, Z. Y.; Liu, J. Q.; Zhang, H. A universal, rapid method for clean transfer of nanostructures onto various substrates. *ACS Nano* **2014**, *8*, 6563–6570.

[96] Ye, F.; Lee, J.; Feng, P. X. L. Atomic layer MoS_2-graphene van der Waals heterostructure nanomechanical resonators. *Nanoscale* **2017**, *9*, 18208–18215.

[97] Kinoshita, K.; Moriya, R.; Onodera, M.; Wakafuji, Y.; Masubuchi, S.; Watanabe, K.; Taniguchi, T.; Machida, T. Dry release transfer of graphene and few-layer h-BN by utilizing thermoplasticity of polypropylene carbonate. *npj 2D Mater. Appl.* **2019**, *3*, 22.

[98] Pizzocchero, F.; Gammelgaard, L.; Jessen, B. S.; Caridad, J. M.; Wang, L.; Hone, J.; Bøggild, P.; Booth, T. J. The hot pick-up technique for batch assembly of van der Waals heterostructures. *Nat. Commun.* **2016**, *7*, 11894.

[99] Dai, Y. C.; Qi, P. F.; Tao, G. Y.; Yao, G. J.; Shi, B. B.; Liu, Z. X.; Liu, Z. C.; He, X.; Peng, P.; Dang, Z. B. et al. Phonon-assisted upconversion in twisted two-dimensional semiconductors. *Light Sci. Appl.* **2023**, *12*, 6.

[100] Xu, H. Y.; Akbari, M. K.; Zhuiykov, S. 2D semiconductor nanomaterials and heterostructures: Controlled synthesis and functional applications. *Nanoscale Res. Lett.* **2021**, *16*, 94.

[101] Zhang, Z. W.; Chen, P.; Duan, X. D.; Zang, K. T.; Luo, J.; Duan, X. F. Robust epitaxial growth of two-dimensional heterostructures, multiheterostructures, and superlattices. *Science* **2017**, *357*, 788–792.

[102] Sahoo, P. K.; Memaran, S.; Xin, Y.; Balicas, L.; Gutiérrez, H. R. One-pot growth of two-dimensional lateral heterostructures via sequential edge-epitaxy. *Nature* **2018**, *553*, 63–67.

[103] Kang, K.; Lee, K. H.; Han, Y. M.; Gao, H.; Xie, S. E.; Muller, D. A.; Park, J. Layer-by-layer assembly of two-dimensional materials into wafer-scale heterostructures. *Nature* **2017**, *550*, 229–233.

[104] Zhang, C. D.; Chuu, C. P.; Ren, X. B.; Li, M. Y.; Li, L. J.; Jin, C. H.; Chou, M. Y.; Shih, C. K. Interlayer couplings, moiré patterns, and 2D electronic superlattices in MoS_2/WSe_2 hetero-bilayers. *Sci. Adv.* **2017**, *3*, e1601459.

[105] Lin, Y. C.; Ghosh, R. K.; Addou, R.; Lu, N.; Eichfeld, S. M.; Zhu, H.; Li, M. Y.; Peng, X.; Kim, M. J.; Li, L. J. et al. Atomically thin resonant tunnel diodes built from synthetic van der Waals heterostructures. *Nat. Commun.* **2015**, *6*, 7311.

[106] Li, M. Y.; Shi, Y. M.; Cheng, C. C.; Lu, L. S.; Lin, Y. C.; Tang, H. L.; Tsai, M. L.; Chu, C. W.; Wei, K. H.; He, J. H. et al. Epitaxial growth of a monolayer WSe_2-MoS_2 lateral p-n junction with an atomically sharp interface. *Science* **2015**, *349*, 524–528.

[107] Yuan, L.; Zheng, B. Y.; Kunstmann, J.; Brumme, T.; Kuc, A. B.; Ma, C.; Deng, S. B.; Blach, D.; Pan, A. L.; Huang, L. B. Twist-angle-dependent interlayer exciton diffusion in WS_2-WSe_2 heterobilayers. *Nat. Mater.* **2020**, *19*, 617–623.

[108] Kang, K.; Xie, S. E.; Huang, L. J.; Han, Y. M.; Huang, P. Y.; Mak, K. F.; Kim, C. J.; Muller, D.; Park, J. High-mobility three-atom-thick semiconducting films with wafer-scale homogeneity. *Nature* **2015**, *520*, 656–660.

[109] Xie, S. E.; Tu, L. J.; Han, Y. M.; Huang, L. J.; Kang, K.; Lao, K. U.; Poddar, P.; Park, C.; Muller, D. A.; DiStasio, R. A. et al. Coherent, atomically thin transition-metal dichalcogenide superlattices with engineered strain. *Science* **2018**, *359*, 1131–1136.

[110] Jin, G.; Lee, C. S.; Okello, O. F. N.; Lee, S. H.; Park, M. Y.; Cha, S.; Seo, S. Y.; Moon, G.; Min, S. Y.; Yang, D. H. et al. Heteroepitaxial van der Waals semiconductor superlattices. *Nat. Nanotechnol.* **2021**, *16*, 1092–1098.

[111] Zhou, X. W.; Zhang, Z. N.; Zeng, X. L.; Wu, Y. P.; Xu, F. Y.; Zhang, C. M.; Li, X.; Wu, Z. M.; Kang, J. Y. Direct synthesis of moiré superlattice through chemical vapor deposition growth of monolayer WS_2 on plasma-treated HOPG. *Nano Res.* **2022**, *15*, 8587–8594.

[112] Zheng, H. H.; Guo, H. L.; Chen, S. L.; Wu, B.; Li, S. F.; He, J.; Liu, Z. W.; Lu, G.; Duan, X. D.; Pan, A. L. et al. Strong interlayer coupling in twisted transition metal dichalcogenide moiré superlattices. *Adv. Mater.* **2023**, *35*, 2210909.

[113] Kim, K.; Yankowitz, M.; Fallahazad, B.; Kang, S.; Movva, H. C. P.; Huang, S. Q.; Larentis, S.; Corbet, C. M.; Taniguchi, T.; Watanabe, K. et al. van der Waals heterostructures with high accuracy rotational alignment. *Nano Lett.* **2016**, *16*, 1989–1995.

[114] K.; DaSilva, A.; Huang, S. Q.; Fallahazad, B.; Larentis, S.; Taniguchi, T.; Watanabe, K.; LeRoy, B. J.; MacDonald, A. H.; Tutuc, E. Tunable moiré bands and strong correlations in small-twist-angle bilayer graphene. *Proc. Natl. Acad. Sci. USA* **2017**, *114*, 3364–3369.

[115] Andersen, T. I.; Scuri, G.; Sushko, A.; De Greve, K.; Sung, J.; Zhou, Y.; Wild, D. S.; Gelly, R. J.; Heo, H.; Bérubé, D. et al. Excitons in a reconstructed moiré potential in twisted WSe_2/WSe_2 homobilayers. *Nat. Mater.* **2021**, *20*, 480–487.

[116] Wu, B.; Zheng, H. H.; Li, S. F.; Wang, C. T.; Ding, J. N.; He, J.; Liu, Z. W.; Wang, J. T.; Liu, Y. P. Enhanced homogeneity of moiré superlattices in double-bilayer WSe_2 homostructure. *ACS Appl. Mater. Interfaces* **2023**, *15*, 48475–48484.

[117] Wang, L.; Meric, I.; Huang, P. Y.; Gao, Q.; Gao, Y.; Tran, H.; Taniguchi, T.; Watanabe, K.; Campos, L. M.; Muller, D. A. et al. One-dimensional electrical contact to a two-dimensional material. *Science* **2013**, *342*, 614–617.

[118] Xu, Y.; Liu, S.; Rhodes, D. A.; Watanabe, K.; Taniguchi, T.; Hone, J.; Elser, V.; Mak, K. F.; Shan, J. Correlated insulating states at fractional fillings of moiré superlattices. *Nature* **2020**, *587*, 214–218.

[119] Shao, G. L.; Xue, X. X.; Liu, X.; Zhang, D. L.; Jin, Y. Y.; Wu, Y. W.; You, B. Y.; Lin, Y. C.; Li, S. S.; Suenaga, K. et al. Twist angle-dependent optical responses in controllably grown WS_2 vertical homojunctions. *Chem. Mater.* **2020**, *32*, 9721–9729.

[120] Xu, M. Z.; Ji, H. J.; Zheng, L.; Li, W. W.; Wang, J.; Wang, H. X.; Luo, L.; Lu, Q. B.; Gan, X. T.; Liu, Z. et al. Reconfiguring

nucleation for CVD growth of twisted bilayer MoS_2 with a wide range of twist angles. *Nat. Commun.* **2024**, *15*, 562.
[121] Xu, M. Z.; Ji, H. J.; Zhang, M. W.; Zheng, L.; Li, W. W.; Luo, L.; Chen, M. D.; Liu, Z.; Gan, X. T.; Wang, X. W. et al. CVD synthesis of twisted bilayer WS_2 with tunable second harmonic generation. *Adv. Mater.* **2024**, *36*, 2313638.
[122] Chang, S. J.; Wang, S. Y.; Huang, Y. C.; Chih, J. H.; Lai, Y. T.; Tsai, Y. W.; Lin, J. M.; Chien, C. H.; Tang, Y. T.; Hu, C. M. van der Waals epitaxy of 2D *h*-AlN on TMDs by atomic layer deposition at 250 °C. *Appl. Phys. Lett.* **2022**, *120*, 162102.
[123] Zhang, X.; Lai, J. W.; Gray, T. Recent progress in low-temperature CVD growth of 2D materials. *Oxf. Open Mater. Sci.* **2023**, *3*, itad010.
[124] Yang, H. T.; Hu, R. Q.; Wu, H.; He, X. L.; Zhou, Y.; Xue, Y. Z.; He, K. X.; Hu, W. S.; Chen, H. S.; Gong, M. M. et al. Identification and structural characterization of twisted atomically thin bilayer materials by deep learning. *Nano Lett.* **2024**, *24*, 2789–2797.
[125] Lu, M. Y.; Ji, H. N.; Chen, Y. X.; Gao, F. L.; Liu, B.; Long, P.; Deng, C.; Wang, Y.; Tao, J. D. Machine learning assisted layer-controlled synthesis of MoS_2. *J. Mater. Chem. C* **2024**, *12*, 8893–8900.
[126] Xu, M. Z.; Tang, B. J.; Lu, Y. H.; Zhu, C.; Lu, Q. B.; Zhu, C.; Zheng, L.; Zhang, J. Y.; Han, N. N.; Fang, W. D. et al. Machine learning driven synthesis of few-layered WTe_2 with geometrical control. *J. Am. Chem. Soc.* **2021**, *143*, 18103–18113.
[127] Tang, B. J.; Lu, Y. H.; Zhou, J. D.; Chouhan, T.; Wang, H.; Golani, P.; Xu, M. Z.; Xu, Q.; Guan, C. T.; Liu, Z. Machine learning-guided synthesis of advanced inorganic materials. *Mater. Today* **2020**, *41*, 72–80.
[128] Wu, F. C.; Lovorn, T.; MacDonald, A. H. Topological exciton bands in moiré heterojunctions. *Phys. Rev. Lett.* **2017**, *118*, 147401.
[129] Yu, H. Y.; Liu, G. B.; Tang, J. J.; Xu, X. D.; Yao, W. Moiré excitons: From programmable quantum emitter arrays to spin-orbit-coupled artificial lattices. *Sci. Adv.* **2017**, *3*, e1701696.
[130] Wu, F. C.; Lovorn, T.; Macdonald, A. H. Theory of optical absorption by interlayer excitons in transition metal dichalcogenide heterobilayers. *Phys. Rev. B* **2018**, *97*, 035306.
[131] Jin, C. H.; Regan, E. C.; Yan, A. M.; Iqbal Bakti Utama, M.; Wang, D. Q.; Zhao, S. H.; Qin, Y.; Yang, S. J.; Zheng, Z. R.; Shi, S. Y. et al. Observation of moiré excitons in WSe_2/WS_2 heterostructure superlattices. *Nature* **2019**, *567*, 76–80.
[132] Pan, H. N.; Wu, F. C.; Das Sarma, S. Quantum phase diagram of a moiré-Hubbard model. *Phys. Rev. B* **2020**, *102*, 201104(R).
[133] Morales-Durán, N.; Hu, N. C.; Potasz, P.; Macdonald, A. H. Nonlocal interactions in moiré Hubbard systems. *Phys. Rev. Lett.* **2022**, *128*, 217202.
[134] Pan, H. N.; Wu, F. C.; Das Sarma, S. Band topology, Hubbard model, Heisenberg model, and dzyaloshinskii-Moriya interaction in twisted bilayer WSe_2. *Phys. Rev. Res.* **2020**, *2*, 033087.
[135] Devakul, T.; Crépel, V.; Zhang, Y.; Fu, L. Magic in twisted transition metal dichalcogenide bilayers. *Nat. Commun.* **2021**, *12*, 6730.
[136] Kumar, A.; Hu, N. C.; MacDonald, A. H.; Potter, A. C. Gate-tunable heavy fermion quantum criticality in a moiré Kondo lattice. *Phys. Rev. B* **2022**, *106*, L041116.
[137] Angeli, M.; MacDonald, A. H. Γ valley transition metal dichalcogenide moiré bands. *Proc. Natl. Acad. Sci. USA* **2021**, *118*, e2021826118.
[138] Des Cloizeaux, J. Energy bands and projection operators in a crystal: Analytic and asymptotic properties. *Phys. Rev.* **1964**, *135*, A685–A697.
[139] Des Cloizeaux, J. Analytical properties of *n*-dimensional energy bands and wannier functions. *Phys. Rev.* **1964**, *135*, A698–A707.
[140] Marzari, N.; Vanderbilt, D. Maximally localized generalized wannier functions for composite energy bands. *Phys. Rev. B* **1997**, *56*, 12847–12865.
[141] Kaushal, N.; Dagotto, E. Moiré kanamori-Hubbard model for transition metal dichalcogenide homobilayers. *Phys. Rev. B* **2023**, *107*, L201118.
[142] Guo, H. L.; Zhang, X.; Lu, G. Shedding light on moiré excitons: A first-principles perspective. *Sci. Adv.* **2020**, *6*, eabc5638.
[143] Gross, E. K. U.; Kohn, W. Local density-functional theory of frequency-dependent linear response. *Phys. Rev. Lett.* **1985**, *55*, 2850–2852.
[144] Marques, M. A. L.; Maitra, N. T.; Nogueira, F. M. S.; Gross, E. K. U.; Rubio, A. *Fundamentals of Time-Dependent Density Functional Theory*; Springer: Berlin, 2012.
[145] Refaely-Abramson, S.; Sharifzadeh, S.; Govind, N.; Autschbach, J.; Neaton, J. B.; Baer, R.; Kronik, L. Quasiparticle spectra from a nonempirical optimally tuned range-separated hybrid density functional. *Phys. Rev. Lett.* **2012**, *109*, 226405.
[146] Refaely-Abramson, S.; Sharifzadeh, S.; Jain, M.; Baer, R.; Neaton, J. B.; Kronik, L. Gap renormalization of molecular crystals from density-functional theory. *Phys. Rev. B* **2013**, *88*, 081204(R).
[147] Refaely-Abramson, S.; Jain, M.; Sharifzadeh, S.; Neaton, J. B.; Kronik, L. Solid-state optical absorption from optimally tuned time-dependent range-separated hybrid density functional theory. *Phys. Rev. B* **2015**, *92*, 081204.
[148] Wing, D.; Haber, J. B.; Noff, R.; Barker, B.; Egger, D. A.; Ramasubramaniam, A.; Louie, S. G.; Neaton, J. B.; Kronik, L. Comparing time-dependent density functional theory with many-body perturbation theory for semiconductors: Screened range-separated hybrids and the *GW* plus Bethe-salpeter approach. *Phys. Rev. Mater.* **2019**, *3*, 064603.
[149] Gupta, N.; Sachin, S.; Kumari, P.; Rani, S.; Ray, S. J. Twistronics in two-dimensional transition metal dichalcogenide (TMD)-based van der Waals interface. *RSC Adv.* **2024**, *14*, 2878–2888.
[150] Liu, K. H.; Zhang, L. M.; Cao, T.; Jin, C. H.; Qiu, D. N.; Zhou, Q.; Zettl, A.; Yang, P. D.; Louie, S. G.; Wang, F. Evolution of interlayer coupling in twisted molybdenum disulfide bilayers. *Nat. Commun.* **2014**, *5*, 4966.
[151] Zhao, X. G.; Shi, Z. M.; Wang, X. J.; Zou, H. S.; Fu, Y. H.; Zhang, L. J. Band structure engineering through van der Waals heterostructing superlattices of two-dimensional transition metal dichalcogenides. *InfoMat* **2021**, *3*, 201–211.
[152] T. X.; Jiang, S. W.; Li, L. Z.; Zhang, Y.; Kang, K. F.; Zhu, J. C.; Watanabe, K.; Taniguchi, T.; Chowdhury, D.; Fu, L. et al. Continuous Mott transition in semiconductor moiré superlattices. *Nature* **2021**, *597*, 350–354.
[153] Tong, Q. J.; Yu, H. Y.; Zhu, Q. Z.; Wang, Y.; Xu, X. D.; Yao, W. Topological mosaics in moiré superlattices of van der Waals heterobilayers. *Nat. Phys.* **2017**, *13*, 356–362.
[154] Li, T. X.; Jiang, S. W.; Shen, B. W.; Zhang, Y.; Li, L. Z.; Tao, Z.; Devakul, T.; Watanabe, K.; Taniguchi, T.; Fu, L. et al. Quantum anomalous hall effect from intertwined moiré bands. *Nature* **2021**, *600*, 641–646.
[155] Förg, M.; Baimuratov, A. S.; Kruchinin, S. Y.; Vovk, I. A.; Scherzer, J.; Förste, J.; Funk, V.; Watanabe, K.; Taniguchi, T.; Högele, A. Moiré excitons in $MoSe_2$-WSe_2 heterobilayers and heterotrilayers. *Nat. Commun.* **2021**, *12*, 1656.
[156] Zhang, L.; Zhang, Z.; Wu, F. C.; Wang, D. Q.; Gogna, R.; Hou, S. C.; Watanabe, K.; Taniguchi, T.; Kulkarni, K.; Kuo, T. et al. Twist-angle dependence of moiré excitons in $WS_2/MoSe_2$ heterobilayers. *Nat. Commun.* **2020**, *11*, 5888.
[157] Zheng, H. H.; Wu, B.; Wang, C. T.; Li, S. F.; He, J.; Liu, Z. W.; Wang, J. T.; Duan, J. A.; Liu, Y. P. Moiré enhanced potentials in twisted transition metal dichalcogenide trilayers homostructures. *Small* **2023**, *19*, 2207988.
[158] Zheng, H. H.; Wu, B.; Wang, C. T.; Li, S. F.; He, J.; Liu, Z. W.; Wang, J. T.; Duan, J. A.; Liu, Y. P. Exploring the regulatory effect of stacked layers on moiré excitons in twisted $WSe_2/WSe_2/WSe_2$ homotrilayer. *Nano Res.* **2023**, *16*, 10573–10579.
[159] Tran, K.; Moody, G.; Wu, F. C.; Lu, X. B.; Choi, J.; Kim, K.; Rai, A.; Sanchez, D. A.; Quan, J. M.; Singh, A. et al. Evidence for moiré excitons in van der Waals heterostructures. *Nature* **2019**, *567*, 71–75.
[160] Seyler, K. L.; Rivera, P.; Yu, H. Y.; Wilson, N. P.; Ray, E. L.; Mandrus, D. G.; Yan, J. Q.; Yao, W.; Xu, X. D. Signatures of moiré-trapped valley excitons in $MoSe_2/WSe_2$ heterobilayers. *Nature* **2019**, *567*, 66–70.
[161] Zhang, N.; Surrente, A.; Baranowski, M.; Maude, D. K.; Gant, P.;

Castellanos-Gomez, A.; Plochocka, P. Moiré intralayer excitons in a $MoSe_2/MoS_2$ heterostructure. *Nano Lett.* **2018**, *18*, 7651–7657.
[162] Lin, B. H.; Chao, Y. C.; Hsieh, I.; Chuu, C. P.; Lee, C. J.; Chu, F. H.; Lu, L. S.; Hsu, W. T.; Pao, C. W.; Shih, C. K. et al. Remarkably deep moiré potential for intralayer excitons in $MoSe_2/MoS_2$ twisted heterobilayers. *Nano Lett.* **2023**, *23*, 1306–1312.
[163] Wu, B.; Zheng, H. H.; Li, S. F.; Ding, J. N.; He, J.; Zeng, Y. J.; Chen, K. Q.; Liu, Z. W.; Chen, S. L.; Pan, A. L. et al. Evidence for moiré intralayer excitons in twisted WSe_2/WSe_2 homobilayer superlattices. *Light Sci. Appl.* **2022**, *11*, 166.
[164] E. M.; Ruiz-Tijerina, D. A.; Danovich, M.; Hamer, M. J.; Terry, D. J.; Nayak, P. K.; Ahn, S.; Pak, S.; Lee, J.; Sohn, J. I. et al. Resonantly hybridized excitons in moiré superlattices in van der Waals heterostructures. *Nature* **2019**, *567*, 81–86.
[165] Tang, Y. H.; Gu, J.; Liu, S.; Watanabe, K.; Taniguchi, T.; Hone, J.; Mak, K. F.; Shan, J. Tuning layer-hybridized moiré excitons by the quantum-confined stark effect. *Nat. Nanotechnol.* **2021**, *16*, 52–57.
[166] Koperski, M.; Nogajewski, K.; Arora, A.; Cherkez, V.; Mallet, P.; Veuillen, J. Y.; Marcus, J.; Kossacki, P.; Potemski, M. Single photon emitters in exfoliated WSe_2 structures. *Nat. Nanotechnol.* **2015**, *10*, 503–506.
[167] Srivastava, A.; Sidler, M.; Allain, A. V.; Lembke, D. S.; Kis, A.; Imamoğlu, A. Optically active quantum dots in monolayer WSe_2. *Nat. Nanotechnol.* **2015**, *10*, 491–496.
[168] Chakraborty, C.; Kinnischtzke, L.; Goodfellow, K. M.; Beams, R.; Vamivakas, A. N. Voltage-controlled quantum light from an atomically thin semiconductor. *Nat. Nanotechnol.* **2015**, *10*, 507–511.
[169] He, Y. M.; Clark, G.; Schaibley, J. R.; He, Y.; Chen, M. C.; Wei, Y. J.; Ding, X.; Zhang, Q.; Yao, W.; Xu, X. D. et al. Single quantum emitters in monolayer semiconductors. *Nat. Nanotechnol.* **2015**, *10*, 497–502.
[170] Tran, T. T.; Bray, K.; Ford, M. J.; Toth, M.; Aharonovich, I. Quantum emission from hexagonal boron nitride monolayers. *Nat. Nanotechnol.* **2016**, *11*, 37–41.
[171] Schmitt, D.; Bange, J. P.; Bennecke, W.; AlMutairi, A.; Meneghini, G.; Watanabe, K.; Taniguchi, T.; Steil, D.; Luke, D. R.; Weitz, R. T. et al. Formation of moiré interlayer excitons in space and time. *Nature* **2022**, *608*, 499–503.
[172] Liu, E. F.; Barré, E.; Van Baren, J.; Wilson, M.; Taniguchi, T.; Watanabe, K.; Cui, Y. T.; Gabor, N. M.; Heinz, T. F.; Chang, Y. C. et al. Signatures of moiré trions in $WSe_2/MoSe_2$ heterobilayers. *Nature* **2021**, *594*, 46–50.
[173] Kim, H.; Dong, D. F.; Okamura, Y.; Shinokita, K.; Watanabe, K.; Taniguchi, T.; Matsuda, K. Dynamics of moiré trion and its valley polarization in a microfabricated $WSe_2/MoSe_2$ heterobilayer. *ACS Nano* **2023**, *17*, 13715–13723.
[174] Sung, J.; Zhou, Y.; Scuri, G.; Zólyomi, V.; Andersen, T. I.; Yoo, H.; Wild, D. S.; Joe, A. Y.; Gelly, R. J.; Heo, H. et al. Broken mirror symmetry in excitonic response of reconstructed domains in twisted $MoSe_2/MoSe_2$ bilayers. *Nat. Nanotechnol.* **2020**, *15*, 750–754.
[175] Zeng, C.; Zhong, J. H.; Wang, Y. P.; Yu, J.; Cao, L. K.; Zhao, Z. L.; Ding, J. N.; Cong, C. X.; Yue, X. F.; Liu, Z. W. et al. Observation of split defect-bound excitons in twisted WSe_2/WSe_2 homostructure. *Appl. Phys. Lett.* **2020**, *117*, 153103–153107.
[176] Scuri, G.; Andersen, T. I.; Zhou, Y.; Wild, D. S.; Sung, J.; Gelly, R. J.; Bérubé, D.; Heo, H.; Shao, L. B.; Joe, A. Y. et al. Electrically tunable valley dynamics in twisted WSe_2/WSe_2 bilayers. *Phys. Rev. Lett.* **2020**, *124*, 217403.
[177] Wu, B.; Zheng, H. H.; Li, S. F.; Wang, C. T.; Ding, J. N.; He, J.; Liu, Z. W.; Wang, J. T.; Liu, Y. P. Effect of layered-coupling in twisted WSe_2 moiré superlattices. *Nano Res.* **2023**, *16*, 3435–3442.
[178] Zheng, H. H.; Wu, B.; Li, S. F.; He, J.; Chen, K. Q.; Liu, Z. W.; Liu, Y. P. Evidence for interlayer coupling and moiré excitons in twisted WS_2/WS_2 homostructure superlattices. *Nano Res.* **2023**, *16*, 3429–3434.
[179] Plochocka, P. Excitons in a twisted world. *Nat. Nanotechnol.* **2020**, *15*, 727–729.
[180] Huang, D.; Choi, J.; Shih, C. K.; Li, X. Q. Excitons in semiconductor moiré superlattices. *Nat. Nanotechnol.* **2022**, *17*, 227–238.
[181] Guo, H. L.; Zhang, X.; Lu, G. Moiré excitons in defective van der Waals heterostructures. *Proc. Natl. Acad. Sci. USA* **2021**, *118*, e2105468118.
[182] Villafañe, V.; Kremser, M.; Hübner, R.; Petrić, M. M.; Wilson, N. P.; Stier, A. V.; Müller, K.; Florian, M.; Steinhoff, A.; Finley, J. J. Twist-dependent intra- and interlayer excitons in moiré $MoSe_2$ homobilayers. *Phys. Rev. Lett.* **2023**, *130*, 026901.
[183] Naik, M. H.; Regan, E. C.; Zhang, Z. C.; Chan, Y. H.; Li, Z. L.; Wang, D. Q.; Yoon, Y.; Ong, C. S.; Zhao, W. Y.; Zhao, S. H. et al. Intralayer charge-transfer moiré excitons in van der Waals superlattices. *Nature* **2022**, *609*, 52–57.
[184] Wu, F. C.; Xue, F.; MacDonald, A. H. Theory of two-dimensional spatially indirect equilibrium exciton condensates. *Phys. Rev. B* **2015**, *92*, 165121.
[185] Wang, Z. F.; Rhodes, D. A.; Watanabe, K.; Taniguchi, T.; Hone, J. C.; Shan, J.; Mak, K. F. Evidence of high-temperature exciton condensation in two-dimensional atomic double layers. *Nature* **2019**, *574*, 76–80.
[186] Fang, H. L.; Lin, Q. L.; Zhang, Y.; Thompson, J. Xiao, S. S.; Sun, Z. P.; Malic, E.; Dash, S. P.; Wieczorek, W. Localization and interaction of interlayer excitons in $MoSe_2/WSe_2$ heterobilayers. *Nat. Commun.* **2023**, *14*, 6910.
[187] Nayak, P. K.; Horbatenko, Y.; Ahn, S.; Kim, G.; Lee, J. U.; Ma, K. Y.; Jang, A. R.; Lim, H.; Kim, D.; Ryu, S. et al. Probing evolution of twist-angle-dependent interlayer excitons in $MoSe_2/WSe_2$ van der Waals heterostructures. *ACS Nano* **2017**, *11*, 4041–4050.
[188] Palekar, C. C.; Hagel, J.; Rosa, B.; Brem, S.; Shih, C. W.; Limame, I.; Von Helversen, M.; Tongay, S.; Malic, E.; Reitzenstein, S. Twist angle dependence of exciton resonances in $WSe_2/MoSe_2$ Moiré heterostructures. arXiv September 28, 2023.
[189] Cai, H. B.; Rasmita, A.; Tan, Q. H.; Lai, J.-M.; He, R. H.; Cai, X. B.; Zhao, Y.; Chen, D. S.; Wang, N. Z.; Mu, Z. et al. Interlayer donor-acceptor pair excitons in $MoSe_2/WSe_2$ moiré heterobilayer. *Nat. Nanotechnol.* **2023**, *14*, 5766.
[190] Remez, B.; Cooper, N. R. Leaky exciton condensates in transition metal dichalcogenide moiré bilayers. *Phys. Rev. Res.* **2022**, *4*, L022042.
[191] Guo, H. L.; Zhang, X.; Lu G. Tuning moiré excitons in Janus heterobilayers for high-temperature Bose-Einstein condensation. *Sci. Adv.* **2022**, *8*, eabp9757.
[192] Deng, S.; Chu, Y. C.; Zhu, Q. Z. Moiré exciton condensate: Nonlinear Dirac point, broken-symmetry Bloch waves, and unusual optical selection rules. *Phys. Rev. B* **2022**, *106*, 155410.
[193] Baek, H.; Brotons-Gisbert, M.; Koong, Z. X.; Campbell, A.; Rambach, M.; Watanabe, K.; Taniguchi, T.; Gerardot, B. D. Highly energy-tunable quantum light from moiré-trapped excitons. *Sci. Adv.* **2020**, *6*, eaba8526.
[194] Zhang, L.; Wu, F. C.; Hou, S. C.; Zhang, Z.; Chou, Y. H.; Watanabe, K.; Taniguchi, T.; Forrest, S. R.; Deng, H. Van der Waals heterostructure polaritons with moiré-induced nonlinearity. *Nature* **2021**, *591*, 61–65.
[195] Yu, H. Y.; Yao, W. Electrically tunable topological transport of moiré polaritons. *Sci. Bull.* **2020**, *65*, 1555–1562.
[196] Fitzgerald, J. M.; Thompson, J. J. P.; Malic, E. Twist angle tuning of moiré exciton polaritons in van der Waals heterostructures. *Nano Lett.* **2022**, *22*, 4468–4474.
[197] Chu, Z. D.; Regan, E. C.; Ma, X. J.; Wang, D. Q.; Xu, Z. F.; Utama, M. I. B.; Yumigeta, K.; Blei, M.; Watanabe, K.; Taniguchi, T. et al. Nanoscale conductivity imaging of correlated electronic states in WSe_2/WS_2 moiré superlattices. *Phys. Rev. Lett.* **2020**, *125*, 186803.
[198] H. Y.; Li, S. W.; Regan, E. C.; Wang, D. Q.; Zhao, W. Y.; Kahn, S.; Yumigeta, K.; Blei, M.; Taniguchi, T.; Watanabe, K. et al. Imaging two-dimensional generalized Wigner crystals. *Nature* **2021**, *597*, 650–654.
[199] Huang, X.; Wang, T. M.; Miao, S. N.; Wang, C.; Li, Z. P.; Lian, Z.; Taniguchi, T.; Watanabe, K.; Okamoto, S.; Xiao, D. et al.

Correlated insulating states at fractional fillings of the WS_2/WSe_2 moiré lattice. *Nat. Phys.* **2021**, *17*, 715–719.

[200] Li, T. X.; Zhu, J. C.; Tang, Y. H.; Watanabe, K.; Taniguchi, T.; Elser, V.; Shan, J.; Mak, K. F. Charge-order-enhanced capacitance in semiconductor moiré superlattices. *Nat. Nanotechnol.* **2021**, *16*, 1068–1072.

[201] Shimazaki, Y.; Schwartz, I.; Watanabe, K.; Taniguchi, T.; Kroner, M.; Imamoğlu, A. Strongly correlated electrons and hybrid excitons in a moiré heterostructure. *Nature* **2020**, *580*, 472–477.

[202] Liu, E. F.; Taniguchi, T.; Watanabe, K.; Gabor, N. M.; Cui, Y. T.; Lui, C. H. Excitonic and valley-polarization signatures of fractional correlated electronic phases in a WSe_2/WS_2 moiré superlattice. *Phys. Rev. Lett.* **2021**, *127*, 037402.

[203] Gu, J.; Ma, L. G.; Liu, S.; Watanabe, K.; Taniguchi, T.; Hone, J. C.; Shan, J.; Mak, K. F. Dipolar excitonic insulator in a moiré lattice. *Nat. Phys.* **2022**, *18*, 395–400.

[204] Wang, X.; Xiao, C. X.; Park, H.; Zhu, J. Y.; Wang, C.; Taniguchi, T.; Watanabe, K.; Yan, J. Q.; Xiao, D.; Gamelin, D. R. et al. Light-induced ferromagnetism in moiré superlattices. *Nature* **2022**, *604*, 468–473.

[205] Shabani, S.; Halbertal, D.; Wu, W. J.; Chen, M. X.; Liu, S.; Hone, J.; Yao, W.; Basov, D. N.; Zhu, X. Y.; Pasupathy, A. N. Deep moiré potentials in twisted transition metal dichalcogenide bilayers. *Nat. Phys.* **2021**, *17*, 720–725.

[206] Li, H. Y.; Li, S. W.; Naik, M. H.; Xie, J. X.; Li, X. Y.; Wang, J. Y.; Regan, E.; Wang, D. Q.; Zhao, W. Y.; Zhao, S. H. et al. Imaging moiré flat bands in three-dimensional reconstructed WSe_2/WS_2 superlattices. *Nat. Mater.* **2021**, *20*, 945–950.

[207] Li, H. Y.; Li, S. W.; Naik, M. H.; Xie, J. X.; Li, X. Y.; Regan, E.; Wang, D. Q.; Zhao, W. Y.; Yumigeta, K.; Blei, M. et al. Imaging local discharge cascades for correlated electrons in WS_2/WSe_2 moiré superlattices. *Nat. Phys.* **2021**, *17*, 1114–1119.

[208] Imada, M.; Fujimori, A.; Tokura, Y. Metal-insulator transitions. *Rev. Mod. Phys.* **1998**, *70*, 1039–1263.

[209] Senthil, T. Theory of a continuous Mott transition in two dimensions. *Phys. Rev. B* **2008**, *78*, 045109.

[210] Szasz, A.; Motruk, J.; Zaletel, M. P.; Moore, J. E. Chiral spin liquid phase of the triangular lattice Hubbard model: A density matrix renormalization group study. *Phys. Rev. X* **2020**, *10*, 021042.

[211] Balents, L. Spin liquids in frustrated magnets. *Nature* **2010**, *464*, 199–208.

[212] Georges, A.; Kotliar, G.; Krauth, W.; Rozenberg, M. J. Dynamical mean-field theory of strongly correlated fermion systems and the limit of infinite dimensions. *Rev. Mod. Phys.* **1996**, *68*, 13–125.

[213] Liu, Y. Y.; Stradins, P.; Wei, S. H. Van der Waals metal-semiconductor junction: Weak Fermi level pinning enables effective tuning of schottky barrier. *Sci. Adv.* **2016**, *2*, e1600069.

[214] Zhang, M. J.; Zhao, X.; Watanabe, K.; Taniguchi, T.; Zhu, Z.; Wu, F. C.; Li, Y. Q.; Xu, Y. Tuning quantum phase transitions at half filling in 3L-$MoTe_2/WSe_2$ moiré superlattices. *Phys. Rev. X* **2022**, *12*, 041015.

[215] Tang, Y. H.; Su, K. X.; Li, L. Z.; Xu, Y.; Liu, S.; Watanabe, K.; Taniguchi, T.; Hone, J.; Jian, C. M.; Xu, C. K. et al. Evidence of frustrated magnetic interactions in a Wigner-Mott insulator. *Nat. Nanotechnol.* **2023**, *18*, 233–237.